ATMOSPHERIC GUIDING OF ELECTROMAGNETIC WAVES

Brian P. Condon

A Thesis Submitted for the Degree of PhD
at the
University of St Andrews

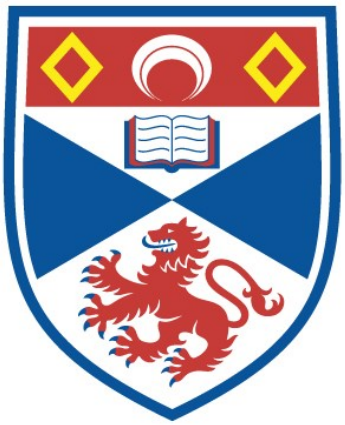

1993

ATMOSPHERIC GUIDING OF ELECTROMAGNETIC WAVES

A thesis presented by
Brian P Condon B Sc (Hons) St And
to the
University of St Andrews
in application for the degree of
Doctor of Philosophy
March 1993

DECLARATION

I hereby certify that this thesis has been composed by me, that it is a record of my own work and that it has not previously been presented in partial or complete fulfilment of any other degree or professional qualification.

In submitting this thesis to the University of St Andrews, I wish access to it to be subject to the condition that, for a period of 5 years from the date of submission, this thesis shall be made available for use only with the written consent of Dr Arthur Maitland. I understand that the title and abstract of this thesis will be published during the period of restricted access and that after the expiry of this period, this thesis shall be made available for use in accordance with the regulations of the University Library for the time being in force, subject to any copyright in the work not being affected thereby, and a copy of the work may be supplied to any *bona fide* library or research worker.

Brian P Condon

CERTIFICATE

I hereby certify that Brian P Condon has fulfilled the conditions of the Resolution and Regulations appropriate to the degree of Doctor of Philosophy.

A. Maitland
Research Supervisor

ACKNOWLEDGEMENTS

I would like to thank Arthur Maitland for a classic example of "lateral thinking" in coming up with the idea. I am grateful for his support and enthusiasm during the course of the research.

The financial support for the research was provided by DRA Electronics Division. Thank you to Dave Parkes and his colleagues (particularly Keith Trafford) for their interest and their challenging questions.

I acknowledge, with thanks, the work of the Millimetre Wave Group of the Department of Physics and Astronomy. I am especially grateful to Graham Smith for adapting the microwave interferometer to my experiment and for help in making the measurements.

I am grateful to the staff of the Mechanical Workshop of the Department, particularly Jim Clark and Willie Smith for their skill and excellent work.

Thanks to all the members of Laser 1, particularly Bill Dawber, Peter Hirst and Natalie Ridge for useful discussions. Additional thanks are due to Natalie Ridge for proof-reading and to Peter Hirst for help with drawing some of the figures and taming most of the uncooperative computers during the final print-out. Thank you to Mary Maitland for her wonderful cooking and for accompanying me to the opera.

Finally, I could not have completed this work without the help of my partner, Kate Lyle. No more commuting to Scotland!

DEDICATION

to my grandparents

Eric and Irene Rankin

ABSTRACT

We propose to alter the propagation conditions experienced by a microwave beam by the generation of a "laser beam atmospheric waveguide". The waveguide is formed by tailored refractive index changes caused by the absorption of a small part of the energy of an annular laser beam. The objective is to increase the microwave radiation field experienced by a target through improved directionality rather than total radiated power from the source.

The equations governing the propagation of high power laser beams in the paraxial limit and their interactions (both linear and non-linear) with an absorbing atmosphere are derived and studied. The mechanisms which lead to the formation of the guide and the effects of the propagation environment are considered in detail and the full paraxial form of the thermal blooming wave equation is derived from first principles.

Refractive index changes in air caused by the passage of a 1 kW CW CO_2 Gaussian laser beam are studied theoretically and both linear and non-linear cases examined. In the linear case, it is predicted that the laser beam produces a refractive index change of greater than 1 part in 10^5 for a 1 second beam exposure. In the non-linear case, the iterative scheme developed predicts self-interaction and beam break-up after less than 0.5 s. For an annular beam, refractive index changes of 3 parts in 10^5 are predicted for the linear case.

The influence of refractive index fluctuations on microwave radiation is modelled using a ray-tracing algorithm to investigate the behaviour of microwave radiation in an atmospheric waveguide. For a step-index guide of 5 cm radius, there is strong guiding so that even with a small perturbation in refractivity, rays with a wide range of launch angles are trapped. In the case of a guide with a quadratic refractive index profile, small changes in refractive index (1 part in 10^6) produce weak guiding where only rays with trajectories very close to the optic axis are trapped. As the refractive index change increases, more divergent rays are trapped until a transition to strong guiding occurs at a critical value (changes in refractive index of the order of 1 part in 10^4).

A number of implementations of the waveguiding concept are proposed and evaluated. For the purposes of an experimental verification, a specially designed Annular Beam Director ("ABD") of an on-axis type is tested. Annular laser beams are propagated over short distances in the laboratory and the results presented. Measurements made with a rotating wire laser beam analyser indicate that the ABD performs well.

Experiments designed to measure refractive index changes caused by a 1 kW CW CO_2 laser beam of Gaussian profile are described. Measurements are made at wavelengths of 633 nm using a specially configured Michelson interferometer and at 3 mm using a millimetre wave quasi-optical FM noise measurement system. Typical results indicate refractive index changes of the order of 1 part in 10^6 at both the wavelengths considered.

The guiding of microwave radiation is verified using a 1 kW CW CO_2 annular laser beam, produced by the ABD, into which microwave energy is injected using a small copper reflector located at the centre of the annulus. In one implementation, the microwave energy is coupled out of the guide with a second copper reflector. In a second implementation, the microwave detector unit is located on the optic axis and the laser beam is terminated in an annular beam dump. The results show clear evidence that the high power laser beam forms a waveguide, increasing the amount of microwave radiation reaching the detector by a factor of 1.5.

CONTENTS

1. INTRODUCTION

The principle of guiding radiation in engineered waveguide structures is well known in radar and optics. In the atmosphere, refractive index variations can cause bending or trapping of microwave radiation (so-called "ducting" or "superrefraction") extending the range of a radar significantly further than a straight line of sight. If the natural phenomenon of ducting could be replicated in a controlled manner, we would have a powerful technique for improving the performance of microwave systems.

We propose to alter the propagation conditions experienced by a microwave beam through the formation of a "laser beam atmospheric waveguide". The waveguide is formed by tailored refractive index changes caused by absorption of a small part of the energy of the beam. This waveguide will enable the transmission of microwave radiation with less loss than the inverse square law of pure free-space propagation dictates. The objective is to increase the microwave radiation field experienced by the target through improved directionality rather than total radiated power from the source.

In this thesis, laser propagation in the atmosphere is described and the mechanisms governing the formation of an atmospheric waveguide are investigated theoretically and experimentally. Novel structures for the implementation of the guide and the injection of the radiation to be guided are presented.

1.1 Statement of the problem

A high power laser beam propagating through the real atmosphere interacts with its environment in a number of ways. The most important of these interactions are absorption, scattering, thermal blooming, turbulence induced beam spread and wander and optical breakdown.

Existing work in this field has concentrated on theoretical (largely numerical) studies of laser propagation (Gebhardt [1], Ulrich and Wallace [2]) with some laboratory simulations using low power lasers (a few mW or W) propagating in high pressure gases or absorbing liquids (Hayes *et al* [3] Buser *et al* [4], and McLean *et al* [5]). The motivation has been to maximise energy deposition on some target at a given range. To date, little experimental data have been published on thermal blooming in uncontrolled environments. There has been no publication of experiments designed to test the formation of laser waveguides in air at normal atmospheric pressure.

Thermal blooming and optical breakdown can cause significant changes in the refractive index of the atmosphere. If the refractive index changes could be configured to form a hollow tube, then we would have a structure rather like an optical fibre waveguide. The "core" of the waveguide would be be at ambient temperature and the "cladding" would be heated by the laser to a higher temperature. The refractive index in the core will be higher than that in the cladding. Electromagnetic waves injected into the core will be guided provided they strike the cladding at angles less than the acceptance angle for the waveguide.

It is important however, not to think of an atmospheric waveguide as a solid piece of equipment which has a constant length and diameter and is fixed in space and time. A laser beam generated waveguide could have a time-varying diameter or position and it may not be possible precisely to control the waveguide parameters if the propagation conditions vary along the guide.

The problem addressed in this thesis is to assess and apply known theory to the creation of an atmospheric optical waveguide, to extend this theory where necessary (and possible) and to conduct experiments to test the theory and demonstrate the feasibility of the concept.

1.2 Contribution of this thesis

This study is directed to the creation of an atmospheric waveguide and is not therefore intended to be an exhaustive treatment of laser propagation itself. It is however essential to consider those propagation effects which can influence the performance of the waveguide. The contributions of this work fall into two main catagories;

(1) A review of technology and propagation effects based on published literature and an assessment of their system effects.

(2) The development of theory to describe the operation and possible implementation of the waveguide and a series of experiments designed to demonstrate feasibility.

In the first catagory there are the following distinct contributions to the field;

- a review and assessment of relevant published sources, principally US and Soviet journals;
- calculation of the thermal blooming threshold conditions;
- an extension of these calculations to include the thermal non-linear refractive index; and
- an evaluation of the laser sources available to provide guiding.

In the second catagory, the following original contributions are made to the field;

- calculation of the conditions necessary to produce guiding in the case of a laser-produced annular atmospheric waveguide;
- experiments in normal laboratory conditions designed to measure the refractive index changes produced by pulsed and cw laser beams;
- measurements of bloomed and unbloomed beam profiles;
- design of a beam director capable of producing the required beam profile;
- considerations of beam and launching geometries for guiding structures;
- the inter-relationship of refractive index changes producd by the laser and perceived by microwave radiation in the 10-300 GHz frequency range; and

- calculations based on a new approach to the non-linear nature of thermal blooming.

These contributions should provide a basis for a better understanding of the physics of thermal blooming in near-real environments and give some insight into the challenges involved in building working systems based on these ideas.

1.3 Project approach

This project began in October 1987 with a six month period of feasiblity study. The field of laser propagation in the atmosphere was examined in detail and the status of work internationally was researched. Basic theory was developed to provide an order of magnitude estimate of the threshold condition for thermal blooming and to provide a basis upon which to extend theoretical and experimental knowledge. This period ended with a formal project report [6] which presented the results of the feasibility study and in which recommendations were made for further investigations of the waveguide concept.

Further investigations began in April 1988 with the establishment of a propagation studies laboratory. Experiments have been conducted with a 1.2 kW cw CO_2 laser. Measurements of the refractive index changes produced by the laser beam propagating through the air and direct measurements of the laser beam profile have been made. Annular beams have been propagated in the laboratory and their suitability for guiding microwave radiation has been assessed. The experimental work was concluded in October 1991.

The research conducted in the period October 1987 to October 1991 is reported here.

1.4 An assessment of the technology

The use of laser radiation in forming a guiding channel for the improved propagation of other types of energy was first proposed by G. A. Askar'yan of the P. N. Lebedev Physics Institute in 1968 [7]. Askar'yan's theoretical paper proposed the formation of an annular laser beam which could be used to guide infra-red or microwave radiation, sound waves or charged particles. Work on this concept continued in two main areas;

> Annular laser beams produced by blocking the centre of the beam with a screen or plate or by the use of the TEM^{*}_{01} stable resonator mode. This method uses the change of refractive index caused by the heating of the air by the laser pulse to establish the waveguide.
>
> High power laser pulses used to form a "cleared" channel. This method generally uses a laser powerful enough to cause optical breakdown [8]. As the laser pulse propagates, it forms a tube of heated air down which radiation can be sent.

Newman and Smith of United Technologies Research Centre, USA [9], proposed the use of the TEM^{*}_{01} mode (the so-called "doughnut mode") to guide submillimetre radiation (λ = 100 μm) over a 1 km path. They calculated that with a CO_2 laser of pulse energy 400J and a pulse

length of less than 166 ms, the spreading of the submillimetre wave beam of initial diameter 10 cm could be completely controlled. In the absence of the guiding beam, the microwave beam could be expected to have a diameter of 100 cm at the target. Thus, by guiding, the intensity of the radiation at a target could be increased by a factor of 100.

Newman and Smith reported the success of a laboratory experiment in which a CO_2 laser beam was propagated through a high pressure cell containing CO_2. The laser could be switched between TEM_{00} and TEM_{01}^* modes. A cw CO_2 probe beam was used to measure the guiding effect of the TEM_{01}^* mode. An increase in relative on-axis intensity of a factor of about 3 was observed.

Lax *et al* [10] discuss the propagation of a train of laser pulses where the duration of each pulse is short compared to the hydrodynamic response time of the propagation medium but where the interpulse interval is long enough to allow hydrodynamic expansion between pulses. This is a way of attempting to maximise the laser range and energy deposition on the target because pulses later in the train benefit from the cleared channel created by earlier pulses.

Yeh *et al* [11] and Schoen *et al* [12] propose the use of multiple aperture laser systems in an attempt to reduce the effect of thermal blooming; again this work is directed at maximising the laser energy deposition on the target.

Walsh and Ulrich [13] mention a rigorous solution to the problem of modelling the propagation of two or more laser beams from a single

aperture, each beam having a different wavelength, beam profile and atmospheric absorption cross-section but they do not give a reference or any results of this model.

Between 1971 and 1981 Soviet publications ceased. Although the Former Soviet Union is now, in general, making the results of its scientific work in this period available, no research in this field has been reported. It is, therefore, difficult to speculate about the direction which that work has taken. In 1981, however, Askar'yan and Mukhadamadovich published a paper which discusses the suppression of the effects of small-scale self-focussing by rotation, shaking and rocking of the laser beam [14]. Such results could have been obtained with a field-tested device.

Laser propagation work reported at SPIE's Optoelectronics and Laser Conference in Los Angeles in January 1990 is now dominated by the "strategic missions" for high power laser propagation from ground-to-space for Ballistic Missile Defence ("BMD") applications. T. J. Karr of Lawrence Livermore National Laboratory [15] reports the results of a computer simulation which predicts the formation of beam instabilities caused by thermal blooming which generate three-dimensional filaments or ribbon structures in the air correlated to disturbances on the beam.

Karr *et al* [16] also report experiments using a low power beam from an argon ion laser propagated through carbon tetrachloride to measure small scale thermal blooming effects. They claim that this is the first clear experimental demonstration of large amplification of small-scale spatial perturbations by Stimulated Thermal Rayleigh

Scattering ("STRS") of a cw laser beam propagating through an absorbing medium.

Quigley *et al* [17] of Los Alamos National Laboratory have used a single pulse, chemical CO_2 laser capable of pulse energies of up to 350 J to clear a 5 cm diameter hole through a stratos-like cloud in a cloud chamber. The results show that complete clearing can be achieved. The mechanism is shown to be droplet shattering followed by evaporation. The channel closure is dominated by turbulent mixing and not droplet recondensation. The application is to create a cleared channel with good optical quality to support the ground-to-space propagation of radiation from a laser weapon.

Research effort has been concentrated in providing adaptive optics to correct for thermal blooming. Higgs *et al* [18] report experiments with a 10 kW HF Chemical laser operating on multiple lines near 2.9 μm. These wavelengths are strongly absorbed by water vapour and CO_2 in the atmosphere. Experiments are reported over a 100 - 400 m horizontal path showing rapid on-set of thermal blooming with over 60 per cent of the laser power being absorbed into the air over a period of 400 ms.

It should also be noted that of the 30 papers presented to the SPIE conference in January 1990 (a peak year), only 5 papers reported experimental work. This underlines the requirement for novel experiments to assist this developing field.

1.4.1 Evidence of deployment

There is no evidence in the published literature that devices capable of guiding electromagnetic waves using annular laser beams have been deployed. The following factors would however indicate that such devices may exist;

- The use of high power lasers capable of producing annular beams in coordination with microwave sources. The microwave antenna would either be located coaxially with the laser or some kind of beam steering equipment would enable precise alignment of the beams. If the waveguide were to be passive (such as in listening or monitoring devices) then the use of annular laser beams with sensitive microphones or microwave detectors would be expected.

- The use of lasers which appear to be more powerful than necessary to perform their apparent task; unusually powerful laser communications links or ranging/target designation lasers are examples.

- The production of high power chemical lasers at wavelengths which are strongly absorbed by the atmosphere.

1.4.2 Conclusion

A thorough review of published sources indicates that the concept of laser waveguiding is considered to be effective in guiding electromagnetic radiation in strictly controlled experiments. There is no published work to date which demonstrates the concept in real or near-real environments.

In the wider field of laser propagation studies, very limited data have been published specifically on the thermal blooming of high power laser beams in air at atmospheric pressure. Studies performed to date use low power lasers and absorbing liquids or gases in high pressure cells in an attempt to simulate these effects. There is much theoretical work using computer codes and numerical simulations. Analytical theory uses linearised forms of the (non-linear) thermal blooming equations in an attempt to model the effects.

An aim of this thesis is to contribute to the understanding of thermal blooming by providing new experimental results.

REFERENCES FOR CHAPTER 1

1 Gebhardt F G, Applied Optics, **15**, No 6, p 1479 (1976)

2 Ulrich P B and Wallace J, Journal of the Optical Society of America, **63**, No 1, p 8 (1973)

3 Hayes J N, Ulrich P B and Aitken A H, Applied Optics, **11**, p 257 (1972).

4 Buser R G, Rohde R S, Berger P J, Gebhardt F and Smith D C, Applied Optics, **14**, No 11, p 2740 (1975)

5 McLean E A, Sica L and Glass A J, Applied Physics Letters, **13**, No 11, p369 (1968)

6 Condon B P and Maitland A, "Atmospheric Guiding of Electromagnetic Waves, Report on the Feasibility Study and Proposal for further funding" for RSRE Malvern, 31 March 1988

7 Askar'yan G A, Soviet Physics JETP, **28**, No 4 p732 (1968)

8 Askar'yan G A and Tarasova N M, JETP Letters, **20**, p123 (1974)

9 Newman L A and Smith D C, Applied Physics Letters, **38** No 8 p 590 (1981)

10 Lax M, Batteh J H and Agrawal G P, Journal of Applied Physics **52,** No 1 p109 (1981)

11 Yeh C, Pearson J E and Brown W P, Applied Optics, **15** , p 293

12 Schoen N C and Noveseller D E, Applied Optics, **22**, p3366

13 Walsh J L and Ulrich P B, "Thermal Blooming in the Atmosphere" published in "Laser Beam Propagation in the Atmosphere" edited by J W Strohbehn, ISBN 3-540-08812-1-1, published by Springer-Verlag (1978)

14 Askar'yan G A and Mukhamadzhanov M A, Soviet Physics Technical Physics, **26** No 9, p1163 (1981)

15 Karr T J, "Propagation of High Energy Laser Beams through the Earth's Atmosphere", Peter B Ulrich, Leroy E Wilson Editors, Proc SPIE 1221, p26 (1990)

16 Karr T J, Rushford M C, Murray J R, Morris J R, Journal of the Optical Soiciety of America B; Optical Physics, **8**, No 5, p993 (1991)

17 Quigley G P, Webster R B, Caramana E J, Morse R L and York G W, Applied Optics, **30**, No 21 p 3041 (1991)

18 Higgs C, Fouche D G and Pearson C F, "Intense Laser Beams", Richard C Wade, Peter B Ulrich, Editors, Proc SPIE 1628, p210 (1992)

2. ATMOSPHERIC PROPAGATION OF LASER BEAMS

2.1 Introduction

A number of applications require a detailed understanding of laser propagation in the atmosphere. These include communications, weaponry, remote sensing and remote chemical analysis, laser radar, target designation, energy transmission and laser safety management.

Laser propagation environments vary from vacuum or near vacuum conditions in space applications to propagation through optically thick clouds or dust for target designation. The performance of systems may also depend on the propagation direction. For example, ground-to-space propagation of laser radiation is more difficult to achieve with accuracy than space-to-ground propagation. This is because, in the first case, the thermal blooming interactions occur close to the transmitting point where small deviations can have a large effect on the beam arriving outside the atmosphere.

Propagation effects fall into three main areas, vacuum propagation where performance is diffraction-limited, "linear" propagation where the effects are independent of the laser power or intensity and "nonlinear" propagation where the effects are dependent on the laser power or intensity. These three areas and some typical effects are shown in Table 2.1.

Vacuum	Linear Effects	Nonlinear Effects
diffraction	scatter absorption	thermal blooming bending turbulence air breakdown (10^6 - 10^8 Wcm^{-2})

Table 2.1. Propagation Effects

In this section, the propagation of laser radiation is considered and basic theory is developed to provide the basis for a model of laser propagation in the real atmosphere.

2.2 Wave propagation in horizontally homogeneous media

Maxwell's equations for a sinusoidal electromagnetic field of frequency ω are

$$\left.\begin{aligned} \nabla \times \mathbf{E} &= -i\omega\mathbf{B}, \\ \nabla \times \mathbf{H} &= \mathbf{J} + i\omega\mathbf{D}. \end{aligned}\right\} \qquad (2.2.1)$$

Where **E** is the electric intensity, **B** is the magnetic flux density, **H** is magnetic intensity, **J** is the current density and **D** is the dielectric displacement. We are to deal with monochromatic fields so we can write the real electric vector field as a function of space and time as

$$\mathcal{E}(\mathbf{r},t) = \frac{1}{2}\left\{\mathbf{E}(\mathbf{r})e^{i\omega t} + \mathbf{E}^{*}(\mathbf{r})e^{-i\omega t}\right\} \qquad (2.2.2)$$

and we could write the other fields in Equation (2.2.1) in the same way. In the cases we consider, we can write the "constitutive relations" as

$$\mathbf{B} = \mu\mathbf{H},\ \mathbf{J} = \sigma\mathbf{E},\ \text{and}\ \mathbf{D} = \varepsilon\mathbf{E} + \mathbf{P} = \varepsilon(1+\chi)\mathbf{E} \qquad (2.2.3)$$

where μ is the permeability, σ is the conductivity, ε is the permittivity, $\mathbf{P}$ is the polarisation, χ is the susceptibility and the propagation medium is assumed to be homogeneous and isotropic. This assumption is reasonable for near horizontal or slant path propagation in the atmosphere. We now substitute Equations (2.2.1-3) into the vector identity

$$\nabla \times \nabla \mathbf{E} = \nabla(\nabla . \mathbf{E}) - \nabla^2\mathbf{E}, \qquad (2.2.4)$$

which holds if we use a Cartesian coordinate system and this yields

$$\nabla(\nabla . \mathbf{E}) - \nabla^2\mathbf{E} = \omega^2\mu\varepsilon\left\{1 + \chi - \frac{i\sigma}{\omega\varepsilon}\right\}. \qquad (2.2.5)$$

In a propagation medium which is spatially uniform, we can assume $\nabla . \mathbf{E} = 0$ and reduce Equation (2.2.5) to

$$\left[\nabla^2 + \omega^2\mu\varepsilon\left\{1 + \chi - \frac{i\sigma}{\omega\varepsilon}\right\}\right]\mathbf{E}(x,y,z) = 0, \qquad (2.2.6)$$

which is the scalar wave equation in general form. We note the identities $\omega^2\mu\varepsilon \equiv \beta^2 \equiv k^2$, where β is the plane wave propagation constant

in the propagation medium. In the real atmosphere, we have $\chi, \sigma \ll 1$ and Equation (2.2.6) becomes

$$\left[\nabla^2 + k^2 \right] \mathbf{E}\ (x, y, z) = 0. \tag{2.2.7}$$

Consider any given vector component of this complex **E** vector

$$\mathbf{E}\ (x, y, z) \equiv \mathbf{u}\,(x, y, z)\, e^{-ikz}. \tag{2.2.8}$$

We know that the transverse profile of a laser beam propagating in the atmosphere changes very slowly with z as the beam spreads, grows or changes shape due to absorption or diffraction effects. The rapid phase variation e^{-ikz} due to the travelling wave component of the beam has been factored out. From Equation (2.2.8) we obtain

$$\nabla^2 \mathbf{E} = \left[\frac{\partial^2 \mathbf{u}}{\partial x^2} + \frac{\partial^2 \mathbf{u}}{\partial y^2} + \frac{\partial^2 \mathbf{u}}{\partial z^2} - 2ik \frac{\partial \mathbf{u}}{\partial z} - k^2 \mathbf{u} \right] e^{-ikz}. \tag{2.2.9}$$

and substituting this equation into Equation (2.2.7) then yields

$$\left[\frac{\partial^2 \mathbf{u}}{\partial x^2} + \frac{\partial^2 \mathbf{u}}{\partial y^2} + \frac{\partial^2 \mathbf{u}}{\partial z^2} - 2ik \frac{\partial \mathbf{u}}{\partial z} \right] e^{-ikz} = 0. \tag{2.2.10}$$

We retain the phase factor as a reminder that the remaining components of **u** vary slowly with z and this enables us to invoke (at least qualitatively) the paraxial approximation using the following inequalities;

$$\left| \frac{\partial^2 \mathbf{u}}{\partial z^2} \right| \ll \left| 2ik \frac{\partial \mathbf{u}}{\partial z} \right| \tag{2.2.11}$$

and

$$\left| \frac{\partial^2 \mathbf{u}}{\partial z^2} \right| \ll \left| \frac{\partial^2 \mathbf{u}}{\partial x^2} \right| , \left| \frac{\partial^2 \mathbf{u}}{\partial y^2} \right| . \tag{2.2.12}$$

This means that we can neglect the second derivative of **u** in the z-direction and rewrite Equation (2.2.10) as

$$\frac{\partial^2 \mathbf{u}}{\partial x^2} + \frac{\partial^2 \mathbf{u}}{\partial y^2} - 2ik \frac{\partial \mathbf{u}}{\partial z} = 0 , \tag{2.2.13}$$

which is the paraxial form of the wave equation. More generally we write

$$\nabla_t^2 \, \mathbf{u}(\mathbf{s}, z) - 2ik \frac{\partial \mathbf{u}(\mathbf{s}, z)}{\partial z} = 0 , \tag{2.2.14}$$

where **s** refers to transverse coordinates **s**(x,y) or **s**(r,θ) in rectangular and cylindrical coordinates, respectively and ∇_t is the Laplacian operating on those coordinates in a plane normal to the propagation axis.

2.2.1 Justification of the paraxial approximation

The paraxial approximation is valid for the problem we address and we justify its use in this section. Any optical beam can always be viewed as comprising the linear superposition of plane waves travelling at various angles to the propagation axis. Consider one component **E** (x,z) of a

plane wave travelling at an angle θ to the z-axis (Figure 2.1). The axial and transverse components of the plane wave are given by

$$\mathbf{E}\,(x,y) = \exp\left(-i\,k\sin\theta - i\,k\cos\theta\right). \qquad (2.2.1.1)$$

The exact form of the reduced wave amplitude **u** (x,z) and its approximate form obtained by invoking the paraxial approximation can be obtained from Equation (2.2.1.1) as

$$\mathbf{u}\,(x,y,z) \equiv -ikx\sin\theta - ikz\,(1-\cos\theta) \approx \exp\left(-i\,k\,\theta + i\,k\,\theta^2\right). \qquad (2.2.1.2)$$

The wave equation in exact form for this example is written

$$\frac{\partial^2 \mathbf{u}}{\partial x^2} + \frac{\partial^2 \mathbf{u}}{\partial y^2} - 2ik\frac{\partial \mathbf{u}}{\partial z} = 0. \qquad (2.2.1.3)$$

From consideration of Equations (2.2.1.2) we write

$$-2ik\frac{\partial \mathbf{u}}{\partial z} = 2k^2\left(1-\cos\theta\right) \approx k^2\left(\theta^2 + \theta^4\right), \qquad (2.2.1.4)$$

$$\frac{1}{\mathbf{u}}\frac{\partial^2 \mathbf{u}}{\partial x^2} = k^2\sin^2\theta \qquad \approx -k^2\left(\theta^2 - \frac{\theta^4}{6}\right), \qquad (2.2.1.5)$$

and

$$\frac{1}{\mathbf{u}}\frac{\partial^2 \mathbf{u}}{\partial z^2} = -k^2\left(1-\cos\theta\right)^2 \approx -k^2\frac{\theta^4}{6}. \qquad (2.2.1.6)$$

In each of these three equations, we have written the exact form of the derivatives of the reduced wave amplitude **u**(x,z) followed by its

approximate form given by invoking the paraxial approximation and using Taylor's expansion to provide terms up to the fourth power. For values of $\theta < 0.5$ radian (say), we have $\theta^4 \ll 1$ and we can ignore terms of greater than the fourth order. In this case, we are justified in rewriting Equations (2.2.1.4-6) to give

$$\left.\begin{aligned} -2ik\frac{\partial \mathbf{u}}{\partial z} &\approx k^2\theta^2 \\ \frac{1}{\mathbf{u}}\frac{\partial^2 \mathbf{u}}{\partial x^2} &\approx -k^2\theta^2 \\ \frac{1}{\mathbf{u}}\frac{\partial^2 \mathbf{u}}{\partial z^2} &\approx 0 \end{aligned}\right\} \quad (2.2.1.7)$$

as solutions of the wave equation. In the case where $\theta = 0.5$ radian (or about 30°), the second derivative of **u** with respect to z in Equation (2.1.1.7) is actually more than two orders of magnitude smaller than the first derivatives in Equations (2.2.1.4 and 5). We conclude that, providing the plane wave components making up a beam travel at angles of less than about 30° to the propagation axis, then the paraxial approximation is valid. In most problems involving the propagation of laser beams, this proviso applies even when beams are focussed.

2.3 The propagation environment

A high power laser beam propagating through the atmosphere interacts with its environment. The interactions depend on the propagation conditions experienced by the beam and these vary widely in the atmosphere. In this section, we briefly describe the structure of the

atmosphere in regions relevant to our problem and then consider the effects of the atmosphere on the propagation of the beam.

The troposphere extends from the earth's surface up to 8 - 18 km, depending on the latitude. It is distinguished by a decrease in temperature with height, with a temperature gradient of 6 - 7°Ckm^{-1}. The zone where the temperature no longer decreases with height is called the tropopause.

The day-time atmosphere divides into three distinct layers below the tropopause; the surface layer (up to 50m), the planetary boundary layer (which includes the surface layer and continues up to 2.2km) and the troposphere (2.2 - 15 km). These layers do not have sharp boundaries and can vary in thickness and altitude according to the time of year or prevailing large-scale weather conditions.

In the surface layer, there is significant small-scale turbulence caused by surface heating and cooling. There are rapid changes in the wind, temperature and humidity. Terrain, vegetation or atmosphere/ocean boundary interactions may also play a part in dictating propagation conditions. Realistic, accurate models for laser and microwave propagation in this region do not currently exist.

The next layer, the planetary boundary layer, is dominated by large-scale convective mixing. The convection is driven by surface heating, with a depth which varies with the time of day and season. In this layer, there is strong vertical mixing and the mean properties change little with height.

In this thesis, we are primarily concerned with propagation in the surface layer, although some applications may require propagation in the planetary boundary layer.

2.4 Diffraction

Diffractive spreading is important because it provides an upper bound for the performance of the optical systems we are to consider and it is logical to introduce it here. The amount of spreading depends on the wavelength of the light, the shape of the phase front and the size of the aperture or beam waist.

The amplitude and irradiance of a gaussian spherical wave have the form

$$\mathbf{E}\,(x, y) = \exp -\left(\frac{x^2 + y^2}{w^2}\right) \tag{2.4.1}$$

and

$$I(x,y) = I_0 \exp -\left(\frac{-2(x^2 + y^2)}{w^2}\right), \tag{2.4.2}$$

respectively, where w is known as the "spot size", x and y are orthogonal axes in a plane normal to the propagation axis and I_0 is the peak irradiance in that plane. By convention, w is defined as the radial distance from the beam's centre where the intensity falls to $I_0 e^{-2}$. We note that for a gaussian beam of TEM_{00} mode, 86 per cent of the energy is contained within the spot.

Consider a gaussian spherical wave propagating in the z-direction, the spot size at range z from the beam waist is given by

$$w(z) = w_0\left\{1+\left(\frac{\lambda z}{\pi w_o^2}\right)^2\right\}^{\frac{1}{2}}, \qquad (2.4.3)$$

where w_0 is the size of the beam waist at the output aperture (z = 0) and λ is the wavelength of the laser. For large z, that is

$$z \gg Z_R = \frac{2\pi w_o^2}{\lambda}$$

we have

$$w(z) \simeq \frac{\lambda z}{\pi w_0} \quad \text{for } z \gg w_0. \qquad (2.4.4)$$

Z_R is known as the "Rayleigh range" and is defined as the the distance at which the spot size has approximately doubled in area. The beam divergence, θ, is given by

$$\theta = \frac{w(z)}{z} = \frac{\lambda}{\pi w_0} \qquad (2.4.5)$$

for values of z greater than Z_R.

2.5 Atmospheric absorption and scatter

A laser beam propagating through the atmosphere suffers attenuation through absorption and scattering. In absorption, energy is lost to the beam and this heats the air. Scattering causes energy to be be diverted from its original direction and redistributed. There are four main

classifications of these effects; molecular absorption and scattering and aerosol absorption and scattering.

The atmospheric transmittance, τ, is defined as

$$\tau \equiv \frac{I(z)}{I_0} = \exp\left\{ \int_0^z \gamma \, dz \right\} \qquad (2.5.1)$$

where z is the range, I_0 is the intensity at z = 0, I(z) is the intensity at z and γ is the total extinction coefficient, given by

$$\gamma = \alpha_m + \alpha_a + \beta_m + \beta_a \, ,$$

where α_m and α_a are the molecular and aerosol absorption coefficients and β_m and β_a are the molecular and aerosol scattering coefficients, respectively.

Molecular absorption and scattering are due to the molecular constituents of the atmosphere. Aerosol absorption and scattering are caused by the colloidal suspension, in air, of solid particles (ice, dust or organic material). Aerosol particle sizes vary from a cluster of a few molecules up to about 20 μm.

2.5.1 Molecular absorption

The molecular absorption of laser radiation in the atmosphere depends critically on the wavelength. Atmospheric absorption is a complicated and irregular function of the wavelength and requires detailed

knowledge of the absorption coefficients of thousands of absorption lines in the vibrational spectra of such gases as H_2O, CO_2, CO, CH_4, N_2O and O_2.

Research completed during the past 20 years has not yet yielded full understanding of all the factors which appear to be involved in molecular absorption. For example, in a recent critical review [1], Grant observed that since 1969, at least 13 measurements of water vapour absorption coefficients in the 8 - 13 μm spectral region have been made. Grant noted considerable disparity between the different water vapour continuum data sets. Agreement between experiment and numerical simulation based on theory is not good. This makes assessment and prediction of the effects of absorption on an atmospheric waveguide difficult. Wherever possible, a range of values of effective absorption coefficients for CO_2 laser radiation will be used, based on an evaluation of published studies.

In the lower atmosphere, the major absorbers for CO_2 laser radiation are water vapour and CO_2. McCoy *et al* [2] give the absorption coefficient due to water vapour as

$$\alpha_H = 4.32 \times 10^{-6} \cdot p \left(P + 193\, p \right) km^{-1}, \qquad (2.5.1.1)$$

where p is the partial pressure of the water vapour in torr and P is the total atmospheric pressure in torr. McCoy measured this absorption in controlled conditions in the laboratory using a specially engineered vapour cell. It was possible to add a known quantity of water vapour to the cell. We eliminate p from Equation (2.5.1.1) by deriving its relation to

parameters which are readily measurable in the real atmosphere; the temperature and relative humidity. The Clausius-Clapeyron Equation can be written

$$\frac{\partial P_s}{\partial T} = \frac{L}{T\,(V_2 - V_1)}\,, \qquad (2.5.1.2)$$

where P_s is the saturation vapour pressure for water (that pressure at which a change of phase occurs at constant temperature), T is the temperature in kelvin, L is the latent heat and V_1 and V_2 are the specific volumes of the liquid and vapour phases, respectively. Under normal atmospheric conditions, V_2 is several orders of magnitude larger than V_1 and we can neglect V_1. If we assume that water vapour behaves as an ideal gas, then we can write

$$pV = R_m T\,, \qquad (2.5.1.3)$$

where R_m is the molar gas constant for a gas with molecular mass M. From Equations (2.5.1.2 and 3) we can write

$$\frac{de_s}{e_s} = \frac{L}{R_{mw}} \cdot \frac{dT}{T^2}\,, \qquad (2.5.1.4)$$

where e_s is, by meteorological convention, the saturation vapour pressure of water. If we assume that L is constant, we can integrate Equation (2.5.1.4) to give

$$\ln e_s = 21.35 - \frac{L}{R_{mw}} \frac{1}{T}\,. \qquad (2.5.1.5)$$

The relative humidity is defined as

$$H = 100 \cdot \frac{e}{e_s}, \qquad (2.5.1.6)$$

where e is the partial vapour pressure. Combining Equations (2.5.1.1, 5 and 6), we can write

$$\left.\begin{aligned} \alpha_H &= 4.32 \times 10^{-6} \cdot e_s \left(P + 193\, e_s \right) \ \text{km}^{-1} \\ \text{where} \quad e_s &= \frac{H}{100} \cdot \exp\left(21.35 - \frac{L}{R_{mw}} \frac{1}{T} \right) \end{aligned}\right\} \qquad (2.5.1.7)$$

The absorption coefficients are calculated and shown in Table 2.2 for a temperature of 25 °C and relative humidities of 10 to 80 per cent. The results of the calculations given by McCoy *et al* are shown for comparison. Graphs of the absorption coefficient for various temperatures and humidities are shown in Figure 2.2.

We now need to consider the part played by CO_2. In the standard atmosphere below about 9 km, Wood *et al* [3] give the following expression for the absorption coefficient due to CO_2;

$$\alpha_C = 1.44 \times 10^2 \left(\frac{295}{T} \right)^{1.5} \exp\left[- \left(\frac{970}{T} \right) \ln 10 \right] \text{km}^{-1}, \qquad (2.5.1.2)$$

where T is the temperature in kelvin. A graph of α_C versus temperature is shown in Figure 2.3.

Relative Humidity (%)	α_H (km^{-1}) from Equation (2.5.1.7)	α_H (km^{-1}) McCoy *et al*
10	0.0127	0.0125
20	0.0352	0.0338
30	0.0673	0.653
40	0.109	0.107
50	0.1605	0.157
60	0.2216	0.215
70	0.2924	0.284
80	0.3729	0.363

Table 2.2 Calculated absorption coefficients for air at 25 °C

The total absortion coefficient, α_{tot}, is given by the sum of the absorption due to water vapour and CO_2. Figure 2.4 is a graph of α_{tot} for a range of temperatures and humidities. This graph shows that the absorption is dominated by α_C at low relative humidities and temperatures. As the relative humidity increases above about 25 per cent, α_H begins to dominate. This result is valid for near horizontal paths up to a few kilometres above sea level.

2.5.2 Scattering

Consider laser radiation of wavelength λ impinging on a scattering centre of radius r_s. If r_s is much smaller than λ, then the radiation will be scattered symmetrically from the scattering centre. This is known as "Rayleigh Scattering" and is due to atoms and molecules.

If r_s is greater than $\frac{\lambda}{10}$ then "Mie Scattering" begins to occur and the radiation becomes preferentially scattered in the forward direction. Mie scattering is due to aerosols and droplets. The forward scattering effect becomes noticeable when r_s is greater than $\frac{\lambda}{4}$. When r_s is greater than λ, extreme forward scattering (which may exhibit lobes) can occur.

If r_s is greater than 10λ then "large particle scatter" occurs and this can be described using the diffraction equations. Scattering from raindrops is an example of this kind of scattering.

The types of particle responsible for atmospheric scattering and typical concentrations are shown in Table 2.3.

Type	Radius (μm)	Concentration (cm^{-3})
air molecules	10^{-4}	10^{19}
haze particles	10^{-2} – 1	10 – 10^{3}
fog droplets, dust	1 – 10	10 – 10^{2}
cloud droplets	1 – 10	10 – 300
raindrops	10^{2} – 10^{4}	10^{-2} – 10^{-5}

Table 2.3 Atmospheric scattering particles

2.6 Atmospheric optical turbulence

Turbulence causes random local fluctuations in the refractive index of the atmosphere. These fluctuations distort the laser wavefront and can cause intensity fluctuations, beam wander and spreading and coherence fluctuations. Optical turbulence causes distant lights and stars to twinkle and objects viewed over hot surfaces (roads in summer, for example) to shimmer.

The refractive index variations are caused by temperature variations which drive the turbulent mixing of the atmosphere. Estimates (Zuev [4]) show that a 1 °C variation in air temperature is accompanied by a refractive index variation of about 10^{-6}. The observed air temperature at a given point can fluctuate over several tenths of a degree during a period of a few milliseconds to several seconds. For a horizontal path in the atmosphere a few kilometres long, the temperature can vary by several degrees.

The primary measure of refractive index fluctuations is called the atmospheric structure parameter, C_n , which is defined by

$$\overline{\left[n(\mathbf{r}_1) - n(\mathbf{r}_2)\right]^2} = C_n^2 r^{2/3} , \qquad (2.6.1)$$

where n is the refractive index and r is the scalar distance between the position vectors $\mathbf{r}_1$ and $\mathbf{r}_2$. The atmospheric structure parameter is not measured directly, but is derived from sensitive temperature probe measurements made at the site of interest.

Close to the ground in the surface layer, optical turbulence is influenced by the aerodynamic roughness of the surface and temperature gradients due to surface heating and radiative cooling. In the planetary boundary layer, the sources of the energy driving the turbulence are wind shear and the buoyancy due to temperature gradients.

The transition from laminar flow to turbulent mixing happens at a critical value of the Reynolds number

$$Re = \frac{vL}{\upsilon} , \qquad (2.6.2)$$

where v is a characteristic velocity, L is a characteristic scale length for the flow process and υ is the viscosity. In the atmosphere, turbulent air forms a cascade of vortices or eddies ("turbules") which diminish in diameter. The size of the largest eddies, L_o, is determined by the scale of the parent flow. Under the influence of inertial forces the large eddies

break up into smaller ones. This cascade process continues until the Reynolds numbers are close to unity. At this stage, viscous forces dominate and the smallest sustainable eddy diameter, l_0 is reached. The diameters L_0 and l_0 are known as the "outer-" and "inner-scales of turbulence", respectively. The value of L_0 close to the ground is of the order of the height of the point of observation. The value of l_0 close to the ground ranges from 1 - 10 mm.

We now have the three factors necessary to describe the turbulence regime of interest. There are two cases to consider; eddies larger than the beam diameter and eddies smaller than the beam diameter.

Eddies larger than the laser beam diameter ($L < 2w$) cause beam wander (Figure 2.5). Churnside *et al* [5] derive an expression for the variance of the beam displacement for a collimated beam as

$$\sigma_c^2 = 0.97\, C_n^2\, D^{-1/3}\, L^3 \qquad (2.6.3)$$

where D is the diameter of the transmitting aperture and L is the path length. This result is valid for $\sqrt{\lambda L}$, $\lambda L/\rho_0 \ll D \ll L_0$ where ρ_0 is the spherical coherence diameter. For a CO_2 laser, with $C_n^2 = 10^{-13}$ (strong turbulence), D = 0.1m and L = 10 km, the variance of the beam displacement is less than 1cm.

The second case to consider is when the eddies are smaller than the beam (Figure 2.6). If $l \ll \sqrt{\lambda L}$ then the eddies act as scattering centres causing Rayleigh scattering and consequent beam spreading. When $l \approx \sqrt{\lambda L}$ Rayleigh scattering still occurs, but coherence is maintained between the main beam and the scattered radiation. The two "beams"

interfere producing fringes. The fringes modulate the heating of the air and generate in-phase refractive index patterns. The main beam is scattered by the index variations, transferring more energy to the weak beam further along the path. The weak beam is "amplified" producing scintillations along the beam path. These scintillations can grow as more and more energy is transferred from the main beam. This process is called "Stimulated Thermal Rayleigh Scattering" ("STRS") and is an example of "Turbulence Thermal Blooming Interaction" ("TTBI"). The effect of STRS is to degrade the quality and coherence of the beam. In guiding applications STRS may actually help in the formation of the waveguide because heat is still transferred to the air.

2.7 Thermal blooming

2.7.1 Qualitative treatment

It was noted in Section 2.5 that energy removed from a laser beam by absorption results in heating of the propagation medium. The resulting density decrease in the medium creates a lower refractive index in the beam path. The gradient of the index causes the laser beam to be refracted towards the outer region of higher index. This is known as thermal blooming because of the resulting appearance of the beam observed in early experiments. The amount of temperature rise is dictated by the residence time of a "parcel" of air as it crosses the beam due either to the wind or to transverse movement of the beam (known as "slewing"). Density and temperature profiles and resulting beam bending are shown schematically in Figure 2.7. The blooming pattern is generated by a combination of two effects; radial outward bending by

the thermal lens effect and ray bending towards the cooler (upwind) region. These effects result in the crescent-shaped irradiance profiles typical of thermal blooming and shown in wave-optics simulations and experiments due to Gebhardt [6] and reproduced in Figure 2.8.

2.7.2 History and developments

Thermal blooming was first reported by Leite, Moore, and Whinnery of Bell Laboratories in 1964 [7]. They were attempting to measure Raman scattering in liquids by placing a liquid-filled cell inside a HeNe laser cavity. They noticed changes in the absorbency of the liquid caused by heating. They went on to investigate the effect and found a transient power density change. The laser output increased to some peak and was then reduced due to thermal defocussing caused by a thermal lens generated by thermal blooming.

In 1966, Rieckhoff [8] reported a "new" non-linear effect in the propagation of light through an absorbing liquid placed outside a laser cavity. Rieckhoff's experiments showed the non-linear dependence of the relative beam diameter on laser power. Leite *et al* responded [9] with a paper claiming priority and proposing the thermal lens effect as a power limiting device for a cw argon ion laser.

The first Soviet publication was in 1967 by Akhmanov *et al* [10] who reported a theoretical and experimental investigation of non-linear defocussing of a cw laser beam in water. They reported the observation of a "steady-state" condition and developed a linear hydrodynamic model to explain this. A second Soviet paper by Raizer [11] provided further

theoretical work based on geometric optics and ray tracing to model self focussing and defocusing in weakly absorbing media.

Callen *et al* [12] reported experiments on the time-development of thermal blooming of a gaussian beam which formed into a series of concentric annuli. Six years later, Ulrich [13] accounted for these results using a self-consistent non-linear numerical analysis.

The first observations of thermal blooming caused by a CO_2 laser beam in liquids were made by Inaba *et al* in 1968 [14]. They noted power dependent effects and recorded the characteristic crescent shaped patterns on Kalvar film.

During the late sixties and early seventies, there was a steady flow of publications reporting thermal blooming investigations. Most of the work was conducted in the USA, with some contributions from the USSR. In 1969, Gebhardt and Smith published an important paper which introduced the idea of a "distortion number" [15]. A distortion number is a dimension-less combination of the physical parameters of the problem such as beam power, absorption coefficient, range, wind speed and beam radius. These parameters were to become useful in the development of "scaling laws" to model and compare the performances of competing laser systems.

Soviet investigators published a number of papers relevant to this thesis. In about 1971, Soviet publication in the open literature ceased. The final Soviet paper, by Askar'yan and Pogosyan [16] discussed the focussing of a visible laser beam by the "thermal track" of an annular beam from a Nd YAG laser. The lasers were aligned co-axially and the experiments

were conducted in water or plexiglass. It was not until 1981 that another Soviet paper by Askar'yan and Mukhadamovich was published [17]. This paper discusses the suppression of the small scale effects of thermal blooming by rocking, shaking or rotating the laser.

In 1972, a number of investigators (for example Hayes, Ulrich and Aitken [18]) began to publish the results of wave-optics codes used to analyse the thermal blooming effect in the atmosphere. No experiments involving the propagation of laser radiation in the uncontrolled atmosphere were reported in the open literature.

As a result of the work done mainly at the US Air Force Weapons Laboratory in the sixties and seventies, it became apparent that laser technology could not form the basis for a mobile weapons system capable of damaging mission targets. The energies required to be focussed at a target necessitated very large, heavy systems which needed clean environments and intensive technical support. Even if systems could have been miniaturised and made rugged enough to cope with difficult environments, thermal blooming provided insurmountable difficulties in targeting and focussing. Since that time, laser technology has provided the key components for sophisticated target designation and ranging systems.

The field of thermal blooming studies gained increased importance due to the Strategic Defense Initiative ("SDI"). In July 1987, the American Physical Society published a report on the science and technology of directed energy weapons ("DEW") [19]. This report highlighted thermal blooming as a major concern in the development of DEW systems and concluded that "A major effort under realistic field conditions is

necessary before any substantial commitment to ground-based laser systems can be made...the ability to provide atmospheric compensation of high intensity laser beams is important, yet problematic.".

Significant research programs were under way in the USA but little has so far been published. However, in January 1989, at the SPIE conference, T J Karr of the Lawrence Livermore National Laboratory gave an invited paper on "Thermal Blooming Compensation Instabilities" [20] This paper described numerical simulations of a 50 kW CO_2 laser beam propagating over ranges of 0.3 - 3 km. The results presented were described as "preliminary and tentative" but showed intense beam break-up due to thermal blooming only 0.3 s after the beam is turned on.

2.7.3 Thermal blooming threshold conditions;

In this section we present an order of magnitude estimate of thermal blooming in an ideal gas.

Consider an unfocussed laser beam of total power, P, being emitted from an aperture of radius, a, into air at atmospheric pressure. It is assumed that the beam has an intensity distribution which has a maximum on the beam axis and falls to zero at radius a. The number, N, of wavelengths of the radiation contained in a path of length L can be written

$$N = \frac{nL}{\lambda}, \qquad (2.7.3.1)$$

where n is the refractive index and λ is the atmospheric wavelength of the laser radiation. After the beam is turned on, the refractive index will vary with time because of the heating of the air produced by the absorption of energy from the beam. The variation in N is given by

$$\Delta N = \frac{L}{\lambda} \delta n. \qquad (2.7.3.2)$$

For air, over a wide range of values of temperature, pressure and electric field, n can be written as

$$(n-1) = k\rho, \qquad (2.7.3.3)$$

where ρ is the density and k is the Gladstone-Dale constant. Under standard conditions, $(n-1) \approx 3 \times 10^{-4}$. If the density varies by a small amount , $\delta\rho$, the corresponding change in the refractive index can be obtained from Equation (2.7.3.3) as

$$\frac{\delta(n-1)}{n_o - 1} = \frac{\delta\rho}{\rho_o} \equiv s \ , \qquad (2.7.3.4)$$

where n_o and ρ_o are the values of the refractive index and density just before the laser beam is switched on. Equation (2.7.3.4) can be rewritten as

$$\delta n = (n_o - 1)\, s. \qquad (2.7.3.5)$$

As energy from the laser beam is absorbed by the atmosphere, the value of s changes. The equation of state is

$$pV = m R T, \tag{2.7.3.6}$$

where p is the pressure, V is the volume occupied by m mole of gas, T is the absolute temperature, and R is the universal gas constant. From the equation of state, we can obtain the thermal expansion coefficient , β, defined by

$$\beta = -\frac{1}{V}\left(\frac{\partial V}{\partial T}\right)_P = \frac{1}{T}. \tag{2.7.3.7}$$

Finally, we must consider the temperature rise when heating at constant pressure. If γ is the ratio of molar specific heats C_P and C_V, then we have

$$C_P = \frac{\gamma}{\gamma - 1} R. \tag{2.7.3.8}$$

If we slowly add a small amount of heat dQ per mole to the gas and assume that it is free to expand at constant pressure, then from Equations (2.7.3.7 and 8) we find

$$\frac{d\rho}{\rho} = -\frac{dV}{V} = -\beta \frac{dQ}{C_P} = -\frac{\gamma - 1}{\gamma RT} dQ. \tag{2.7.3.9}$$

Rewriting the differentials $d\rho$ and dQ in terms of the small quantities s and q_v we have

$$\frac{d\rho}{\rho} = s \text{ and } dQ = \frac{RT}{p_o} q_v, \tag{2.7.3.10}$$

where p_o is the ambient pressure and q_v is the heat energy deposited per unit volume.

We can relate q_v and the beam intensity, I, as follows

$$q_v = \alpha I t_o, \qquad (2.7.3.11)$$

where α is the atmospheric absorption coefficient at the laser wavelength and t_o is the heating time. Combining Equations (2.7.3.7 - 11) we obtain the value of s at an arbitrary range, r, in the beam after heating for a time t_o;

$$s(r) = -\frac{\gamma - 1}{P_0 \gamma} \alpha I(r) t_o . \qquad (2.7.3.12)$$

In deriving this equation, we have assumed that there is no air movement through the beam and that the intensity remains constant at radius r throughout the heating time. The main sources of air movement are wind, turbulence and convection. The most significant of these will be wind.

We can attempt to estimate the effect of wind if we imagine a wind moving with velocity, v, normal to the propagation axis. The rate at which heat is absorbed from the laser beam will depend on the intensity distribution across the beam. In order to obtain an order of magnitude estimate of the value of s including wind effects, we shall set I(r) equal to the peak intensity and note that we have

$$t_o = \frac{a}{v}, \qquad (2.7.3.13)$$

where a is the radius of the beam.

From Equations (2.7.3.2, 5, 12, 13) we obtain

$$\Delta N = -(n_o - 1)\frac{L}{\lambda}\frac{\gamma - 1}{\gamma p_o}\alpha I_o \frac{a}{v}, \qquad (2.7.3.14)$$

where I_o is the peak beam intensity. Note that as $v \rightarrow 0$, ΔN becomes very large. This corresponds to the formation of a "stagnation zone" where the beam encounters a region of still air. The still air is not cleared from the beam until convection occurs. Significant changes in the refractive index of the air can occur and these may completely disrupt the beam, causing gross aberrations and severe transmission loss.

We now assign a path length, L. In order to obtain an estimate of the lowest power level at which thermal blooming could happen, we choose L to be large. The choice we make is

$$L \approx \frac{(2a)^2}{\lambda} . \qquad (2.7.3.15)$$

This path length is the Rayleigh range. The total beam power and the on-axis intensity may be related by the equation

$$P \approx \pi a^2 I_o. \qquad (2.7.3.16)$$

If we now combine Equations (2.7.3.14 - 16) and set $\delta N = -1$, we obtain an expression for the onset of thermal blooming in a transverse flow

$$P_t = \frac{\pi}{4} \frac{\gamma p_o}{\gamma - 1} \frac{1}{\alpha (n_o - 1)} \frac{\lambda^2 v}{a}. \qquad (2.7.3.17)$$

In setting $\delta N = -1$, we are assuming that a phase change of one wavelength is characteristic of thermal blooming (Aitken *et al* [21]). We can now find a value for P_t, for a laser beam of wavelength 10 μm, noting that the constants have the following values;

$$p_o = 10^5 \text{ Nm}^{-2}, \qquad n_o = 3 \times 10^{-4},$$
$$\gamma = 1.4, \qquad \lambda = 10^{-5} \text{ m}$$

and we find that the threshold power is

$$P_t = 0.1 \frac{v}{\alpha a} \text{ W}. \qquad (2.7.3.18)$$

With the following values

$$\left.\begin{aligned} \alpha &= 3 \times 10^{-3} \text{ m}^{-1} \\ a &= 10^{-2} \text{ m} \\ v &= 0.3 \text{ ms}^{-1} \end{aligned}\right\} \qquad (2.7.3.19)$$

substituted into Equation (2.7.3.18), we find that the threshold for thermal blooming in air is 1 kW. The choices for α and a represent a CO_2 laser beam of 10.6 μm propagating in air at atmospheric pressure. We can see that thermal blooming can occur at fairly low power levels. The Rayleigh range for this example is about 40 m. At the Rayleigh range, the beam has been attenuated by approximately 13 per cent.

The temperature change associated with this example can be estimated from the equation

$$\frac{\delta T}{T} = -\frac{\delta \rho}{\rho} = -s \qquad (2.7.3.20)$$

This equation is for an ideal gas at constant pressure. The values of s and δT are -9.1×10^{-4} and 0.27 K, respectively. This temperature change is comparable with that produced by random atmospheric turbulence which will produce positive and negative refractive index changes along the beam path. We can therefore expect some net cancellation of the effects of turbulence. The refractive index changes produced by the laser beam will have the same sign along the entire length of the beam and for a cw laser or a pulsed laser with a high enough repetition rate, a cumulative effect is expected.

2.7.4 Extension to annular beams and guiding

We have shown that thermal blooming can occur at fairly low power levels We now need to extend this work to cover annular beams and, in particular, to estimate the powers at which we might expect to produce a guiding effect.

An annular laser beam propagating in air will produce a tube of heated air. By analogy with a step-index optical fibre, the centre of the tube, "the core", will be at ambient temperature and will be surrounded by a region of heated air, "the cladding". Electromagnetic waves injected into the core will be guided providing that they strike the cladding at angles less than the critical angle for the wave guide, given by

$$n = \sin \theta_c \,, \qquad (2.7.4.1)$$

where n is the refractive index of the cladding and θ_c is the critical angle. For an annular beam, we shall assume

$$P_a \approx \pi \left(r_2 - r_1 \right)^2 I_o , \qquad (2.7.4.2)$$

where P_a is the power of the annular beam and r_1 and r_2 are the inner and outer radii of the annulus, respectively. From Equations (2.7.3.5, 12, 13) and Equation (2.7.4.2) we obtain

$$\delta n = -(n_o - 1) \frac{\gamma - 1}{\gamma \rho_o} \alpha \frac{P_a}{\pi \left(r_2 - r_1 \right)^2} \frac{a}{v} . \qquad (2.7.4.3)$$

Notice that this equation appears to be independent of the wavelength of the radiation used to form the guide. However, the absorption coefficient, α, is very wavelength dependent. The absorption coefficient will also depend on the environmental conditions experienced by the beam (such as fog, rain or smoke). If we substitute for the constants and set $a = r_2$, we find

$$\delta n = 8.6 \times 10^{-10} \frac{\alpha P_a}{\pi \left(r_2 - r_1 \right)^2} \frac{r_2}{v} . \qquad (2.7.4.4)$$

With the following data,

$$\left.\begin{aligned} \alpha &= 3 \times 10^{-3}\ \mathrm{m}^{-1} \\ v &= 0.3\ \mathrm{ms}^{-1} \\ r_1 &= 0.02\ \mathrm{m} \\ r_2 &= 0.03\ \mathrm{m} \end{aligned}\right\} \qquad (2.7.4.5)$$

we find

$$\delta n = 8.2 \times 10^{-10} P_a. \qquad (2.7.4.6)$$

If the angle a core ray makes with the propagation axis of the laser beam is ϕ, then we can write,

$$\phi = 90 - \theta_c \qquad (2.7.4.7)$$

for guiding. If we assume that we can align the waveguide and the beam to be guided to an accuracy of 3 mrad, then we can derive the laser beam power required to produce the necessary refractive index change. We again consider a laser beam of wavelength 10.6 μm propagating in a region with transverse flow conditions and use the same parameters used in Section 2.7.3. The critical angle in this case is 89.83° and to achieve guiding, the laser must produce an index change of 4×10^{-6}. If this value is used for δn in Equation (2.7.4.6), then we find that the beam power required is 4.88 kW, about five times the calculated threshold value.

The numerical aperture, $\mathcal{N}$, for the annular waveguide is given by

$$\mathcal{N} = \sqrt{2\, n\, \delta n}\ . \qquad (2.7.4.8)$$

For this example, $\mathcal{N} \approx 0.003$. We note that optical fibres typically have numerical apertures in the range 0.1 - 0.2.

The calculations outlined in Sections 2.7.3 and 4 provide an order of magnitude estimate of the thermal blooming effect and show that refractive index changes large enough to produce a useful waveguide may be achieved with existing laser sources.

FIGURES FOR CHAPTER 2

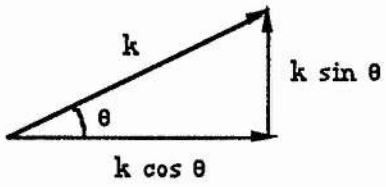

Figure 2.1 Axial and transverse components

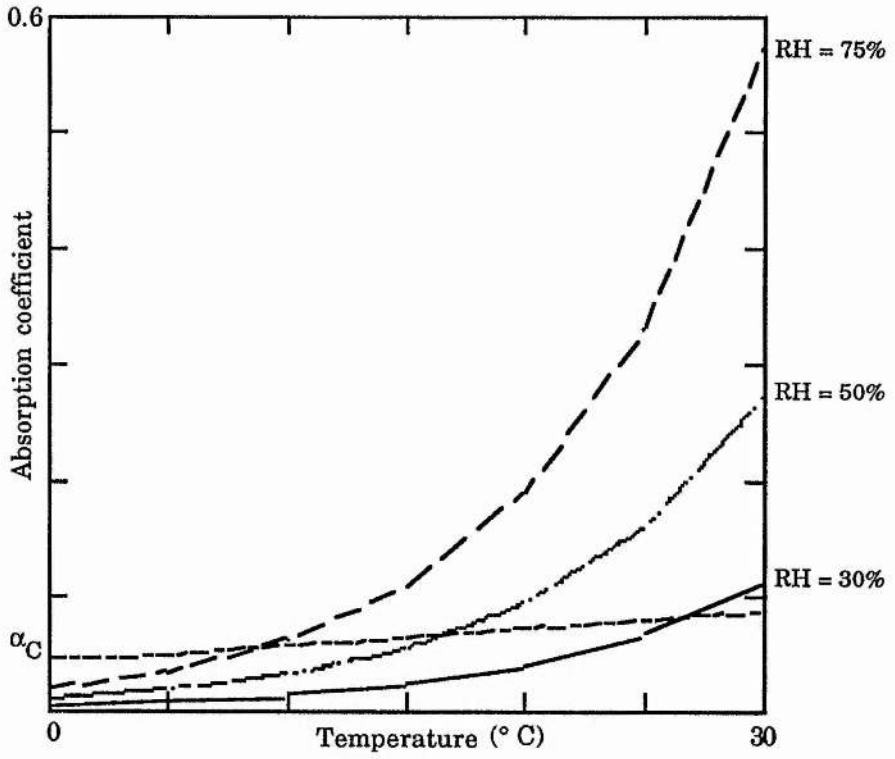

Figure 2.2 Absorption coefficients (per km) due to water vapour and CO_2 (α_C) for a range of temperatures and humidities

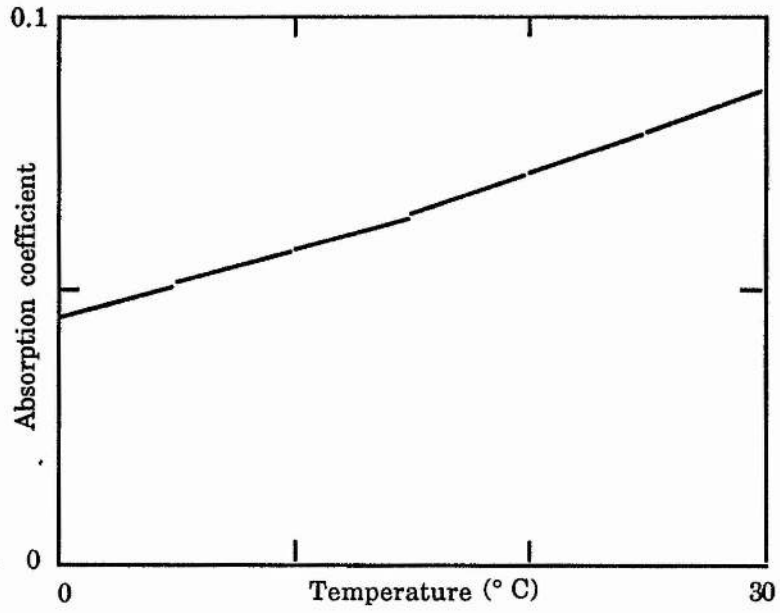

Figure 2.3 Absorption coefficient (per km) for CO_2

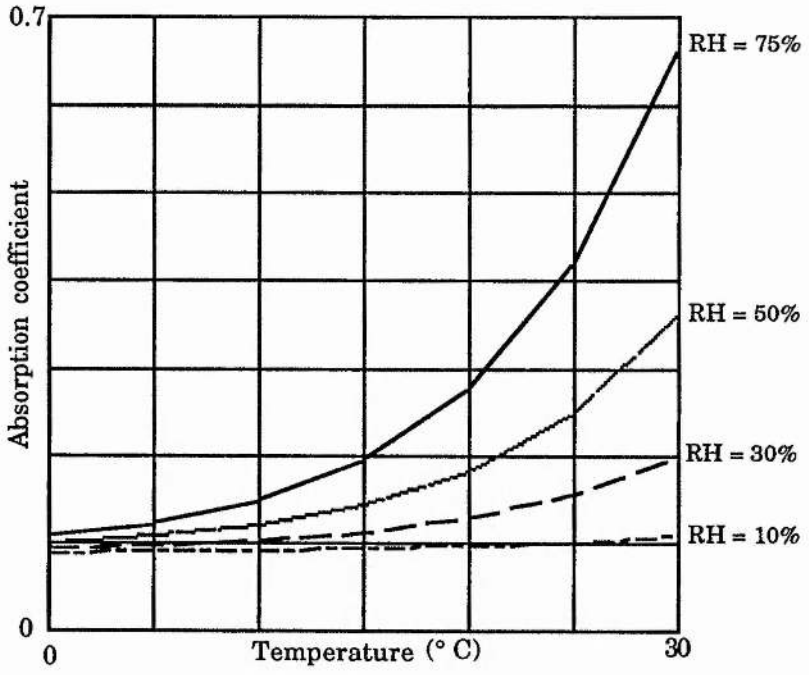

Figure 2.4 Total absorption coefficient (per km)

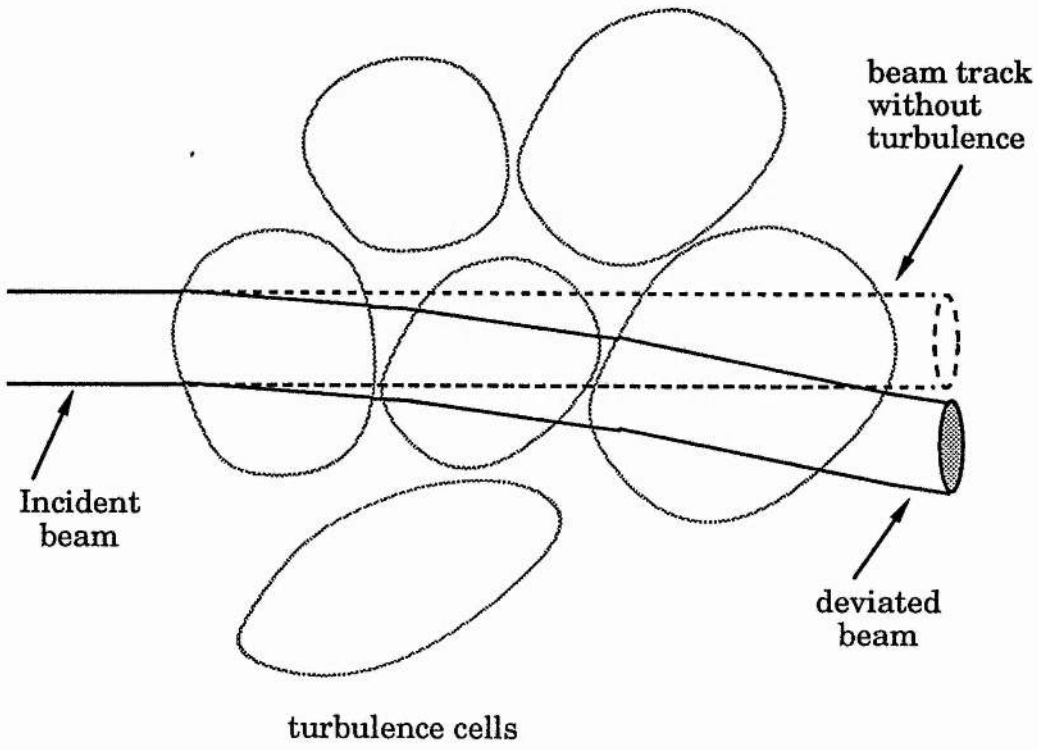

Figure 2.5 The effect of eddies larger than the beam diameter

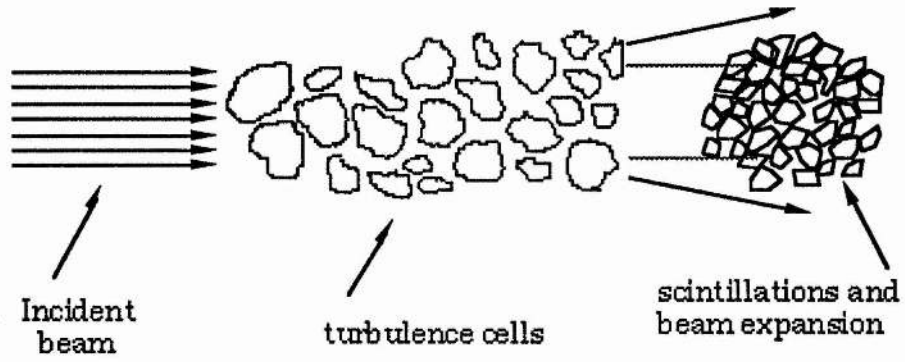

Figure 2.6 The effect of eddies smaller than the beam diameter

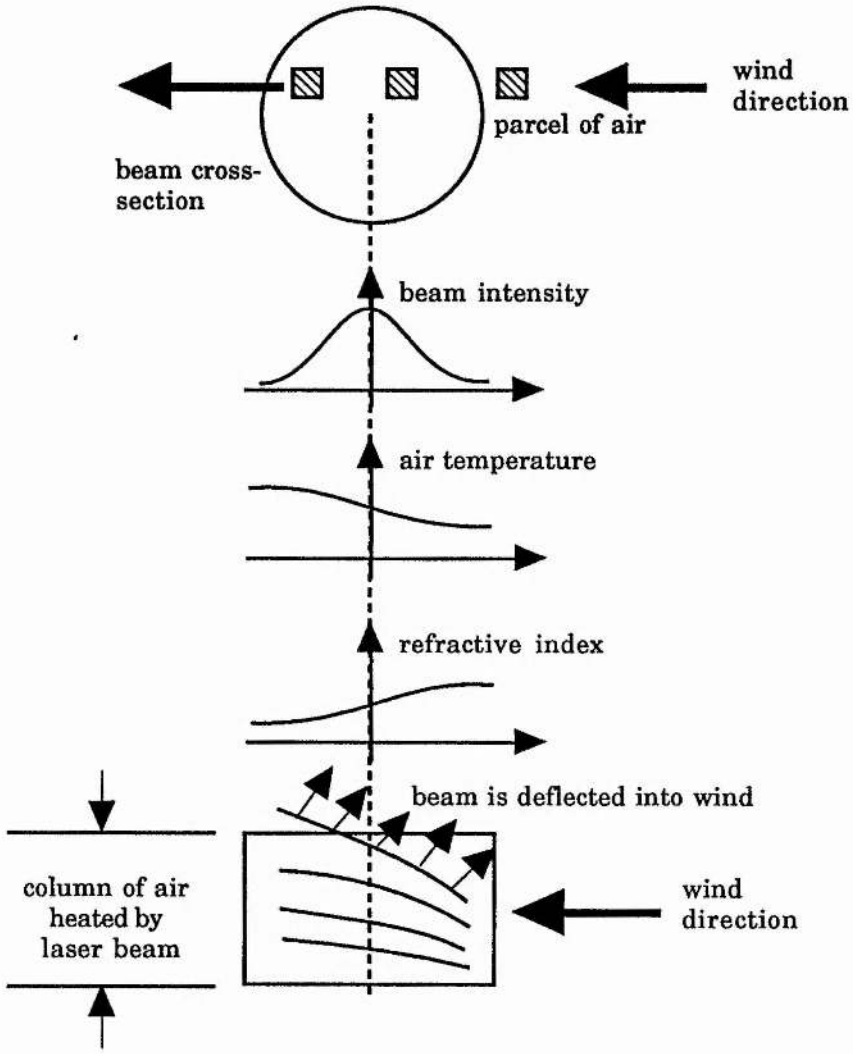

Figure 2.7 Deflection of a high power laser beam by the wind

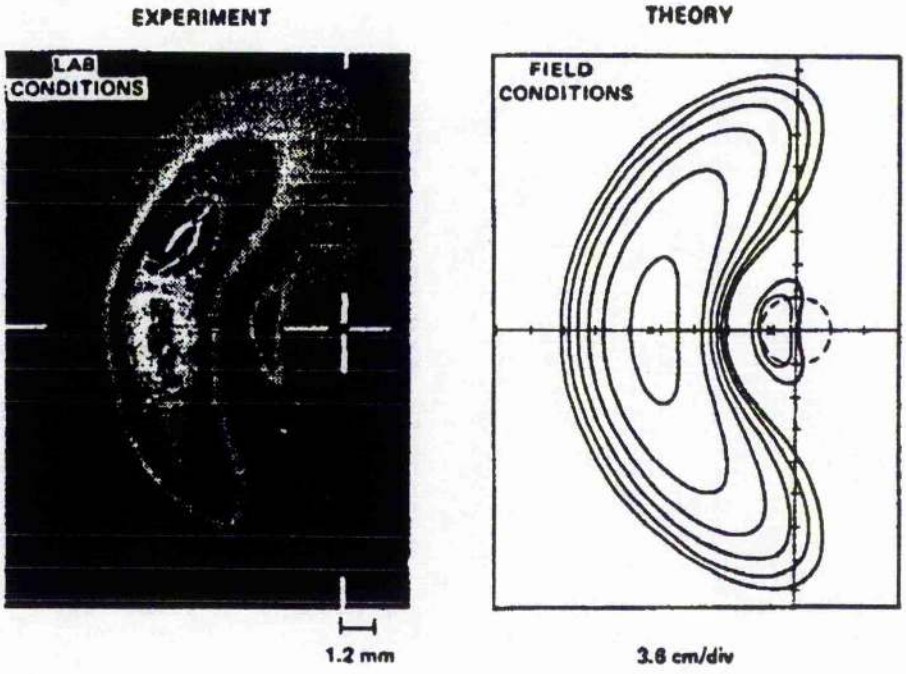

Figure 2.8 Thermal blooming patterns given by Gebhardt [6]

REFERENCES FOR CHAPTER 2

1 Grant W B, Applied Optics, **29**, No 4, p451, February 1990

2 McCoy J H, Rensch D B and Long R K, Applied Optics, **8**, No 7, p 1471, July 1969

3 Wood A D, Camac M and Gerry E T, Applied Optics, **10**, No 8, p 1877, August 1971

4 Zuev V E, "Laser Beams in the Atmosphere" published by Consultants Bureau, New York (1982)

5 Churnside J H and Lataitis R J Applied Optics, **29**, No 7, p 926, 1 March 1990

6 Gebhardt F G, Applied Optics, 15, No 6, p 1479 (1976)

7 Leite R C C, Moore R S, and Whinnery J R, Applied Physics Letters **22**, No 3, p129 (1964)

8 Rieckhoff K E, Applied Physics Letters **9**, No 2, p 87 (1966)

9 Leite R C C, Porto S P S and Damen T C, Applied Physics Letters **10**, No 3, p100 (1967)

10 Akhmanov S A, Krindach D P Sukorukov A P and Khoklov, JETP Letters **6**, No 2, p39 (1967)

11 Raizer Yu P, Soviet Physics JETP **25**, No 2, p470 (1967)

12 Callen W R, Huth B G and Pantell R H, Applied Physics Letters **11**, No 3, p103 (1967)

13 Ulrich P B, Journal of the Optical Society of America **63**, No 7, p897 (1973)

14 Inaba H and Ito H, IEEE Journal of Quantum Electronics **QE-4**, p45 (1968)

15 Gebhardt F G and Smith D C, Applied Physics Letters **14**, No 2 p52 (1969)

16 Askar'yan G A and Pogosyan, Soviet Physics JETP **33**, p700 (1971)

17 Askar'yan G A and Mukhamadzhanov M A, Soviet Physics Technical Physics, **26** No 9, p1163 (1981)

18 Hayes J N, Ulrich P B and Aitken A H, Applied Optics **11**, No 2 p257 (1972)

19 "Report to the American Physical Society of the study group on science and technology of directed energy weapons", Reviews of Modern Physics **59**, No 3, Part II (1987)

20 Karr T J, "Propagation of High Energy Laser Beams through the Earth's Atmosphere", Peter B Ulrich, Leroy E Wilson Editors, Proc SPIE 1221, pp26 - 55, (1990)

21 Aitken A H, Hayes J N and Ulrich P B, Applied Optics **12**, p193 (1973)

3 WAVEGUIDE FORMATION AND PERFORMANCE

3.1 Introduction

In this Chapter, ways of producing annular laser beams are reviewed, and new ideas described. Using the material and methods introduced in Chapter 2, the interaction of an annular beam with a blooming medium will be further developed. This will enable the formation of the guide to be modelled. Once formed, the radiation to be guided must be coupled into the guide. We shall examine the types of radiation that may be guided and evaluate the performance of the guide.

3.2 Annular laser beams

Annular laser beams can be produced in three main ways;

- beams of the TEM_{01}^{*}, or "doughnut" mode
- beams from unstable cavities
- beams produced by specially designed instruments containing mirrors and axicons or other beam splitting elements

We shall examine these methods and evaluate them with our application in mind.

3.2.1 The doughnut mode

In 1981, Newman and Smith [1] proposed the use of the TEM_{01}^{*} stable resonator mode for guiding a weaker laser beam. A subsequent paper by Hauser and Davis [2] provided a theoretical study of the induced refractive index changes based on the concept of an instantaneous heat source in the zero wind case. They concluded that channel formation was feasible provided that the main beam was less than half the intensity of the channel forming beam.

In most practical laser systems, the doughnut mode is a linear combination of the TEM_{10} and TEM_{01} Hermite Gaussian modes (Siegman [3], Maitland and Dunn[4]). These modes oscillate separately and independently, with slightly different oscillation frequencies because of the astigmatism introduced by the Brewster-angled windows in the laser. The time-averaged total power is then circularly symmetric about the axis (Figure 3.1).

The doughnut mode can be described using the following equation

$$I(r) = \frac{r^2}{w^2} \exp\left(-\frac{2r^2}{w^2}\right), \qquad (3.2.1.1)$$

where I is the beam intensity at radial distance r and w is the spot size. A surface plot of Equation (3.2.1.1) and a transverse beam profile, obtained by setting r equal to x, are shown in Figures 3.2 and 3.3.

The doughnut mode initially appeared to be an attractive solution for waveguide generation because this mode maintains its profile as it propagates. In Section 3.3, we shall consider this further.

Examination of the beam profiles in Figures 3.2 and 3.3 raises a number of major practical difficulties, as follows:

- The desired size of the clear aperture dictates the size of the laser output aperture. For large systems, this would require very large (and therefore expensive) optics. The high masses involved could also lead to problems in applications where rapid tracking and pointing were required;

- lack of control of the beam profile parameters such as the ratio between waveguide "wall thickness" (spot size) and clear aperture; and

- inefficient use of the gain volume in the laser cavity.

For some applications, it may be possible to use lasers operating so as to produce the doughnut mode and the performance of this beam profile will be examined below.

3.2.2 Beams from unstable resonators

Unstable resonators can produce annular beams in the near field. Unfortunately, within a very short distance (in the Fresnel zone) from the output mirror, the near field pattern develops a strong but small

"spot of Arago" in the centre of the annulus. In high power systems, this spot is powerful enough to cause optical damage.

The far field pattern (Fraunhofer diffraction) has a central lobe on axis, surrounded by side lobes (diffraction rings) of decreasing amplitude. The angular width of the central lobe will correspond to the diffraction-limited far field pattern for a slit or circular aperture corresponding to the diameter of the near field pattern.

Despite the many advantages of unstable resonators for producing high powers it is not considered feasible to implement waveguide structures in this way.

3.2.3 Annular beam convertors

We now consider the design of beam convertors intended to turn a "solid" laser beam (normally Gaussian in profile) into an annular beam. A proposed design for an annular beam convertor is shown in Figure 3.4. A gaussian input beam is directed onto a conical element (1) (known as an "axicon"). In this design, the axicon is mounted on three wire supports (or "spider") but it could be mounted on a transparent optical flat made of Zinc Selenide or Germanium. The beam is split by the axicon and captured by a circular angled reflector. The reflecting surfaces are diamond turned copper with gold coatings. The resulting beam has the required annular profile.

An off-axis design is shown schematically in Figure 3.5. The "solid" input beam impinges on a circular conical mirror/splitter (1). The

resulting beam is directed onto an annular mirror (2) which corrects the distortions introduced by mirror (1). The output beam has the required annular profile. This design has the advantage that the microwave feed horn does not block the beam.

3.2.4 Other methods of waveguide generation

We have devised several other ways of generating the waveguide and these will be covered briefly here.

3.2.4.1 Multiple diverging beams

An atmospheric waveguide generated by multiple diverging beams is shown in Figures 3.6 and 7. Several "solid" (Gaussian) beams are propagated. As the range increases, the laser beams spread due to their divergence and the waveguide begins to form. The distance at which the waveguide begins to form could be chosen by altering the output divergence of the laser beams or changing the pointing angle of the laser beams. In another possible implementation of this idea (Figure 3.8), the direction of pointing of the laser output is chosen so that the laser beams are focussed at, or some distance behind, the target. This may have the effect of "focussing" the microwave energy. There are two obvious problems with this idea;

- as the inner aperture of the waveguide narrows, we might expect increased leakage of the radiation to be guided

- if the laser intensity is high, then focussing the beams may produce severe non-linear effects and beam break-up. We could, perhaps, avoid this problem by making sure that the beam foci are well beyond the target.

3.2.4.2 Rotating mirror waveguide generator

The waveguide is generated by a rapidly rotating beam steering mirror arrangement (shown in Figure 3.9). This could be a practical way of producing small diameter (2-3 cm) waveguides for very high frequency operation. The beam is scanned, tracing out a Lissajous figure which forms the walls of the waveguide. The scan rotation rate must be high enough to compenste for the effects of cooling or beam clearing by wind.

3.3 Annular beam structure

We now consider the propagation of an annular beam where the axis of propagation of the radiation to be guided and the axis of propagation of the annulus are aligned so that the angle between them is equal to the divergence angle of the annular beam. This arrangement is shown in Figure 3.10.

For a collimated Gaussian beam with intensity I, we can write

$$I = I_o \exp\left(-\frac{y^2}{w^2}\right) \qquad (3.3.1)$$

where y is the transverse beam coordinate normal to the propagation axis, z and w is the beam radius at z = 0. From Figure 3.10, we can write

$$\left.\begin{aligned} I_1 &= I_{o_1} \exp\left(-\frac{y_1^2}{w^2}\right) \\ z_1 &= \frac{z}{\cos\theta} \\ y_1 &= \frac{y}{\cos\theta} + a\,. \end{aligned}\right\} \qquad (3.3.2)$$

From Equation (3.3.1 and 2) we find

$$I_1 = I_{o_1} \exp - \frac{\left(\frac{y}{\cos\theta} + a\right)^2}{w^2}, \qquad (3.3.3)$$

where I_1 is the intensity along the axis z_1 and I_{o_1} is the initial intensity for that axis. I_2 is a reflection of I_1 in the z axis and so we can write

$$I_2 = I_{o_2} \exp - \frac{\left(\frac{y}{\cos\theta} - a\right)^2}{w^2}. \qquad (3.3.4)$$

I, the total beam intensity, is the sum of Equation (3.3.3 and 4) and, after expanding brackets and simplifying, is given by

$$I = I_o \exp - \left[\frac{\left(\frac{y^2}{\cos^2 \theta} + a \right)^2}{w^2} \right] . \cosh\left(2a . \frac{y}{w^2 \cos \theta} \right) \quad (3.3.5)$$

The spot size w is given by Equation (2.4.3);

$$w(z) = w_o \left\{ 1 + \left(\frac{\lambda z}{\pi w_o^2} \right)^2 \right\}^{\frac{1}{2}} \quad (2.4.3)$$

Equation (3.3.5) gives the beam intensity on the y axis for a thin "slice" through the beam. The beam is initially symmetrical about the z axis and we now replace y with r, where $r^2 = x^2 + y^2$. This, combined with Equation (2.4.3) enables us to calculate the beam profile in the x,y plane normal to the propagation axis, z. A surface plot of the beam profile and a graph of Equation (3.3.5) for realistic beam parameters are shown in Figures 3.11 and 3.12. Surface plots for various ranges are shown in Figure 3.13. These figures show the performance of the annular beam in the case where only the effect of beam divergence is included. We can see that as the range (z) increases the central aperture begins to fill as the wall spot size (w) increases. The central aperture is very well defined at 100m and remains reasonably well defined until about 350m from the output aperture. By the time the range has increased to 500m, the clear aperture has completely filled in. So despite our efforts to maintain a clear aperture at long range, we find that the gaussian beam wave nature of the laser beam eventually dominates. We could perhaps overcome this aperture-filling problem by arranging to angle the beams at larger angles.

3.4 Formation of the guide

We now consider the mechanisms which lead to the formation of the guide in more detail. The waveguide is formed by the interaction of the E-field of the beam with the atmosphere. The energy absorbed by the air molecules appears as heat. In the case of a CO_2 laser, absorption of 10.6 μm radiation produces vibrational transitions, increasing the vibrational energy of the atmospheric gases. This energy is internal but the subsequent relaxation processes, particularly those of water molecules, are so rapid that energy transfer into translational energy occurs essentially instantaneously. The temperature increase produces a density change and therefore a refractive index change. Subsequent portions of the laser beam encounter the changes in refractive index and the beam "blooms".

The traditional approach to modelling the problem of propagation in a blooming medium is to note the "smallness" of the absorption coefficient, to treat the refractive index changes as a perturbation and to linearize the thermal blooming relations in an attempt to make the problem tractable. This approach is adopted by the authors cited in Section 1.3. The linearized theory is valid so long as the beam perturbations and the refractive index changes are small. This means that the linear theory is applicable only until there is thermal blooming. We know that for many laser wavelengths, absorption coefficients are often greater than 30 per cent per kilometre and that beam break-up and bending can occur. The use of linearized theory in these circumstances is questionable. Much use is made of numerical techniques in modelling thermal blooming but these generally begin with the linearized Equation (see for example Karr [5]).

We shall develop a new approach to the thermal blooming problem, providing a rigourous derivation of the thermal blooming wave equation. Major steps in the derivation will be included but algebra will be omitted. We recall Equation (2.2.7) and (2.2.8) rewritten as follows

$$\left[\nabla^2 + k^2 n^2\right] u(x, y, z)\, e^{-iknz} = 0 \,. \tag{3.4.1}$$

Where we shall treat $n = n(x,y,z)$ as a full variable and u is a vector component of the E field. Dropping the vector notation and expanding (3.4.1) we obtain

$$\left.\frac{\partial^2 \phi}{\partial x^2}\right|_{yz} + \left.\frac{\partial^2 \phi}{\partial y^2}\right|_{xz} + \left.\frac{\partial^2 \phi}{\partial z^2}\right|_{xy} + k^2 n^2 \phi = 0 \tag{3.4.2}$$

where we have

$$\phi \equiv u \,.\, \psi \quad \text{and} \quad \psi \equiv e^{-iknz} \,. \tag{3.4.3}$$

The first term in Equation (3.4.2) can be written as follows

$$\frac{\partial^2 \phi}{\partial x^2} = \frac{\partial^2 u}{\partial x^2}\,\psi + 2\frac{\partial u}{\partial x}\frac{\partial \psi}{\partial x} + u\,\frac{\partial^2 \psi}{\partial x^2} \,. \tag{3.4.4}$$

The second and third terms of Equation (3.4.2) have the same form. The first and second derivatives of ψ with respect to x are

$$\left.\begin{aligned} &\frac{\partial \psi}{\partial x} = -ikz\frac{\partial n}{\partial x}\,\psi \\ \text{and}\quad &\frac{\partial^2 \psi}{\partial x^2} = -z\psi\left[k^2 z\left(\frac{\partial n}{\partial x}\right)^2 + ik\frac{\partial^2 n}{\partial x^2}\right]. \end{aligned}\right\} \qquad (3.4.5)$$

The first and second derivatives of ψ with respect to y can easily be obtained from Equation (3.4.5). The derivatives of ψ with respect to z are slightly more complicated because the exponent of ψ is a product of n and z. The final set of derivatives is

$$\left.\begin{aligned} &\frac{\partial \psi}{\partial z} = -ik\psi\left(n + z\frac{\partial n}{\partial z}\right) \\ \text{and}\quad &\frac{\partial^2 \psi}{\partial z^2} = -ik\psi\left[-ik\left(n + z\frac{\partial n}{\partial x}\right)^2 + 2\frac{\partial n}{\partial z} + z\frac{\partial^2 n}{\partial z^2}\right]. \end{aligned}\right\} \qquad (3.4.6)$$

From Equation (3.4.1, 4, 5 and 6) we can find the wave equation for thermal blooming as follows

$$e^{-iknz}\nabla^2 u - 2ike^{-iknz}\left[z\frac{\partial u}{\partial x}\frac{\partial n}{\partial x} + z\frac{\partial u}{\partial y}\frac{\partial n}{\partial y} + \frac{\partial u}{\partial z}\left(n + z\frac{\partial n}{\partial z}\right)\right]$$

$$- kue^{-iknz}\left[kz\left(\frac{\partial n}{\partial x}\right)^2 + kz\left(\frac{\partial n}{\partial y}\right)^2 + k\left(n + \frac{\partial n}{\partial z}\right)^2 + i\left(\frac{\partial n}{\partial z} + z\frac{\partial^2 n}{\partial z^2}\right)\right]$$

$$+ k^2 n^2 u e^{-iknz} = 0\,. \qquad (3.4.7)$$

We retain the rapidly varying exponential term as a reminder that the other terms vary slowly with z. As a check, we note that if we set n constant and then invoke the paraxial approximation, Equation (3.4.7) reduces immediately to Equation (2.2.13) which is the paraxial form of the scalar wave equation. We can simplify Equation (3.4.7) using the paraxial approximation and we find

$$e^{-iknz} \cdot \nabla^2 u(x,y) - 2ike^{-iknz}\left[z\frac{\partial u}{\partial x}\frac{\partial n}{\partial x} + z\frac{\partial u}{\partial y}\frac{\partial n}{\partial y} \right]$$

$$- k^2 z^2 u e^{-iknz}\left[\left(\frac{\partial n}{\partial x}\right)^2 + \left(\frac{\partial n}{\partial y}\right)^2 \right] = 0 \quad (3.4.8)$$

This is the full paraxial form of the thermal blooming wave equation derived from first principles.

3.4.1 Refractive Index Changes produced by a laser beam

We need to find the refractive index change in the beam and we therefore need to investigate the mechanisms which lead to the coupling of laser energy into the air. Wood *et al* have performed a detailed analysis of 10.6 μm laser induced chemistry on atmospheric temperature [6]. Under the assumption that complete vibrational equilibrium is reached, we can write

$$\Delta T = \frac{T_i}{4.235\,P}\alpha_C\, u\,(x,y)\left[1 + \frac{\alpha_H}{\alpha_C}\right] t \text{ , in SI units.} \qquad (3.4.1.1)$$

Where ΔT is the temperature change on heating, T_i is the initial temperature and α_H and α_C are the absorption coefficients due to water vapour and CO_2, respectively and t is the heating time. A plot of Equation (3.4.1.1) is shown in Figure 3.14. Recalling the Gladstone-Dale law introduced as Equation (2.7.3.3)

$$(n-1) = k\rho \qquad (2.7.3.3)$$

and assuming that atmospheric air behaves as an ideal gas, we can combine this equation with the equation of state to give

$$\frac{\Delta n}{n_o - 1} = \frac{\Delta \rho}{\rho_o} \equiv -\frac{\Delta T}{T} + \frac{\Delta P}{P}, \qquad (3.4.1.2)$$

where Δn is the refractive index change, n_o is the refractive index before the heating occurs and the other terms are construed in the same way.

If we assume that the air is allowed to expand at constant pressure then we can combine Equation (3.4.1.1 and 2) to give

$$\Delta n = -\frac{(n_o - 1)}{4.235\,P}\,\alpha_C\,\mathbf{u}\,(x,y)\left[1 + \frac{\alpha_H}{\alpha_C}\right]t. \qquad (3.4.1.3)$$

The refractive index at time t can be found using the following equation,

$$n_t = n_o - \frac{(n_o - 1)}{4.235\,P}\,\alpha_C\,\mathbf{u}\,(x,y)\left[1 + \frac{\alpha_H}{\alpha_C}\right]t\,. \qquad (3.4.1.4)$$

The behaviour of this equation is examined for two cases. The first case is the linearized case, where a fixed initial value for the refractive index is assumed. In the second, non-linear case, Equation (3.4.1.4) is treated iteratively in millisecond time-steps. This iterative equation is as follows

$$n_{h+1} = n_h - \frac{(n_h - 1)}{4.235\,P}\,\alpha_C\,\mathbf{u}\,(x,y)\left[1 + \frac{\alpha_H}{\alpha_C}\right]t_h, \qquad (3.4.1.5)$$

where t_h is the heating time and the initial refractive index, n_0, (that value just before the laser is switched on) is used as a seed for the iteration. Equations (3.4.1.4 and 5) exhibit very different behaviour and they are plotted in Figures 3.15a-d, for the beam parameters given in Table 3.1.

The linear case shows a refractive index change over one second of 1.3 parts in 10^5. In Section 2.7.4, we calculated that for guiding, a refractive index change of approximately 4 parts in 10^6 would be required. The results calculated here do not make allowance for the effects of cooling. In the non-linear case, the refractive index changes rapidly reaching a value of 1 (free space) in about 0.5 s.

Parameter	Value
Atmospheric pressure	10^5 Nm^{-2}
Ambient air temperature	20 °C
Relative Humidity	50 per cent
Absorption coefficients	
Water vapour (α_H)	0.094×10^{-3} m^{-1}
Carbon Dioxide (α_C)	0.071×10^{-3} m^{-1}
Total beam power	1,000 W

Table 3.1 Parameters for beam simulations

There are clear problems in the physical interpretation of equations 3.4.1.4 and 5. Equation 3.4.1.4 would eventually return negative values for the refractive index. Equation 3.4.1.5 implies that eventually all the gas in the beam is driven out of the propagation path and not replaced. In early time, both results could be applicable whereas in late time, both results are non-physical. We can though, imagine reasonable, intuitive cases where each equation may be valid.

For pulses or CW beams below the thermal blooming threshold we can imagine that small linear changes in the refractive index might occur. These changes could be small enough so that the effects on the beam in time are negligible.

As the heating time or the beam power increase, we can imagine some critical value, where the transition to the non-linear case can be expected. At these values, equation 3.4.1.5 effectively predicts self-interaction in which feedback processes occur. Later portions of the

beam are affected by the refractive index gradients already generated by earlier portions. This is implicit in our model of the heating as an iterative process; we keep adding small portions of heat each time step but we do not allow cooling. The logical conclusion of this analysis is that all the air is driven "out of the beam" by heating. We know that the heating process can only continue until the heated air becomes so bouyant that it rises out of the beam to be replaced by cooler air from the surrounding regions or until the heating time is long enough to permit the heated air to be cleared from the beam by the wind. This analysis does not permit us to predict over what timescale this process might occur, but we can see that it might be valid until buoyant processes or wind dominate.

3.4.2 Doughnut mode refractive index profile

The doughnut mode intensity profile across the x axis of the laser beam is shown in Figure 3.3. We can use the material developed in previous sections to calculate the refractive index change produced by the doughnut mode. Using Equation (3.4.1.5) and (3.2.1.1) for the transverse, x, axis we can write

$$n_{h+1} = n_h - \frac{(n_h - 1)}{4.235\,P}\,\alpha_C\,\frac{x^2}{w^2}\,\exp\left(-\frac{2x^2}{w^2}\right)\cdot\left[1 + \frac{\alpha_H}{\alpha_C}\right]t_h. \qquad (3.4.2.1)$$

We can use this equation to investigate refractive index changes close to the output aperture for the beam parameters given in Table 3.1. We use the iterative scheme of Section 3.4.1 to calculate the refractive index changes caused by the CO_2 laser beam with the parameters of

Table 3.1. The results of the calculations are shown in Figure 3.16. After 900 ms, we calculate a refractive index change of 3 parts in 10^4. In Figure 3.17, we show the the refractive index changes as a function of time and position across the beam profile.

3.5 The effects of refractive index fluctuations on microwave radiation

3.5 1 Refractivity

The normal value of the refractive index, n, in the atmosphere close to the earth's surface varies between 1.000250 and 1.000400. The refractive index is an inconvenient number to use when dealing with small changes so in propagation studies, a scaled index, N, known as "refractivity" is defined. The refractivity is given by the following equation,

$$N = \left(n - 1\right). 10^{6}. \qquad (3.5.1.1)$$

The atmospheric refractivity therefore varies between 250 and 400 N units close to the earth's surface.

3.5.2 Engineers' Refractive Effects Prediction System ("EREPS")

3.5.2.1 Introduction

In this section, we discuss the application of the Engineer's Refraction Effects Prediction System ("EREPS") [7] to the modelling of laser-generated atmospheric waveguides. EREPS is a software package developed by the Naval Ocean Systems Center Tropospheric Branch, Ocean and Atmospherics Division of the US Navy, to "provide users with assistance in properly assessing electromagnetic propagation effects of the lower atmosphere on proposed radar, electronic warfare, or communication systems". The package comprises a suite of programs which compute propagation factors and radar coverage, an annual climatological surface duct summary for most of the surface of the Earth and an atmospheric ray-tracing alogorithm. The ray-tracing module of EREPS was not specifically designed to tackle the class of problems addressed in this thesis. They are used, however, to predict the effects of large-scale atmospheric ducts on radar and communications systems performance. We shall evaluate the suitability of EREPS for application to the problems tackled in this thesis.

3.5.2.2 Refractivity changes in the atmosphere and waveguiding

It has been observed that the refractivity distribution within the atmosphere is nearly an exponential function of height [8]. The exponential decrease of N with height close to the earth's surface (within 1 kilometre) is sufficiently regular, however, to allow an

approximation of the exponential function by a linear function. This linear function is known as the "standard gradient" and is characterised by a decrease of 39 N-units per kilometre. Gradients that cause effects similar to the standard gradient but which vary between 0 and 79 N-units per km are known as normal gradients.

If the motions of the atmosphere produce a situation where the temperature and humidity distributions create an increasing value of N with height, the wave path is bent upwards and the energy travels away from the earth. This is termed "subrefraction" and rarely occurs naturally.

A standard atmosphere has a refractivity gradient which causes waves to bend downwards towards the earth. If the temperature of the troposphere increases with height (temperature inversion) or the water vapour content decreases rapidly with height, the refractivity gradient will decrease from the standard. This exaggerates the "bending" of the propagating wave. As the refractive index gradient continues to decrease, the radius of curvature of the wave path will approach the radius of curvature of the earth. The refractive index gradient for which the two radii are equal is referred to as the "critical gradient". At the critical gradient, the wave propagates at a fixed height above the ground and travels parallel to the surface of the earth. Refraction between the normal and critical gradients is known as "superrefraction".

Should the refractivity decrease beyond the critical gradient, the radius of curvature for the wave will become smaller than that of the earth and the wave will either strike the earth and undergo surface

reflection, or enter a region of standard refraction and be refracted back upwards, only to reenter the area of refractivity which causes downward refraction. This refractive condition is known as "trapping" since the wave is confined to a narrow region of the troposhere. The common term for this confinement region is a tropospheric "duct" or a tropospheric "waveguide". There are a number of metorological conditions which will lead to the creation of ducts. If these conditions occur aloft such that the base of the duct is above the surface, the duct is referred to as an "elevated duct". The elevated duct is analagous to the laser-generated atmospheric waveguide which we wish to analyse. It is important to remember, however, that tropospheric ducts are essentially two dimensional structures, whereas typical laser waveguides will be three dimensional. The two dimensional models will, therefore, be used to obtain a general understanding of the waveguiding process and to investigate the effects of varying the waveguiding parameters on performance.

3.5.2.3 The ray tracing algorithim and the validity of its application

The purpose of the "RAYS" module of EREPS is to calculate and plot a series of ray-path trajectories on a height-versus range display. The user specifies the refractive index profile, the transmitter height, the elevation angle limits and number of rays desired. We are able to alter EREPS' standard input refractivity profiles and adapt them, "designing" refractivity profiles for atmospheric waveguides of the type considered in this thesis. The ray-trace routine is then invoked and rays are traced based on the results of a series of calculations

performed within each linear-refractivity layer specified in the profile. To give the best compromise of speed and resolution, the independent variable in the ray-trace is elevation angle along the ray. At each step, the elevation angle is incremented and a new height and range are found within the current layer. If the ray leaves the current layer, then the range is calculated at the layer boundary, and the elevation angle is incremented in the next layer above or below. As each layer is entered, the refractivity gradient must be examined to determine if the elevation angle in that layer will be increasing or decreasing. Tests must be included to determine where rays will reach a maximum or minimum height, to ensure that the corresponding elevation angle of zero is considered. For the last step only, a height is calculated at the maximum range within the current layer.

The validity of a ray-tracing model for the laser-generated atmospheric waveguide is considered in two cases. In the first case, if the waveguide is large compared to the wavelength of the radiation to be guided then ray-tracing is a viable tool. This is true, for example, if the radiation to be guided is in the millimetre wave-band and the waveguide has a cross-section of the order of 10 cm. In the second case, according to the principle of linear superposition, any propagating electromagnetic wave can be represented as a set of an infinite number of plane waves propagating with a range of angles and amplitudes. Each plane wave, having a definite direction of energy flow at any particular point, corresponds to a ray propagating in that direction. Thus any propagating waveguide mode can be considered to be composed of an infinite set of individual rays. The guiding condition is satisfied if all of the rays required to define the mode, that is all of the rays with elevation angles within specified

bounds, are guided. Thus the ray tracing algorithm is also valid when the wavelength of the microwave radiation is comparable to the transverse dimensions of the waveguide.

3.5.3 Simulation of laser waveguides using EREPS

The results of EREPS simulations of atmospheric waveguides with various parameters are shown in Plates 1 – 10. The refractivity profile function is defined in N-units at the lower right-hand side of each display. The ray trajectories are shown as a graph of altitude versus range and the other important parameters (transmitter height, number of rays and range of launch angles) are given in the upper right-hand corner.

The first set of results (Plates 1 – 4) show the performance of a step-index atmospheric waveguide of width 10 cm. We note that there is strong guiding so that, even with a small perturbation in the refractivity, rays with a wide range of angles of launch are trapped.

The results of the simulation of quadratic refractivity profile atmospheric waveguides are shown in Plates 5 – 10. In the first parameter sweep (Plates 5 – 8), the spatial extent of the atmospheric waveguide is constant and the magnitude of the refractivity perturbation ("modulation depth") is varied. For small modulation depths, only rays with trajectories very close to the optic axis are guided. As the modulation depth increases, more divergent rays are trapped. The transition to strong guiding occurs very rapidly at a critical value of the modulation depth.

Plates 9 and 10 show the results of a parameter sweep to investigate the importance of the spatial extent of the waveguide. The modulation depth is fixed at a value which is just subcritical for a 10 cm waveguide and the size of the waveguide is increased until guiding occurs. The results show that the transverse dimension of the waveguide has to be increased by an order of magnitude in order to achieve the waveguiding condition. Thus the modulation depth appears to be a much more important parameter than the transverse dimension of the waveguide.

3.6 Summary and conclusions

In this Chapter, the formation and performance of atmospheric waveguides have been examined and a number of methods of generating the waveguide are proposed. We conclude that the most practical way of producing an annular beam is to use an Annular Beam Director specially designed for the purpose.

The refractive index changes produced by the passage of a high power CO_2 laser are calculated and shown to be in the range necessary to produce guiding for a 1 kW beam in both the linear and non-linear cases considered. The theory developed enables us to predict the refractive index changes for a beam with an annular profile. It can be expected that a 1 kW beam will achieve the formation of a guide in times of the order of 1 s, producing refractive index changes of the order of 1 part in 10^4.

At microwave frequencies, we use the ray-tracing algorithm of EREPS to investigate the parameters of an atmospheric waveguide. The importance of precise alignment between the guide and the radiation to be guided (first noted in Section 2.7.4) is underlined by the results of the EREPS results. From consideration of the EREPS simulations and parameter sweeps, we conclude that the magnitude of the refractive index change is a more important parameter than the overall size of the guide.

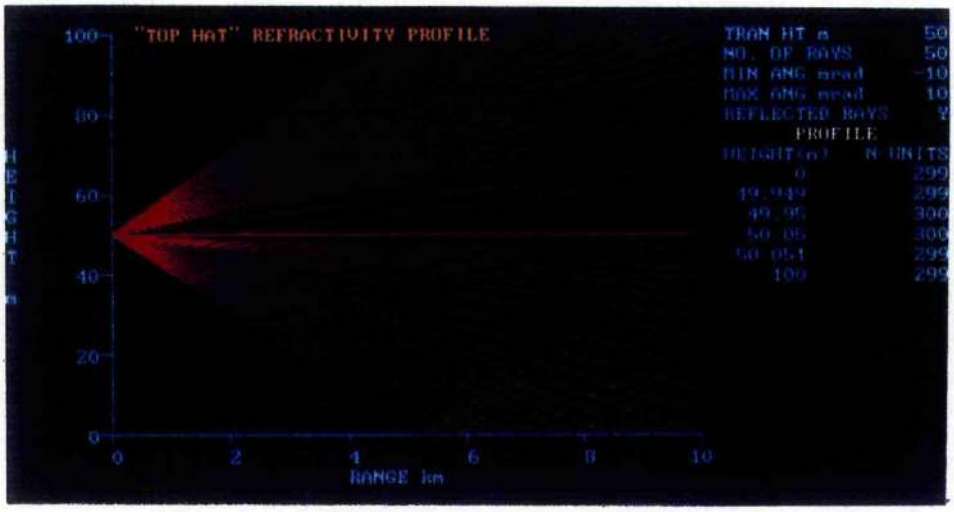

Plate 1

EREPS simulation of 10 cm diameter atmospheric waveguide with a refractivity perturbation of 1 N-unit

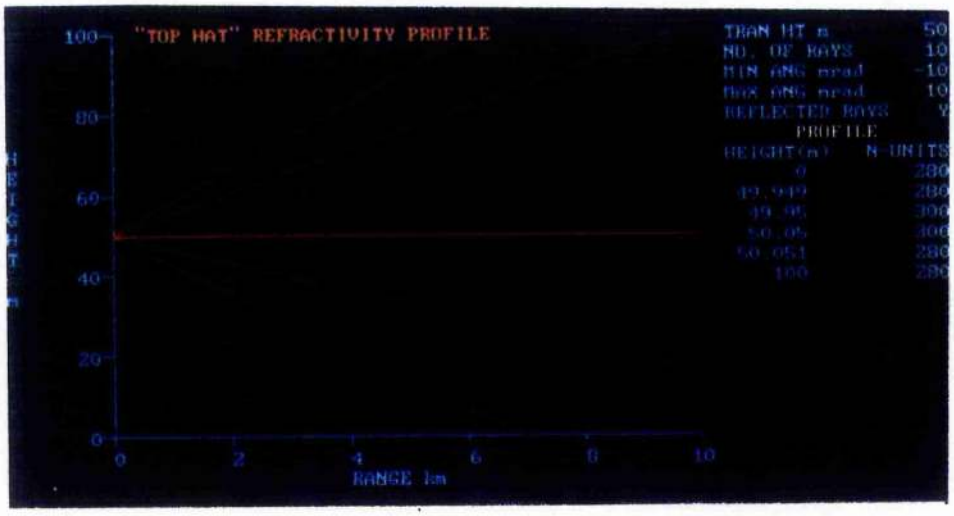

Plate 2

EREPS simulation of 10 cm diameter atmospheric waveguide with a refractivity perturbation of 20 N-units

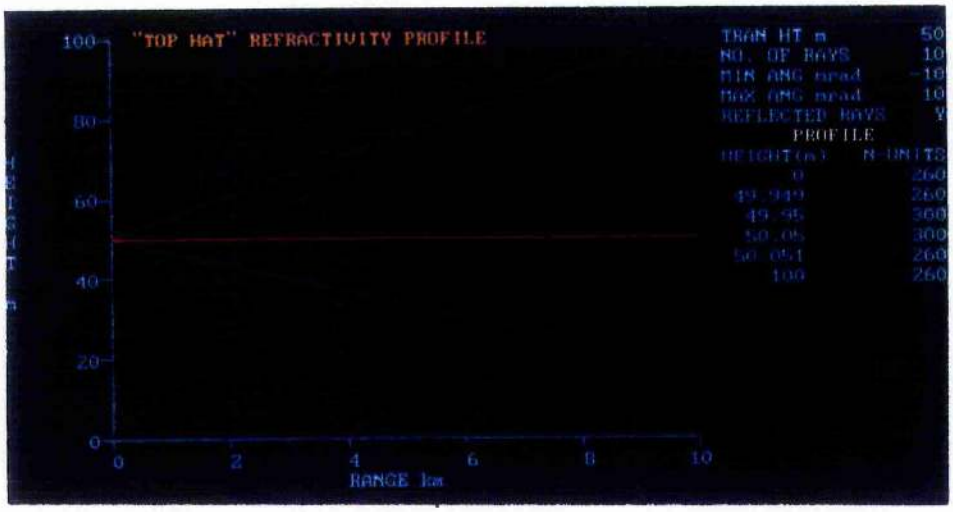

Plate 3

EREPS simulation of 10 cm diameter atmospheric waveguide with a refractivity perturbation of 40 N-units

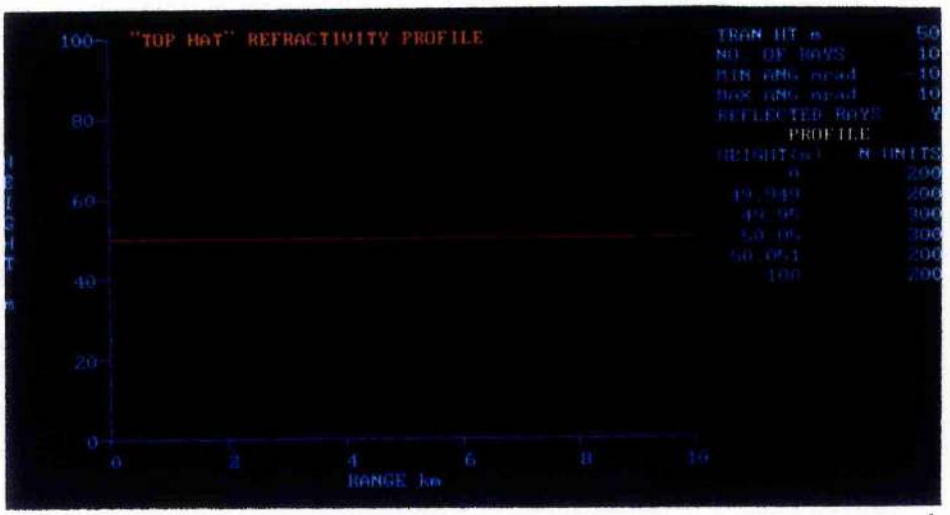

Plate 4

EREPS simulation of 10 cm diameter atmospheric waveguide with a refractivity perturbation of 100 N-units

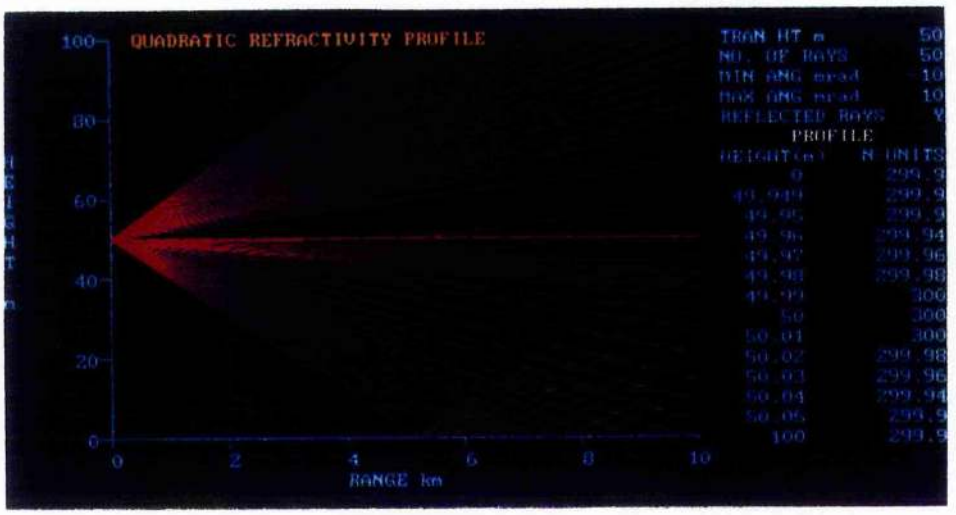

Plate 5

EREPS simulation of 10 cm diameter atmospheric waveguide with a refractivity perturbation of 0.1 N-units

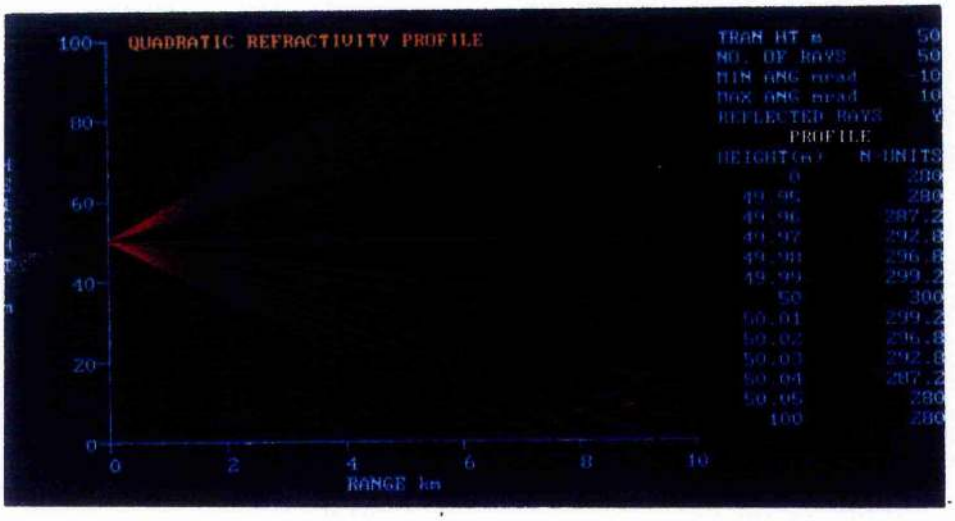

Plate 6

EREPS simulation of 10 cm diameter atmospheric waveguide with a refractivity perturbation of 20 N-units

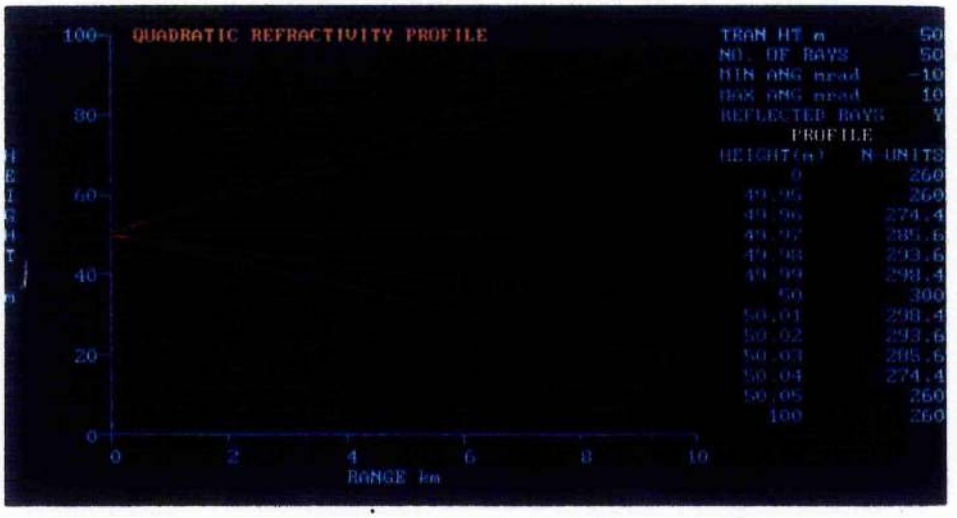

Plate 7

EREPS simulation of 10 cm diameter atmospheric waveguide with a refractivity perturbation of 40 N-units

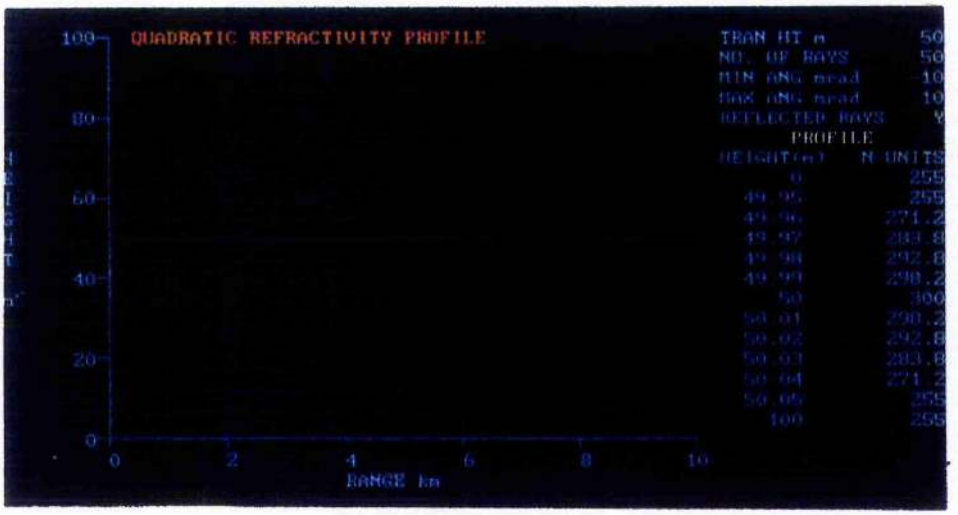

Plate 8

EREPS simulation of 10 cm diameter atmospheric waveguide with a refractivity perturbation of 45 N-units

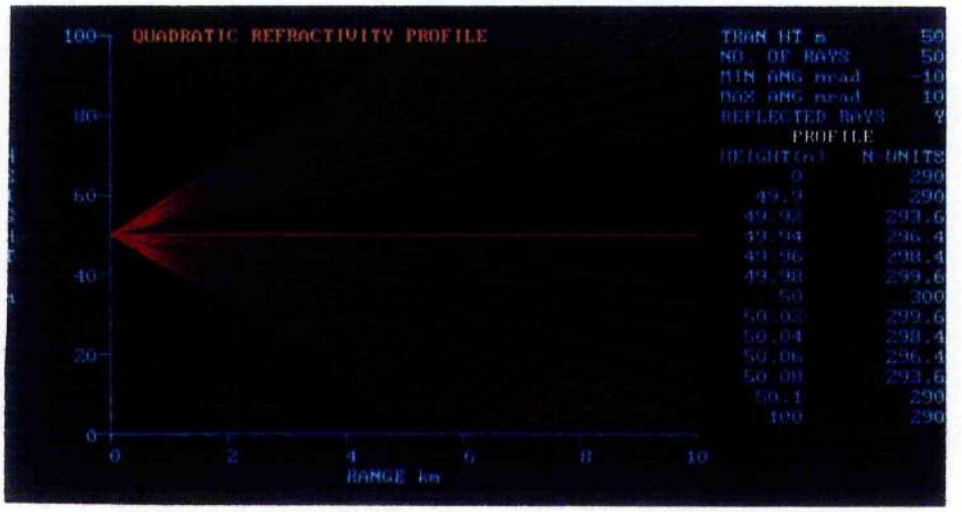

Plate 9

Refractivity perturbation of 10 N-units and an atmospheric waveguide 20 cm in diameter

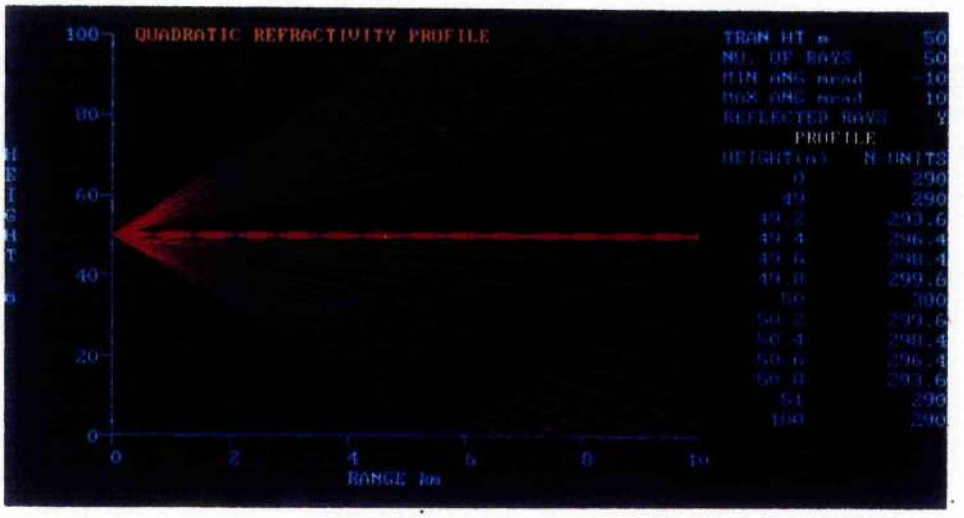

Plate 10

Refractivity perturbation of 10 N-units and an atmospheric waveguide 2 m in diameter

FIGURES FOR CHAPTER 3

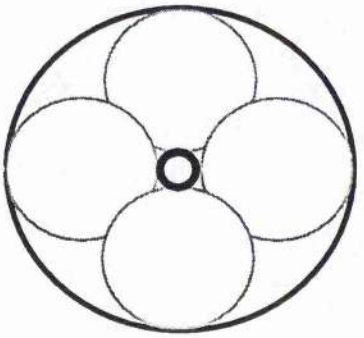

Figure 3.1 The "Doughnut" mode

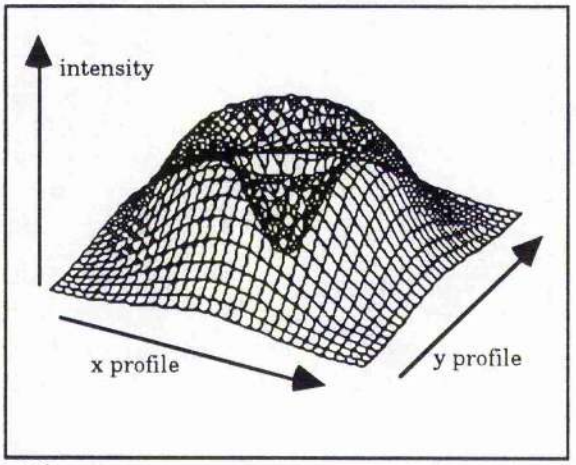

I1

Surface plot using transparent mesh

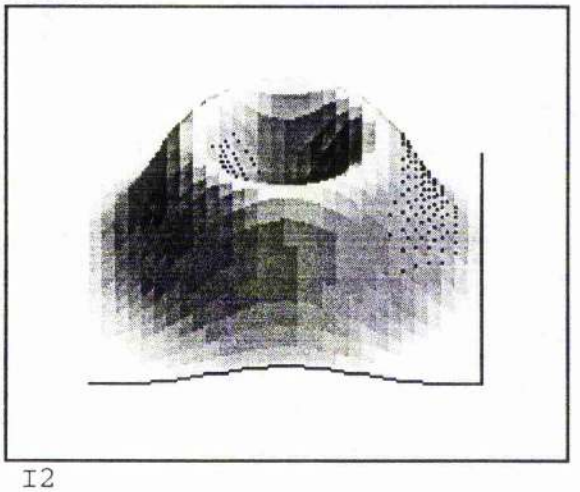

I2

Grey scale shaded plot

Figure 3.2 Illustrative surface plots (arbitrary units) of the doughnut mode from Equation 3.2.1.1

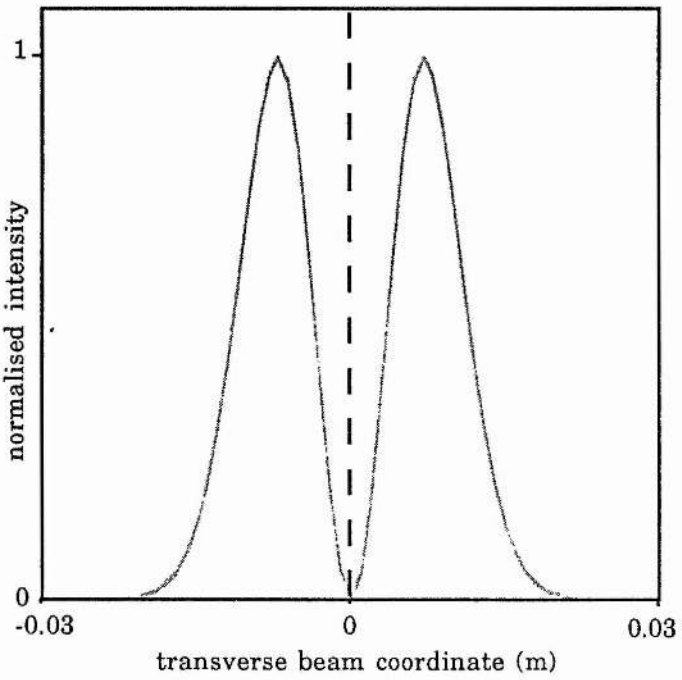

Figure 3.3 Doughnut mode x-profile

Side View

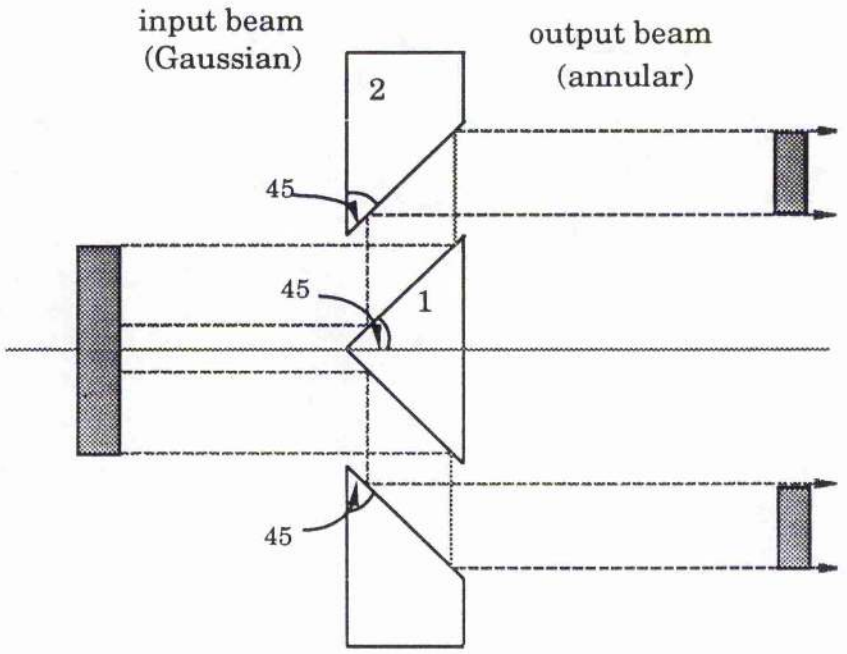

Rear View

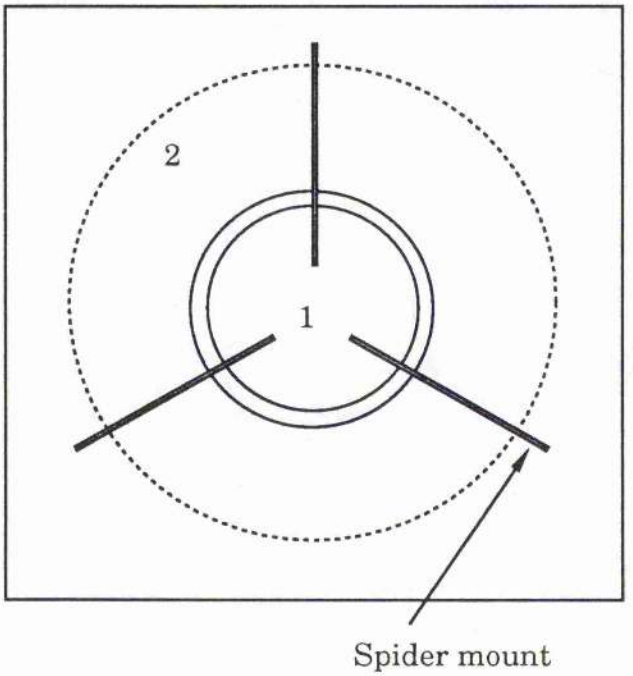

Figure 3.4 Annular beam director design

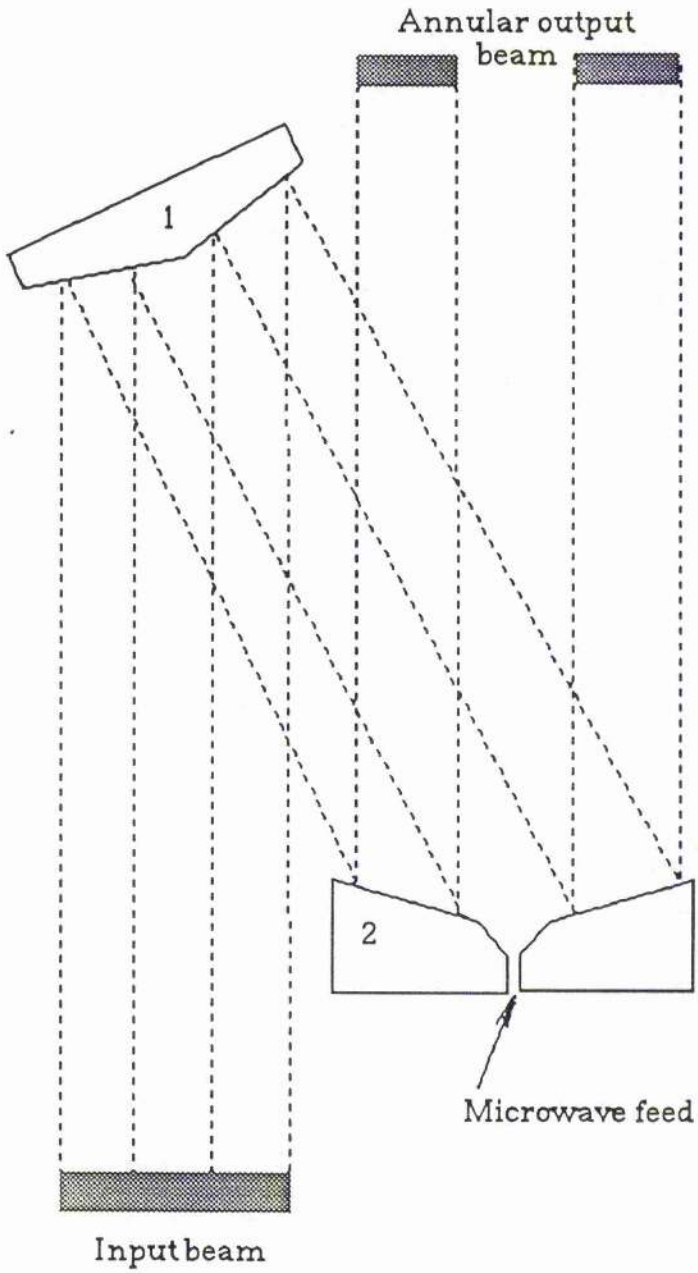

Figure 3.5 Off-axis annular beam director

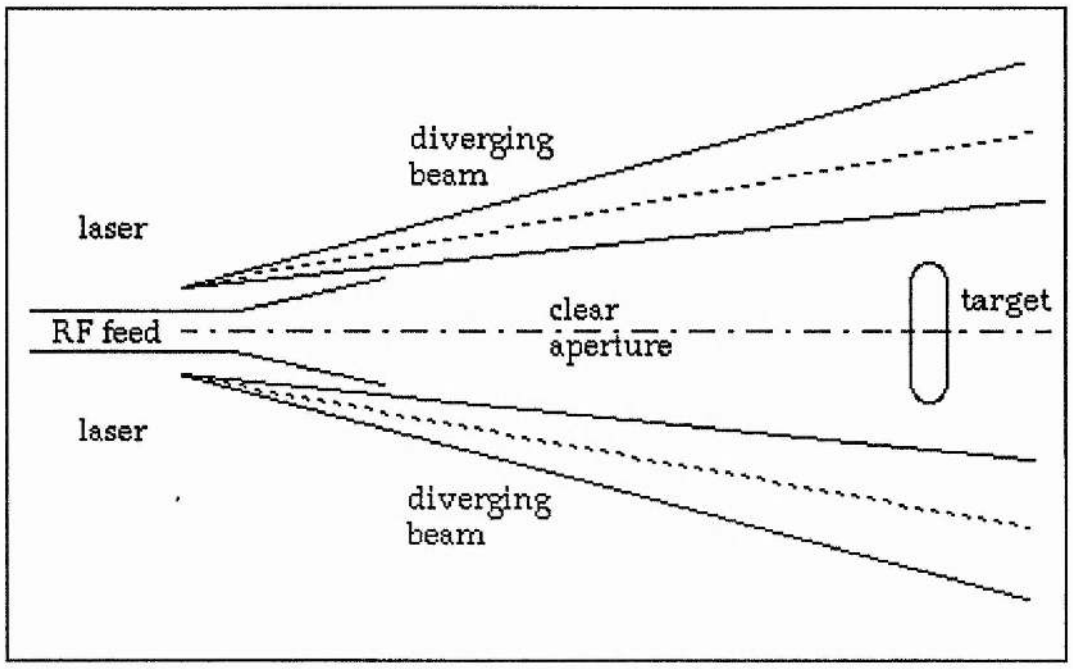

Figure 3.6 Multiple diverging beams, longitudinal section

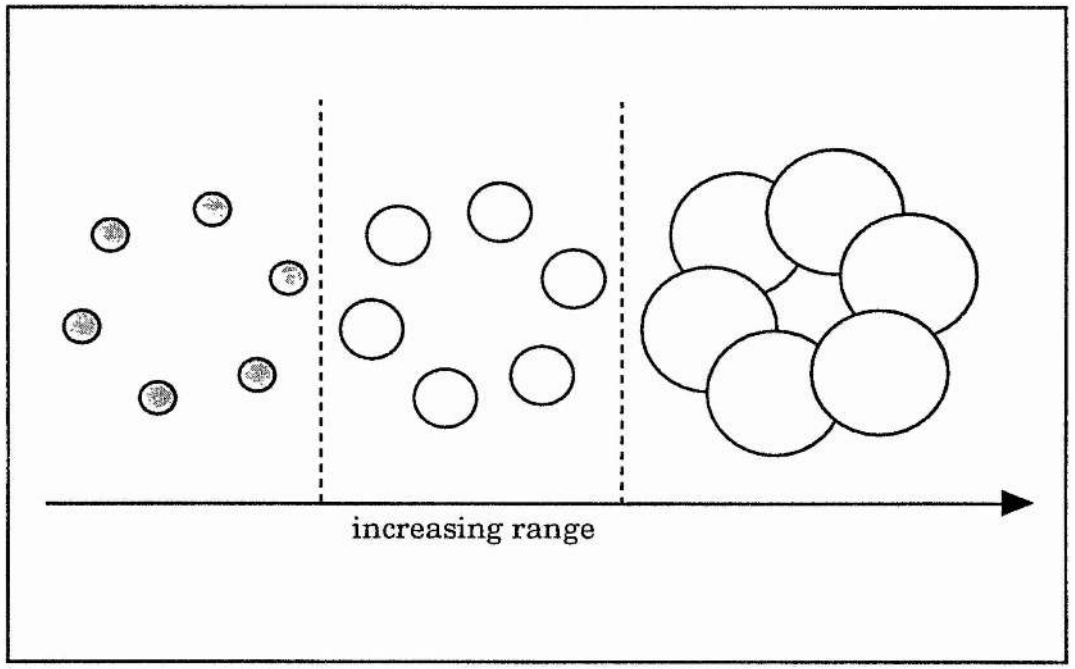

Figure 3.7 Multiple diverging beams, cross section

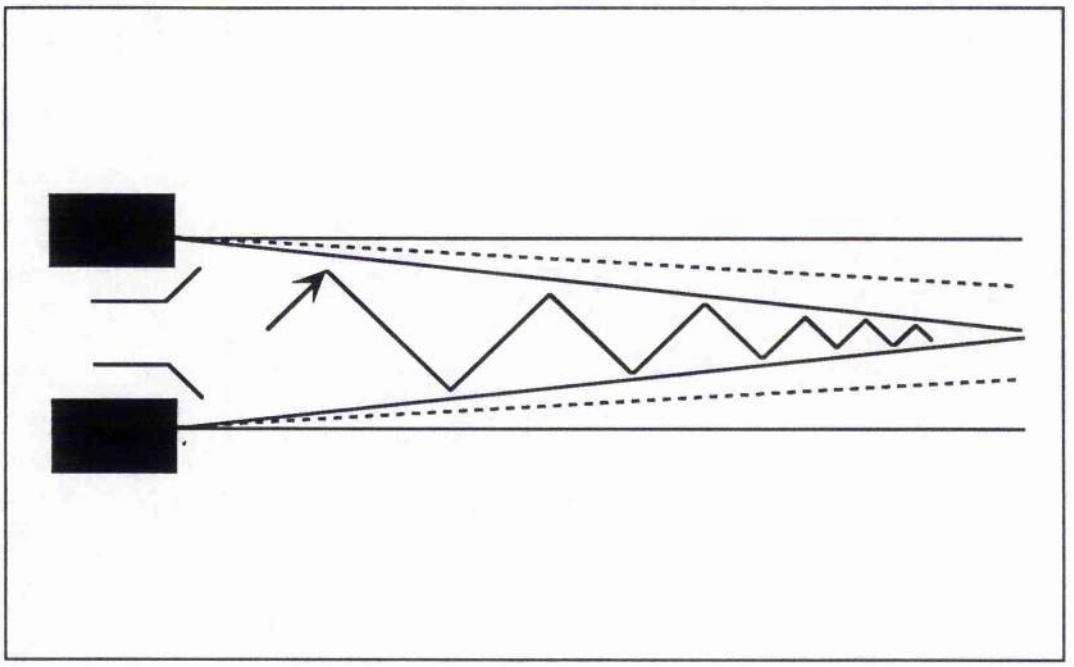

Figure 3.8 Focussing radiation onto a traget

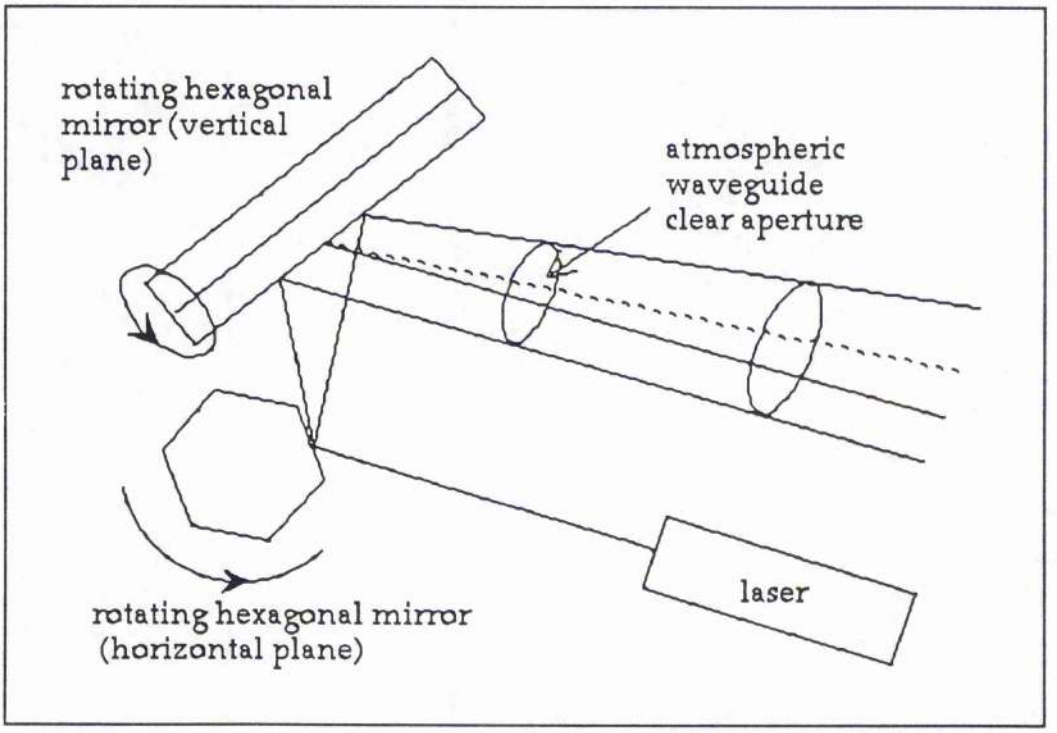

Figure 3.9 Waveguide formation using rotating mirrors

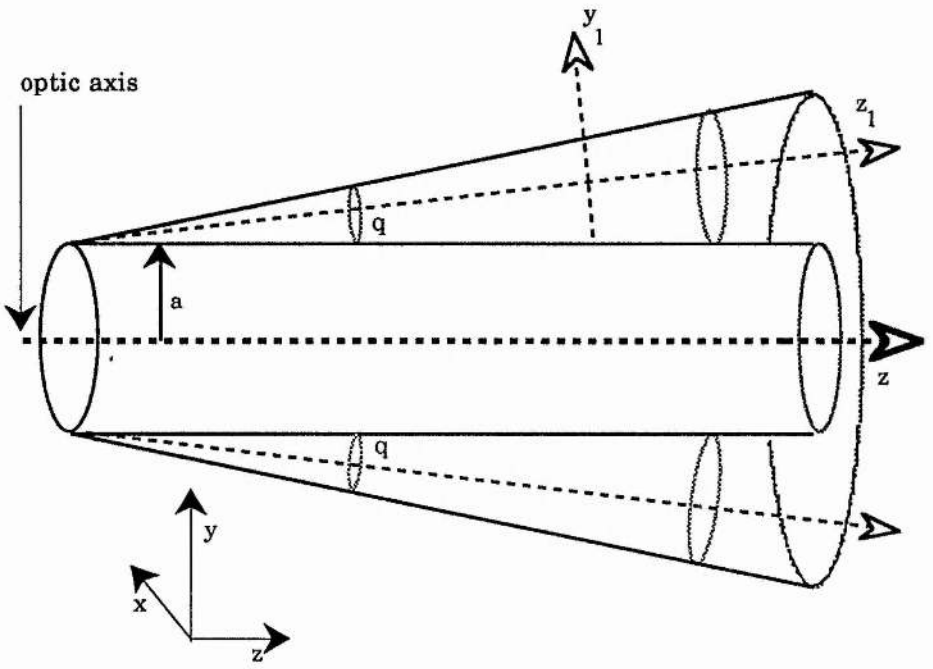

Figure 3.10 Laser and radiation to be guided aligned at the divergence angle of the annulus

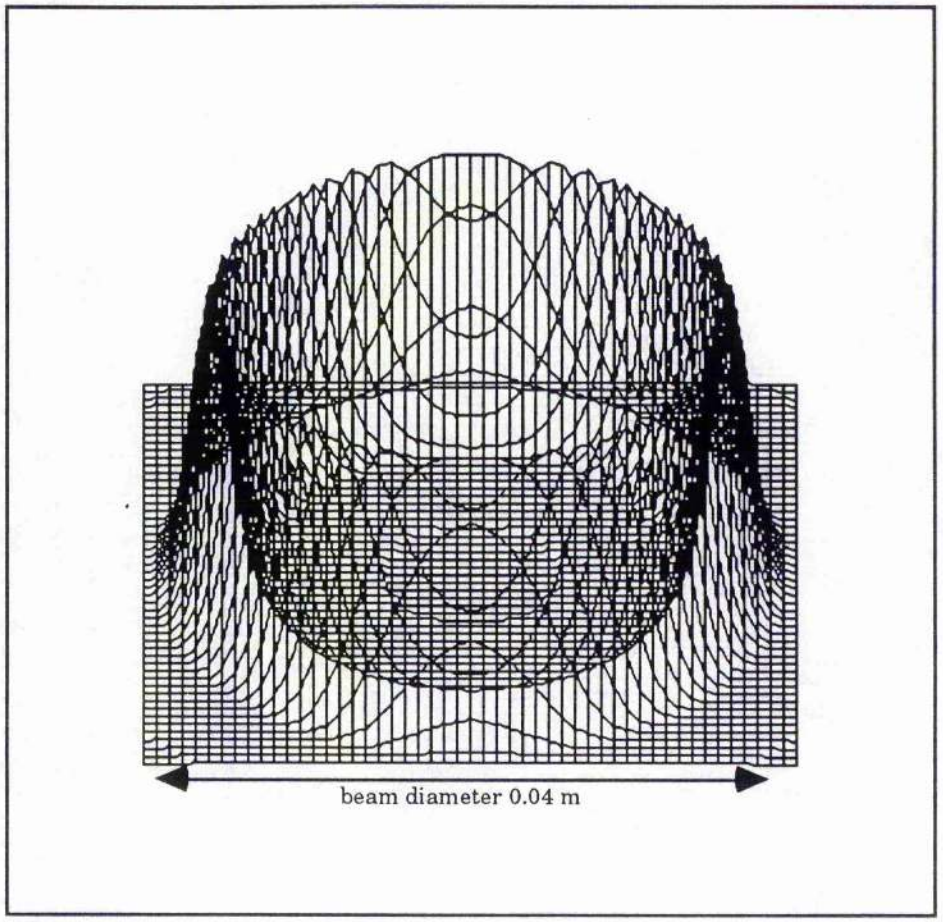

Total Beam power:	1 kW
Total beam diameter:	0.04m
Wall Profile:	Gaussian
Wall spot size (w) at output aperture:	0.01 m
Annulus clear aperture:	0.02m

Figure 3.11 Surface plot of Equation (3.3.5)

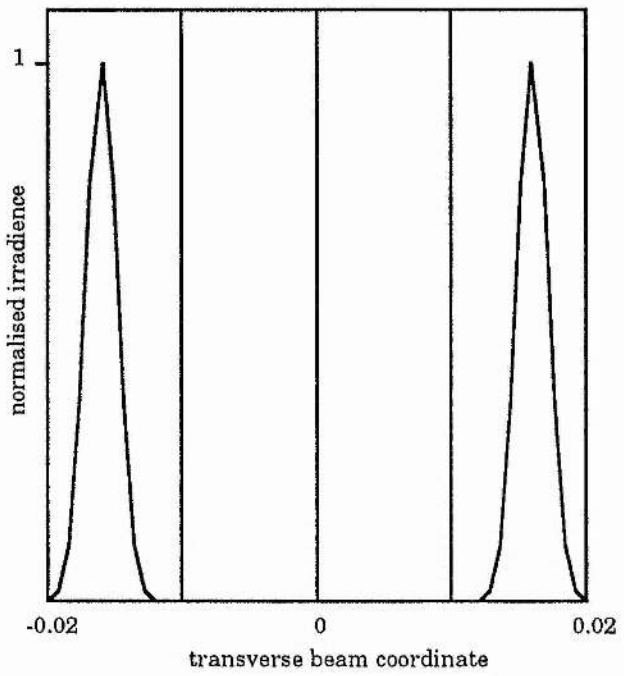

Figure 3.12 Transverse beam profile for Equation (3.3.5), the axis of propagation of the annular beam is at x = 0

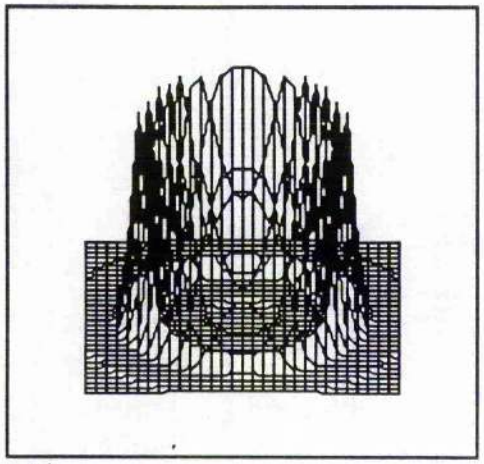

I1

z = 1 m, w = 0.01 m

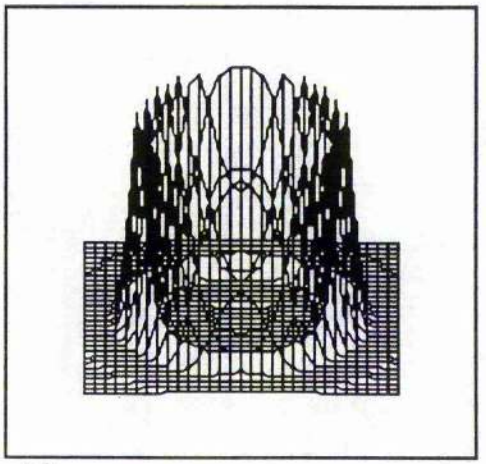

I2

z = 10 m, w = 0.01 m

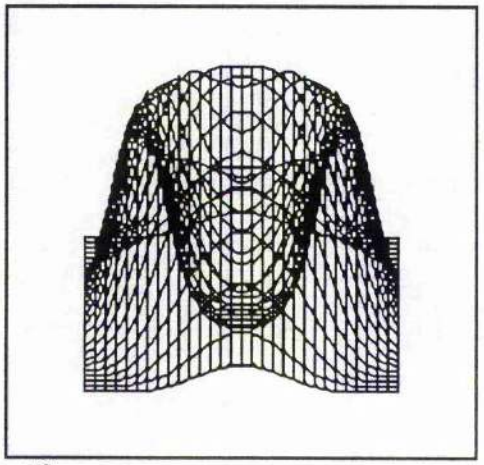

I3

z = 100 m, w = 0.04 m

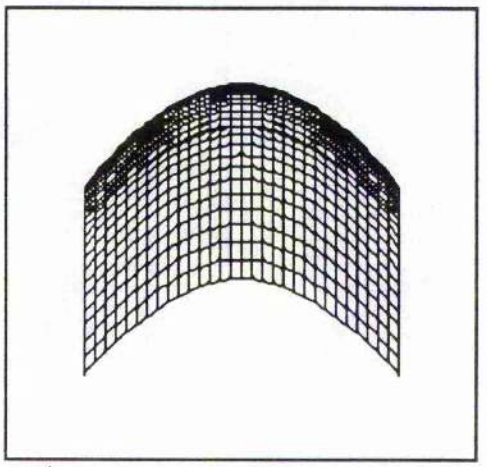

I4

z = 500 m, w = 0.17 m

Figure 3.13 Annular beam behaviour with range

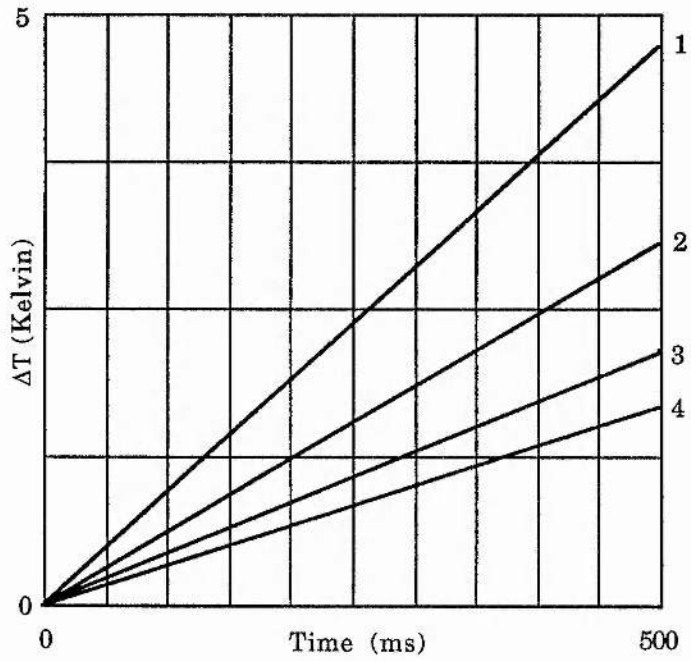

Initial ambient temperature, $T_i = 283$ Kelvin

Traces 1,2,3 and 4 for relative humidities of 75, 50, 30 and 10 per cent, respectively

Figure 3.14 Temperature rise versus time from Equation (3.3.9)

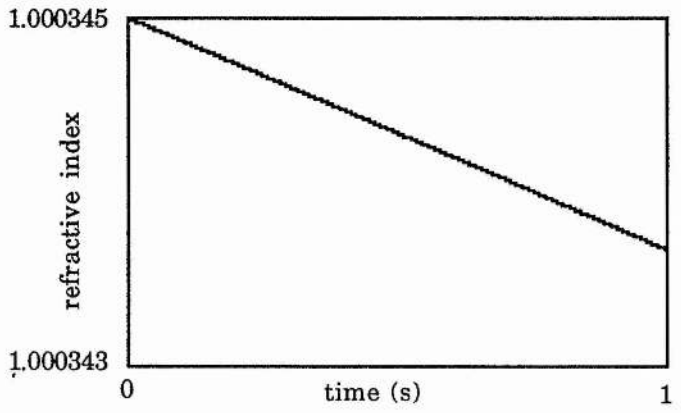

Figure 3.15a Linear change

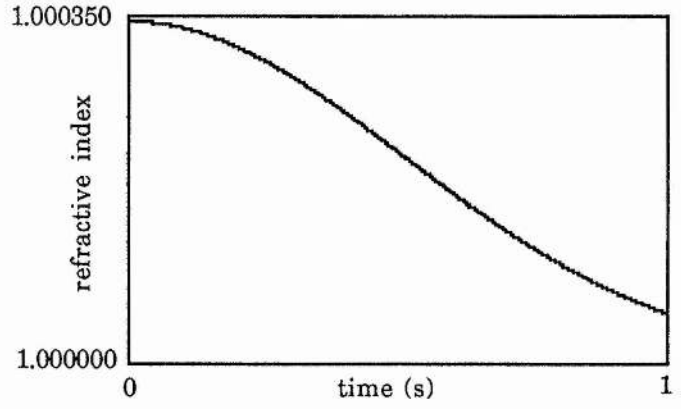

Figure 3.15b Non-linear change

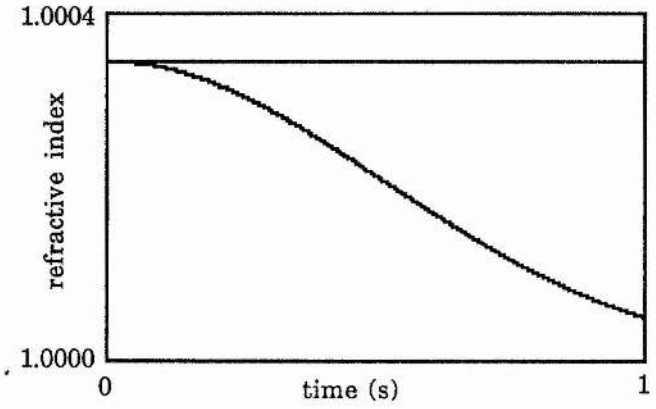

Figure 3.15c Linear and non-linear changes on same scale (upper trace; linear, lower trace; nonlinear)

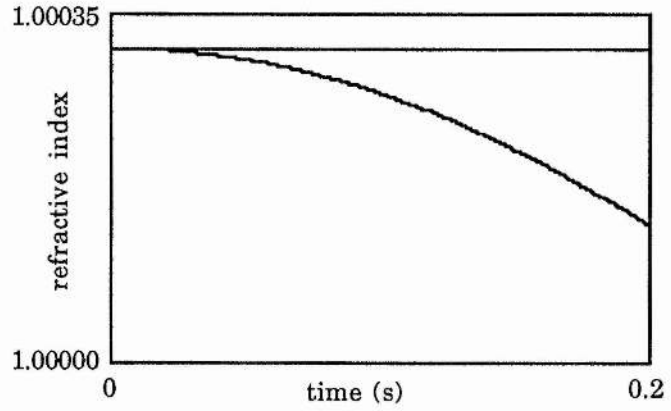

Figure 3.15d Early time behaviour

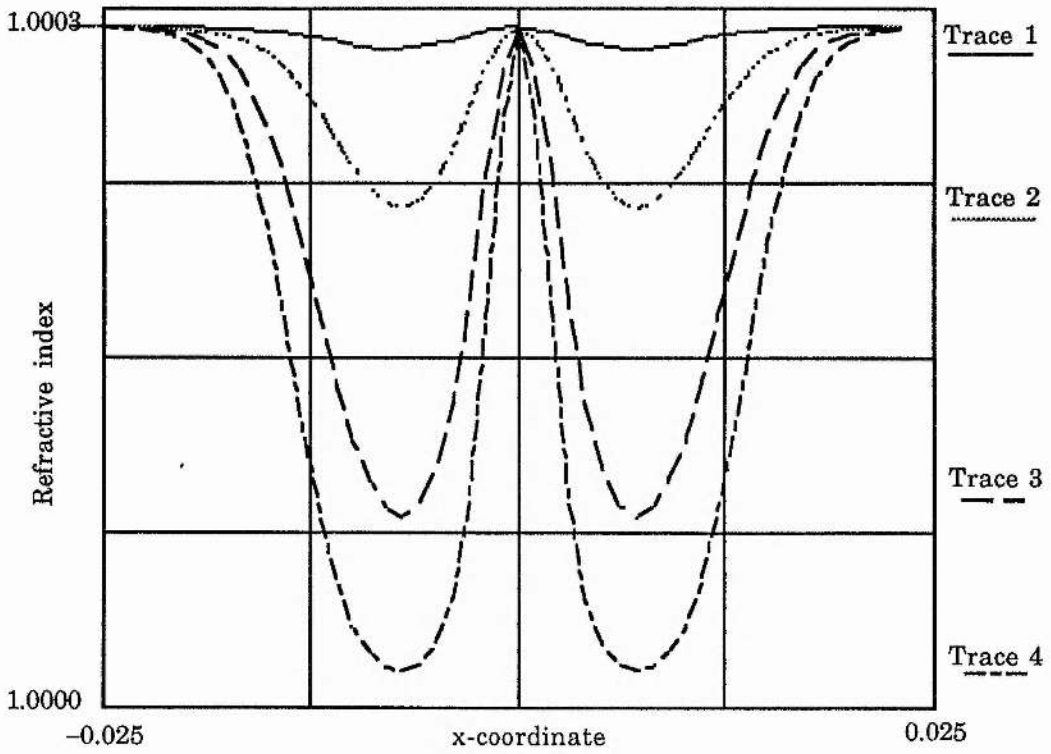

Trace Number	Simulation time (ms)	Peak refractive index change
1	100	1 part in 10^7
2	300	1 part in 10^6
3	600	2 parts in 10^4
4	900	3 parts in 10^4

Figure 3.16 Refractive index changes produced by the doughnut mode simulation of Section 3.4.2

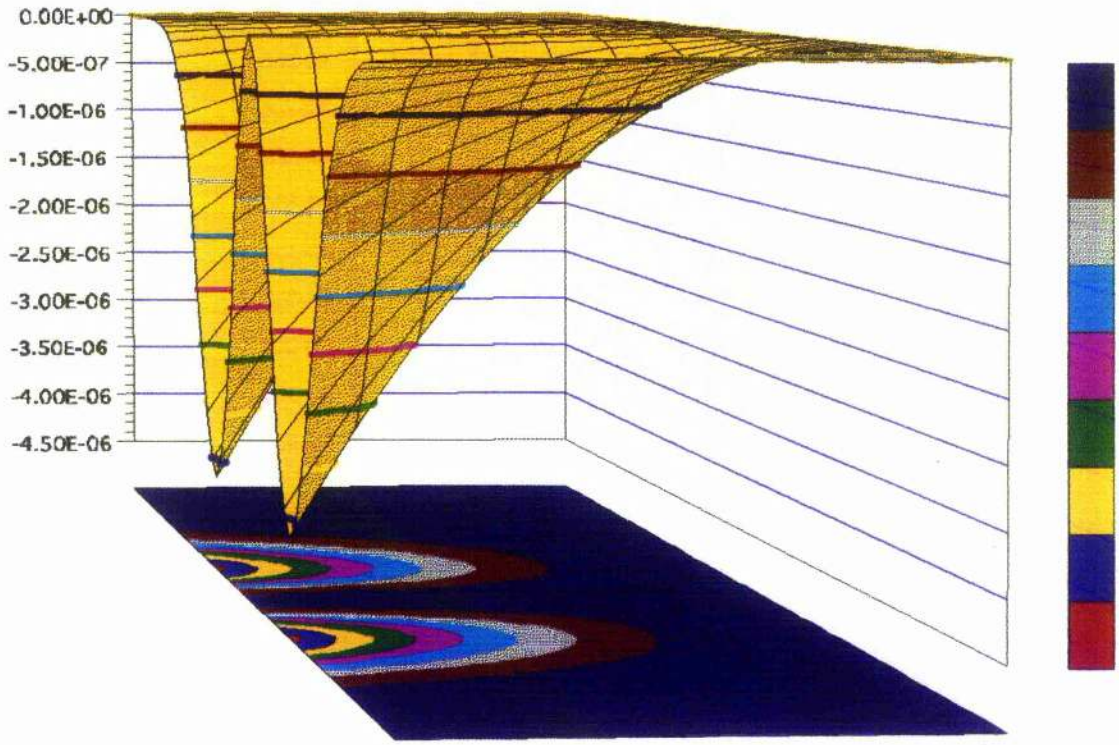

Figure 3.17 Refractive index changes produced by the doughnut mode as a function of time and position across the laser beam profile

REFERENCES FOR CHAPTER 3

1 Newman L A and Smith D C, Applied Physics Letters, **38**, p590 (1981)

2 Hauser N A and Davis C C, Applied Optics, **21**, No 18, p 3384, (1982)

3 Siegman A E, Lasers, pp 685 - 690, ISBN 0 19 855713-2, University Science Books, Mill Valley, California, USA, 1986

4 Maitland A and Dunn M H, Laser Physics, pp 106 - 7 and pp 131 *et seq*, ISBN 7204 0153 4, North Holland Publishing Company, Amsterdam, 1969

5 Karr T J, Propagation of High-Energy Laser Beams through the Earth's Atmosphere, Peter B Ulrich, Leroy E Wilson, Editors, Proc SPIE, p 26 (1990)

6 Wood A D, Camac M and Gerry E T, Applied Optics **10**, No. 8, p 1877 (1971)

7 EREPS: Engineer's Refractive Effects Prediction System Software and User's Manual Code 543, ISBN 0-89006-455-5, Artech House, Boston, USA, 1990.

8 Bean B R and Dutton E J, Radio Meteorology, Dover Publications, Inc., New York, 1968.

4. EXPERIMENTS

4.1 Introduction

In this Chapter, experiments based on the ideas and theoretical models developed in earlier sections of this thesis are described. The experimental approach is to reduce the overall problem of the verification of guiding to a set of simpler, modular experiments which form individual elements of a guiding system. Once the results for individual modules are obtained we can combine all the elements to verify the concept of guiding. An overview of the experiments reported in this thesis is as follows;

- Measurement of the refractive index changes produced by a high power laser beam at optical frequencies;

- Measurement of the refractive index changes produced by a high power laser beam at microwave frequencies;

- The production and propagation of annular high power laser beams in the laboratory using a specially designed annular beam director; and,

- The combination of an annular laser beam and microwave radiation in a verification of the guiding effect.

It was noted in Section 1.1 that previously published experimental work has used low power lasers (mW or a few W) propagating in absorbing liquids or high pressure gases to produce thermal blooming effects. The motivation behind the design of the experiments reported in this thesis is to attempt (insofar as this is practicable and safe in a laboratory environment) to propagate the laser and microwave radiation in "near-real" wind-less conditions. A major consideration in the design of the experiments is the development of methods of working which enable the propagation of high power beams which are not confined in "flight tubes" or similar enclosures but which allow safe operation.

4.2 Description of the high power CO_2 laser system

4.2.1 The MFK unit

The laser used for the experiments is the Laser Ecosse Limited (formerly Ferranti Electronics Limited) MFK Series industrial laser ("MFK"). The MFK is a conventional, fast-axial flow, CW CO_2 laser which has water-cooled discharge tubes. The total cavity length is 24 m. To produce a compact device, the cavity is folded around a cylindrical "spine" using 12 discharge "legs" each of which comprises 2 discharge tubes. The high voltage supply is fed to the centre of the cylindrical structure and each folded leg has two separate central anodes, each feeding one discharge tube. Each anode is fed through a separate ballast resistor from a single high voltage source. The

current is stabilised by saturable reactors in the primary circuit of the high voltage transformer.

A steady flow of gas mixture is drawn through the discharge tubes by a Rootes blower. The exhaust gas from the pump is processed in a recirculation oven and fed back to the laser head. Pulses of fresh gas mixture are added at automatically timed intervals to replace any losses. At start-up and at any time during laser operation, fresh gas can be introduced by operating a manual "purge" cycle.

The laser structure is suspended inside the base tray on a frame support stucture. The design of the support structure means that the laser head is decoupled from any twisting deformation of the base. The laser head stands on wooden blocks on a sturdy steel table. An overview of the MFK's most important characteristics is shown in Table 4.1.

MFK SPECIFICATION	
Output characteristics	
Output wavelength:	10.6 μm.
Output power:	better than 1,000 W.
Output power stability:	±5 per cent over 8 hours.
Mode structure:	$TEM_{0,0,q}$ - slight variations from a pure Gaussian form occur near the output window.
Mode stability:	No changes occur due to cavity warm-up effects.
Beam diameter:	11.0 ± 0.9 mm to $1/e^2$.
Radius of curvature	5.0 ± 1.5 m diverging at the exit aperture of the laser head.
Beam divergence	1.2 mrad

Input Requirements	
Water pressure:	Minimum 2.0 kg cm^{-2} (30 psi). Maximum 5.0 kg cm^{-2} (50 psi).
Water flow:	Up to 10 l per minute.
Power absorbed into water:	15 kW.
Water condition:	Normal tap water at less than 20°C.
Electrical Supply	
Voltage:	380 - 440 V, 3-phase 50 Hz (subject to the setting of the internal tappings).
Voltage stability:	±5 per cent
Voltage transients:	Loss of voltage of more than 10 per cent for more than 1 millisecond may cause the laser to trip-out and require to be restarted.
Current:	38 - 44 A per phase (subject to the setting of the voltage tapping).
Volt-amp rating:	28 kVA.
Gas supplies	
Types and proportions:	Normal commercial grade, Helium 72 per cent, Nitrogen 19 per cent, Carbon Dioxide 7 per cent (supplied separately and controlled from the laser control unit)
Input pressures:	Minimum 2 bar (30 psi), Maximum 3.5 bar (50 psi)
Consumption:	90 l at start-up plus 90 l per hour

Table 4.1: MFK Specifications

4.2.2 The laser beam delivery system

The laser output beam leaves the discharge tube at the top of the cylindrical spine and is deflected through 90 degrees to pass down the "output channel", emerging through a hole in the base of the laser head. In industrial applications, a cutting head is mounted at the end

of the output channel. In the experiments reported in this thesis, the mounting is used to locate a water-cooled beam steering mirror ("output mirror") allowing the beam to be propagated in the laboratory. The output mirror is three-point mounted and can be adjusted for alignment using two micrometers.

The output beam is intercepted by a shutter mirror mid-way down the output channel and directed onto a copper cone, water-cooled calorimeter. The rise in temperature of the water in the calorimeter provides a measure of the output power of the laser accurate to ±5 per cent. The shutter remains in the path of the beam until a solenoid is activated, to flip the mirror out of the path of the beam in 200 ms. The solenoid is operated remotely by a push-switch. When the switch is released, the mirror shutter falls back under gravity into the path of the beam and the beam is terminated safely on the calorimeter.

4.2.3 The flight path and optical table

From the output mirror, the high power laser beam crosses the optical table and is terminated on a water-cooled load. The flight path is chosen to keep the high power beam as far as possible from personnel and equipment. A block diagram of the experimental set-up which also shows some of the precautions adopted for safe working is shown in Figure 4.1.

The optical table can be "floated" on vibration-isolation mounts to reduce the possibility of mechanical disturbance to the interferometers.

4.2.4 Laser beam termination

The high power laser beam is terminated on specially designed beam dumps shown in Figure 4.2 and 4.3. The idea of the "annular" beam dump of Figure 4.3 is due to Hirst [1]. The beam dump in Figure 4.2 overhangs the optical table but is located on a seperate stand and is, therefore, mechanically isolated from the experimental area.

4.2.5 Safety considerations

The laser safety guidelines recommended by the Committee of Vice-Chancellors and Principals [2] are followed during the experiments reported in this thesis. The MFK laser is a Class IV device and is fitted with a number of interlocks designed to assist safe operation. The laser is operated only by authorised personnel and can only be started with a special key. The laboratory is locked during the operation of the laser. Once the laser is running, the beam is terminated inside the covers of the laser head enclosure. The beam can only be propagated into the laboratory by activating the push-switch. This switch is manually operated and cannot be locked in the "on" position. If any of the interlocks are triggered (by opening the laboratory door, for example), the laser shuts down automatically and the discharge is switched off.

Laser safety guidelines suggest that high power beams are confined inside "flight tubes" when propagated in the laboratory environment. In order to ensure that the results of the experiments are not distorted by the presence of cylindrically symmmetric enclosing structures, this

guideline was not followed. Instead, the experimental area is designated an "exclusion zone" and personnel remain behind the perspex safety screen when experiments are in progress (the idea being to confine the people rather than the beam).

4.2.5.1 Alignment procedures

The experiments reported here require the accurate alignment of high power laser beams, low power diagnostic laser radiation (HeNe laser), microwave beams, a zoom lens, annular beam directors and other optical components. Careful and safe alignment procedures were developed. A brief overview of these procedures is given here:

(1) The high power beam is tracked and aligned using burn patterns made on perspex sheets. First, a pattern is taken close to the beam dump and the perspex sheet is left in position. Then, a pattern is taken at the point on the optical table closest to the laser head and the perspex sheet is left in position. The MFK laser is then switched off.

(2) The laboratory is darkened and a HeNe laser is directed up the high power laser beam track. Although the perspex sheets are damaged by the high power beam, if the exposure is short enough, the HeNe laser can still shine through the perspex. The HeNe beam is adjusted until it goes through the centre of the damage on the perspex sheets and enters the output aperture of the MFK laser.

(3) The perspex sheet nearer the MFK laser is removed and, by opening the front cover of the laser head and activating the shutter solenoid, the alignment beam can be seen entering the discharge tube. The alignment beam is adjusted so that

it travels down the centre of the discharge tube. It can clearly be seen striking the first few cavity folding mirrors.

(4) A fire brick, angled away from the optical table, is placed so as to protect the alignment laser and associated optics. A perspex sheet is placed in front of the brick. The MFK laser is restarted and burn patterns are taken at the brick and close to the laser head as before. The MFK laser is switched off and the brick removed. The HeNe laser alignment is again checked. This procedure is repeated until the experimenter is satisfied that the alignment beam path and the high-power laser beam path are co-linear.

The HeNe alignment beam can then be used as a guide to position interferometer components and other diagnostics (the laser beam analyser for example). It is therefore only necessary to switch on the high power laser to check alignment or shortly before a series of experimental runs is made.

4.3 MFK laser performance and beam profile measurements

4.3.1 MFK laser performance

The MFK laser performs well. Rated to provide better than 1,000 W, the unit supplied to St Andrews reliably provided 1,150 W, running for periods of over 10 hours during sequences of experimental work. Breakdowns were experienced twice, when the wedged output coupler failed and had to be replaced. The first failure was caused by thermal stressing of the coupler after a "hot-spot" developed. The hot spot was caused by dust on the outer surface of the coupler. A fan blows filtered air across the face of the coupler to try to avoid this kind of

contamination. The second failure was caused by oil-mist contamination after failure of the oil-filter element. The design of the laser permits the replacement of the rear mirror and output coupler without the need to realign the laser. This was found to be the case.

4.3.2 High power Laser Beam Analyser ("LBA")

The LBA is manufactured by ALL Gmbh, Munich and supplied by Edinburgh Instruments. The LBA is of the rotating wire type reported by Lim and Steen [3]. The high-power laser beam passes through a cylindrical hole in the LBA. The hole is swept by a rotating wire which deflects a very small fraction of the laser energy onto two detectors, one of which registers the x-profile of the beam, the other the y-profile. A schematic due to Lim and Steen is shown as Figure 4.4. Signals from the detectors can be displayed on an oscilloscope which is connected to a printer for making hard copies. The LBA has a "Sync." output which can be used to trigger other diagnostic and recording apparatus when the laser is switched on. The laser's built-in calorimeter can be used to provide a calibration. Typical traces produced by the laser beam analyser are shown in Figure 4.5.

4.4 Measurement of refractivity change produced by a high power Gaussian laser beam using an optical interferometer

4.4.1 Introduction and theory

In Section 3.4, expressions predicting the refractive index change in atmospheric air caused by the passage of a high power laser beam were developed. In this section, experiments designed to detect the refractive index changes produced by the beam are described and results presented. In particular, we focus on the idea of the "dithered" Michelson interferometer which is the building block for our measurements at optical frequencies.

In the early stages of the experimental work reported in this thesis, attempts to measure the refractive index changes caused by the high power laser beam were not successful. Interferometers sensitive enough to detect the refractive index changes are also highly sensitive to noise (electrical and mechanical) and to air movement. In one of a number of discussions (Dawber [4]), the solution of a "dithered" Michelson interferometer was proposed. The implementation of the dithered Michelson described below, enables us to reject random air movement and other noise when we examine the output of the interferometer.

Consider a Michelson interferometer operating, *in vacuo* , with a well collimated beam and straight fringes. We interrogate the fringe pattern using two optical fibres an arbitrary distance apart (say one in the centre of the fringe pattern and one close to the edge). The output from the fibres is fed to two matched detectors. We impose a regular,

repetitive path difference by vibrating one of the interferometer mirrors using a piezo-electric driver and signal generator. The output of one of the detectors is used as the reference signal for a phase sensitive detector (PSD) and we look for the phase difference between the two detectors' signals. Since the light reaching each detector has travelled through different regions of the space making up the interferometer beam, any optical path difference between the light arriving at the detectors will result in the detection of a phase difference by the PSD. We will find a fixed phase difference between the two detectors providing that the time-constant of the phase detection is longer than the inverse frequency of the vibrating mirror (effectively we see the time-averaged phase difference).

If we now place the interferometer in the laboratory, air movements in the arms of the interferometer will cause random changes of phase. These changes will be small, of comparable size in both arms and will cause small variations in the constant phase difference imposed by the vibrating mirror, resulting in the addition of a small amount of "noise". By adjusting the PSD we can bias the output to read zero phase difference when the interferometer is in stable surroundings in the laboratory. Any systematic change between the paths sampled by the fibres will register as a phase change on the PSD. If we cause a phase change by heating the air in that part of the interferometer beam sampled by one of the fibres, we can record the PSD response and use it to calculate the refractive index change caused by the laser beam.

4.4.2 Experimental configuration and procedures

The experimental configuration is shown in Figure 4.6. The high power laser beam passes through one arm of the interferometer. The interferometer is implemented using a spatially filtered and collimated HeNe laser beam ("interferometer beam"). The interferometer beam diameter is chosen so that it is about 5 mm larger than the diameter of the high power laser beam. The collimation of the interferometer is checked by shining the beam on the far wall of the laboratory (about 10m away) and making sure that the beam diameter is constant.

The interferometer is aligned so that one of the fibre detectors "sees" a part of the fringe pattern that the laser beam passes through (which we designate the "signal" output) and the other "sees" an unperturbed region (which we designate the "reference"). To achieve the most sensitive response, fine adjustments are made to the interferometer mirrors so that both the signal and the reference fibres see a maximum of the fringe pattern, where the gradient of the intensity function is a maximum. This also has the benefit of allowing us to maximise the amplitude of the vibrating mirror without "splitting" through more than one fringe.

The reference output is amplified by a Low Noise Amplifier (AIM Electronics Limited LNA 133) and fed to the reference port of the EG&G 5210 Phase Sensitive Detector. The signal output is fed to the signal port of the PSD. The EG&G 5210 is unusual in that it provides a direct measurement of the phase difference between two incoming signals.

The interferometer is so sensitive that any vibration in the building which causes sonic shock (doors slamming or air movement in the laboratory, for example) interferes with the experiment. Air movement is minimised by sealing the laboratory with plastic sheeting and tape (exhaust gases from the laser are fed to the outside air through an exhaust duct) and prohibiting the movement of personnel or talking. The rectifiers in the laser control unit have forced-air cooling and the heated air is expelled into the laboratory close to the optical table. The effects of this on the experiment are minimised by fitting a deflector panel to the control unit which channels the heated air away from the optical table. Mechanical vibrations (from pumps operating nearby) are damped out by the optical table's vibration-isolation legs.

Once the output of the high power laser has stabilised and air movement in the laboratory has subsided, the laser shutter is opened and the interferometer response recorded by monitoring the output of the PSD. The LBA is used to monitor the condition of the CO_2 laser beam. The LBA also provides a synchronisation signal which is used to trigger the diagnostics. The synchronisation signal is monitored and displayed with the output of the PSD. This enables an independent measurement of the laser exposure time.

Before each shot, the temperature and humidity are recorded using the Vaisala probe (HMI 31). The interferometer alignment is checked and the PSD bias adjusted until it registers zero phase difference between the two detectors. When the laser is fired, the beam passes through one arm of the interferometer and some of the laser energy is transferred to the air. The resulting density change is registered by

the interferometer and recorded. The phase change between the two detector signals is a direct output of the PSD.

4.4.3 Results and discussion

Typical results are shown in Figures 4.7-10. It is noted that the results indicate a negative change. The results exhibit common features. After the CO_2 laser is switched on, there is a delay of about 100 ms before the interferometer reacts. Then, the phase changes linearly until the change reaches some peak after about 1 s. The linear changes measured compare favourably with the linear analysis Section 3.4.2. After the peak, the phase remains constant. When the laser is switched off, the phase again changes, tending to return to the value before the laser is fired. The time taken to return to its original state is about twice the time to reach the maximum excursion. A summary of the results shown in Figures 4.7- 10 is given in Table 4.2.

Figure	Maximum Voltage change (mV)	Time taken (s)	Slope (mV/s)	Refractive index change (parts in 10^6)
4.7	220	1.1	200	0.7
4.8	190	1.4	135	0.6
4.9	330	0.6	550	1.0
4.10	400	1.0	400	1.3

Table 4.2 Optical measurement results

The refractive index changes shown in Table 4.2 are calculated using the following procedure. The phase difference between the signal and reference is given by the equation

$$\theta = (k_1 - k_2).d \ , \qquad (4.4.3.1)$$

where k_1 and k_2 are the wave-numbers of the light that passes through the perturbed and unperturbed portions of the interferometer beam, respectively and d is the path difference. Substituting for k_1 and k_2 and rearranging, we find the following relation for the refractive index change caused by the beam as

$$\Delta n = (n_1 - n_2) = \frac{\lambda_0 \theta}{2\pi d} \ , \qquad (4.4.3.2)$$

where λ_0 is the vacuum wavelength of the interferometer radiation (633 nm) and d is the diameter of the high power laser radiation. The PSD gives a direct measurement of the phase (a phase change of ± 180° gives an output of ± 10 V) and so we can write

$$\theta = \frac{V}{V_{max}} \cdot \pi \ , \qquad (4.4.3.3)$$

to express θ in radians, where V is the signal voltage and V_{max} is 10V. From Equations 4.4.3.2 and 3 we can calculate the refractive index changes given in Table 4.2, assuming that the unperturbed refractive index has the value 1.000300.

4.5 Measurement of refractivity change produced by a high power Gaussian laser beam using a microwave interferometer

4.5.1 Theory

The measurements are made using the millimetre wave quasi-optical FM noise measurement system developed by the Millimetre Wave Group at the University of St Andrews and reported by Smith and Lesurf [5]. The system is normally used to measure the free-running FM noise characteristics of many types of diode at W-band. The system utilises a novel, matched, easily tunable quasi-optical cavity in reflection, to act as a carrier suppression filter. This can operate with matched cavity quality factors of several hundred thousand, with almost zero insertion loss, to provide an extremely high discriminator slope at low power levels. Although not designed specifically for measuring refractive index changes, the resonant cavity can be very sensitive to phase changes. Essentially, the system in this application is used as a very sensitive microwave interferometer of the Michelson type, using a calibrated source (rather than a test source) and a fixed cavity. Smith and Lesurf give the relationship between voltage fluctuation ΔV at the detector with frequency variation Δf as

$$\Delta V = V_B \frac{2Q}{f_0} \Delta f \ , \qquad (4.5.1.1)$$

where V_B is the height of the discriminator curve in volts, f_0 is the frequency of the calibrated microwave source and Q is the quality factor of the cavity.

4.5.2 Experimental configuration and results

The experimental configuration is similar to that used for the optical frequency measurements. The laser beam is fired through one arm of the resonant microwave cavity. A simplified schematic of the microwave equipment and the experimental configuration is shown in Figure 4.11. A schematic of the interaction zone between the microwave beam and the laser beam is shown in Figure 4.12. Some difficulties were encountered in setting up this experiment due to the space constraint imposed by the structure of the microwave cavity and the fact that the microwave beam was larger than the laser beam. These difficulties were overcome by some rearrangement of the microwave cavity (the half-cube construction makes this feasible) and by careful alignment of the laser and microwave beams. The microwave beam is Gaussian and so care must be taken to ensure that the laser beam passes through the centre of the microwave beam.

When the laser is fired, the air in the path of the laser heats, changing the effective length of the cavity and causing the voltage deviation of Equation 4.5.1.1. Typical results are given in Table 4.3 and Figures 4.13 - 4.16. In each case, the laser power was 1.15 kW.

Figure	Exposure period (s)	Total voltage change	Voltage change (mV/s)	Calculated frequency change (kHz)	Temp/RH C/%
4.13	3.5	124	35.4	11	27.2 / 26.2
4.14	2.6	184	70.8	15	23.6 / 27.6
4.15	4.8	70	25.0	6	22.7 / 28.4
4.16	2.5	62	26.0	5	22.8 / 28.4

Table 4.3 Microwave Measurement Results

We note that for this experiment V_B = 3.5 volts, f_0 = 90.0 GHz and Q = 150,000 and from Equation 4.1.1.1, we can calculate the frequency variation caused by the laser. The frequency changes produced by the laser correspond to range of refractive index changes between 6 parts in 10^8 and 2 parts in 10^7.

4.5.3 Discussion and conclusions

In this experiment, we have produced a maximum refractive index change of 2 parts in 10^7 which is one order of magnitude smaller than that produced at optical frequencies by the laser. We argue that the microwave result is actually the lower bound of the possible refractive index change because of the experimental configuration. Consideration of Figure 4.12 shows that the laser beam is smaller than the microwave beam and we should attempt to account for the effect of this on the results of the experiment by calculating an upper bound for the refractive index changes. The length of the cavity is

480mm and the microwave beam is Gaussian with a spot size of 20mm. The diameter of the laser beam is 10mm.

Consideration of the intersection of the two Gaussian cylinders, shown in Figure 4.12, enables us to calculate a correction factor, C_1, which allows us to compensate for the mis-match in beam sizes. The intensity for a transverse "slice" of the microwave beam is is given by

$$I = I_o \exp\left(-\frac{y^2}{w^2}\right). \qquad (4.5.3.1)$$

We note that the spot size of the microwave beam is 20 mm. If we assume that the laser beam is well-aligned with the microwave beam, then it will intersect with the central portion of the beam. To calculate our correction factor, we consider the ratio of the laser-intersected portion of the beam with the non-intersected portion of the beam using

$$C_1 = \frac{\int_0^{y_2} I \cdot dy}{\int_0^{y_1} I \cdot dy}, \qquad (4.5.3.2)$$

where C_1 is the correction factor for this example, 0 - y_1 is the positive y-coordinate range intersected by the laser beam and y_1 - y_2 is the remaining section of the microwave beam which does not interact with the laser beam. We assume that the interaction is symmetrical around the centre of the microwave beam.

Evaluating the integrals, we find, for C_1

$$C_1 = \frac{\mathrm{erf}\left(\frac{y_2}{w}\right)}{\mathrm{erf}\left(\frac{y_1}{w}\right)} . \qquad (4.5.3.3)$$

The value of y_2 is the radius of the microwave beam (20 mm). A plot of C_1 for the range of high power laser-beam radii 0 - 20 mm is given in Figure 4.17. The CO_2 laser beam has a radius of 5 mm and from Figure 4.17, we can see that $C_1 = 2$.

There is a second correction factor that we need to evaluate. Let us imagine an experiment where the entire length of the cavity is filled with a slab of dielectric. We would expect to have a much larger effect which scales linearly with the proportion of the length of the cavity filled by the dielectric. In this case, we compare the diameter of the laser beam compared with the length of the cavity and arrive at the second correction factor, C_2, of 48.

The total correction factor is given by the product of C_1 and C_2 and is of the order of 100. The results of the experiments and calculations yield a range of refractive index changes from a lower bound of 1 part in 10^7 to an upper bound of 1 part in 10^5.

4.5.4 Comparison of refractivity changes at optical and microwave frequencies

We note that the optical and microwave experiments of Sections 4.4 and 5, respectively, produce refractive index changes of the same order. In Section 3.4.1, for the linear case, calculated refractive index

changes for a 1 second beam exposure are given as 1 part in 10^5. For the doughnut mode, in the non-linear case (Section 3.4.2), we calculated a refractive index change of 3 parts in 10^4. In Section 2.7.4, we showed that, for guiding, index changes of 4 parts in 10^6 would be required. Thus, we can state that the refractive index changes produced by a CO_2 laser beam, measured by two independent methods, are of the same order as the refractive index changes required to produce an atmospheric waveguide.

4.6 Annular beam propagation

4.6 .1 Annular beam director

The prototype annular beam director ("ABD") is shown in Figure 3.4 and Plates 11-13. The ABD was manufactured by the mechanical workshop in the Physics Department of the University of St Andrews and used to test the idea. It was found to work reasonably well over short distances, but that difficulty aligning the central conical element ("axicon") caused widely diverging beams. No problems were experienced due to the heating of the support wires ("spider"), but they did act as diffraction centres degrading beam quality. It was also felt that some conditioning of the input laser beam was required to give more control of the beam divergence of the ABD. In particular, there may be some advantages in presenting a slightly converging input beam to the ABD. The eventual design is shown in Figure 4.18 together with a list of important specifications. Note that the problems of a spider support structure have been solved by mounting the optical elements on a zinc selenide flat. The ABD was manufactured by

SPECAC Limited of the UK to our design specifications. The ABD is combined with a multi-element zoom lens (x2 beam expander V&S Scientific, Model BE25/200) which can be used to correct for the divergence of the laser and any divergence due to the ABD itself.

4.6.2 Zoom Lens and Annular Beam Director Alignment Procedures

The high-power laser beam track is located in the way described in Section 4.2.5.1 and a HeNe laser aligned co-linearly with it. The zoom lens is mounted on an x-y mount and adjusted until the HeNe beam (which is just visible through the zinc selenide) enters the output aperture of the laser. The alignment of the zoom lens is checked by taking burn patterns down the beam line and the zoom lens adjusted until the beam is the same diameter at the beam dump as at the laser head. The zoom lens is then locked in position.

The ABD is 5-axis mounted. It is placed in position and adjusted until the HeNe alignment laser beam (which is just larger than the centre axicon of the ABD) travels through the zoom lens and enters the output aperture of the laser. Burn patterns are taken and, if necessary, small adjustments can be made to improve the symmetry of the annular beam. Typical annular beam patterns are shown in Figure 4.19 as sections across the x-y plane. Shown for comparison is the calculated pattern based on the results of Section 2.1.

4.6.3 Annular Beam Director Performance

No problems were encountered with the ABD itself. Damage (cracking) was caused to the output element of the zoom lens. This damage ocurred at the same time as the failure of the output coupler of the MFK laser. It seems likely that beam degradation of the high power beam could have been a contributory factor. The manufacturers of the zoom lens report that such failures are quite likely in zinc selenide components operating at high power for long periods.

A major difficulty in working with the ABD is the problem of alignment. The central axicon is small and even a slight error in alignment with the laser leads to a strongly asymmetrical output annulus. Given the need to operate safely, it is not possible to adjust the ABD while the CO_2 laser is running and the laser cannot be operated reliably at low power. One possible solution would be to redesign the ABD positioning system, incorporating remotely-operated micro-positioning elements. As the ABD is so sensitive to tilt, particular consideration should be given to this. Remotely operated positioners would enable adjustments to be made while the high power laser is running. Finally, we could consider mounting the zoom lens and ABD close together on a mounting plane. If the ABD were three-point mounted on the plane with z-translation and tilt/pan then this would ease alignment and produce a compact and reasonably robust one-piece device.

4.7 Experimental verification of laser-generated atmospheric waveguide

In this section, earlier experimental arrangements are combined in experiments designed to verify guiding of microwave radiation by a laser waveguide. The overall set-up is shown in Figure 4.20. The MFK laser head is shown in Plate 14. The laser beam analyser is placed at the end of the beam line, close to the beam dump to monitor the profile of the annular beam. A CCD camera (not shown in Figure 4.20) is mounted on the optical table and is used to monitor the condition of the beam dump.

4.7.1 The optical system

The optical system is the dithered Michelson described in Section 4.4. It is used as a diagnostic and calibration aid, sensing the refractive index change continuously during the course of the experiments. To provide a suitable reference signal, the output of one of the fibres was amplified using a low-noise amplifier (AIM Electronics Limited LNA 133) before being fed into the EG&G 5210 phase sensitive detector.

4.7.2 The microwave system

The microwave source is an InP Gunn diode operating at 78 - 89 GHz. The diode feeds a corrugated horn producing a Gaussian microwave beam. The signal generator which drives the oscillator also provides the reference signal for the EG&G 5210. The microwave detector is

based on a Farran SD012-014-01 diode. The corrugated horns were supplied by Thomas Keating Ltd. Both the oscillator and detector blocks were manufactured by the Millimetre Wave Group at the University of St Andrews.

To couple the radiation into, and out of, the annular laser beam, two polished copper disks are used. The disks are mounted on thin wire supports, set into studs. The studs fit into standard optical mounts which are fixed to the optical table. We shall refer to these items as "microwave reflectors".

The microwave reflectors are aligned in two stages. First, the reflector closest to the microwave detector (R2) is put in position with the face of the disk in a plane normal to the optic axis (we define the optic axis as the centre of the annulus of the high power beam). We rotate R2 through a small angle to avoid back-reflections to the ABD and zoom lens should a portion of the high power laser radiation strike it. The high power laser is switched on, the LBA output is examined and a burn pattern is made. Small adjustments are made until the experimenter is satisfied that the copper disk of R2 is positioned in the centre of the annulus. The support wire can be used as a guide. The reflector is positioned in this way because it will have the largest cross-section with respect to the central "hole" in the laser beam. This helps to ensure that R2 is as close to the centre of the annulus as possible. The reflector nearest the oscillator, R1, is aligned in the same way.

We replace the microwave detector with a thin beam from the HeNe laser. We rotate R2 on its stud until the HeNe beam strikes the back of R1. Then, we rotate R1 until the HeNe beam strikes the centre of the

output horn of the oscillator. R2 and R1 are adjusted in turn until the HeNe alignment beam strikes their centres and then the centre of the output horn of the oscillator.

To check whether or not the microwave reflectors would be affected by the high power laser beam heating the support wires, the HeNe alignment beam is reflected from each of them in turn and directed to the back wall of the laboratory some 10 m away. The HeNe spots do not move even when the high power laser is switched on for several minutes.

The microwave detector is put into position and adjusted until the output from the detector is at a maximum. The output from the detector block is fed to the input of the EG&G 5210. Low signal-to-noise ratios were encountered as the microwave beam is diverging and R1 and R2 are similar in size to the output horn of the oscillator. One way of increasing the signal strength would be to add collimating and focussing elements to the microwave system. Unfortunately, these were not available during the course of these experiments. Another solution is to use the annular beam dump described in Section 4.2.4. The annular beam dump and microwave detector are shown in Figure 4.3. The curved section of waveguide is to help reduce the possibility of damage to the diode from the CO_2 laser. There could also be an effect on the diode output due to heating and this would contribute to noise power. Measurements were made with both experimental arrangements. Three views of the beam track and various components are shown in Plates 15-17.

4.7.3 Experimental procedure

Once the laser and associated diagnostics have been set up, the experimental procedure is comparatively straight-forward. The high power laser is started and allowed to warm-up and stabilise. Before each experimental run, the laser power is recorded and the temperature and humidity in the beam track are measured using the Vaisala probe.

Once the air in the room has stabilised, the high power laser is fired and the output of the microwave detector, the interferometer and the sync. pulse of the LBA are recorded on Tektronix digitising oscilloscopes (Model 2440). The output of the LBA is also monitored on a Tektronix analogue oscilloscope (Model 2235).

4.7.4 Results

Typical results are shown in Figures 4.21 - 4.23. Figure 4.21 is with the initial configuration (with R1 and R2 in position), the remaining figures are with R2 removed and the annular beam dump in use. The process and time-scales indicated by the results are as follows:

(1) The high power laser is switched on and for about 500 ms, the microwave signal drops slightly;

(2) Thereafter, the microwave signal begins to rise and takes about 1s to reach a maximum. If the laser continues to fire, the microwave signal remains constant.

(3) When the laser is switched off, the microwave signal falls and over 1s falls back to a value close its original value.

The results are consistent and repeatable and show clear evidence that the high power laser is forming a guiding structure increasing the amount of microwave radiation which reaches the target by some factor to be evaluated in the analysis below.

To quantify the guiding effect we need to calculate the acceptance angle for the waveguide using the results from the annular beam dump experiments. We assume that since the divergence angle of the microwave transmitter is relatively large (of the order of 30°) and R1 is small compared to its distance from the transmitter, then R1 is uniformly illuminated and defines the position of the beam waist. We also assume that any components of the microwave beam which enter the overmoded waveguide are detected. We therefore calculate the power, P_0, received at the detector by integrating the Gaussian microwave beam profile across the aperture of the overmoded waveguide and we find

$$P_0 = \int_0^{\theta_0} D.I_0 \exp\left(\frac{-D^2\theta^2}{w^2}\right).d\theta \ , \qquad (4.7.4.1)$$

where D is the distance from R1 to the detector, I_0 is a constant, θ is the propagation angle of a microwave ray to the optic axis and w is the spot size. The spot size is given by Equation (2.4.3) and we note that as R1 is inclined at an angle of 45° to the optic axis, the spot size at R1 is given by $w_0 = r/\sqrt{2}$, where r is the radius of R1. When the guide is formed, the total power at the detector, P_1, is given by

$$P_1 = \int_0^{\theta_1} D.I_0 \exp\left(\frac{-D^2\theta^2}{w^2}\right).d\theta. \qquad (4.7.4.2)$$

We now define the guiding power ratio by

$$R \equiv \frac{P_1}{P_0} \qquad (4.7.4.3)$$

and assume that the detector response is linear. Combining Equations (4.7.4.1 - 3) and integrating, we obtain an implicit relation for θ_1 in terms of R and the known experimental parameters as

$$R = \frac{\operatorname{erf}\left(\frac{D\theta_1}{w}\right)}{\operatorname{erf}\left(\frac{D\theta_0}{w}\right)}. \qquad (4.7.4.4)$$

A plot of R against θ_1 is given in Figure 4.24 and from this graph, we can read off the acceptance angle of the guide from the guiding power ratio. Before the laser is switched on, the detector intercepts all rays with propagation angles in the range ± 5 mrad. With reference to Figures 4.22 and 4.23, we see that the power received by the detector increases by a factor of 1.5 some time after the laser is switched on. The propagation angle equivalent to this ratio, given from Equation (4.7.4.4) is 7 mrad. This is the measured acceptance angle of the atmospheric waveguide. It is interesting to note that an increase in received power of 1.5 is the equivalent to reducing the range by a factor of $\sqrt{1.5}$. This experiment was performed over a 1m range; it is reasonable to assume that an experiment over a somewhat longer range (perhaps 100m) would yield a dramatic increase in received

power when the guide is formed. The experimental results are in agreement with the models studied in Chapter 3, which predict weak coupling in the case where the beam divergence of the radiation to be guided is large and there is a mis-match between the source and the numerical aperture of the guide.

4.7.5 Summary and conclusions

In Section 2.7.4, we calculated that a refractive index change of 4 parts in 10^6 would be capable of generating a waveguide provided that the annular beam and the microwave beam could be aligned to better than 3 mrad. The results of the calculations of Section 3.4.2 produced refractive index changes of 1 part in 10^5 in 900 ms. In the optical and microwave experiments (Sections 4.4 and 4.5) we measured refractive index changes of 1 part in 10^6. The EREPS simulation program indicates that, for refractive index changes of the order of 1 part in 10^6, guiding of rays with propagation angles somewhat less than 10 mrad should occur. The theoretical prediction is confirmed by the results of the guiding experiments.

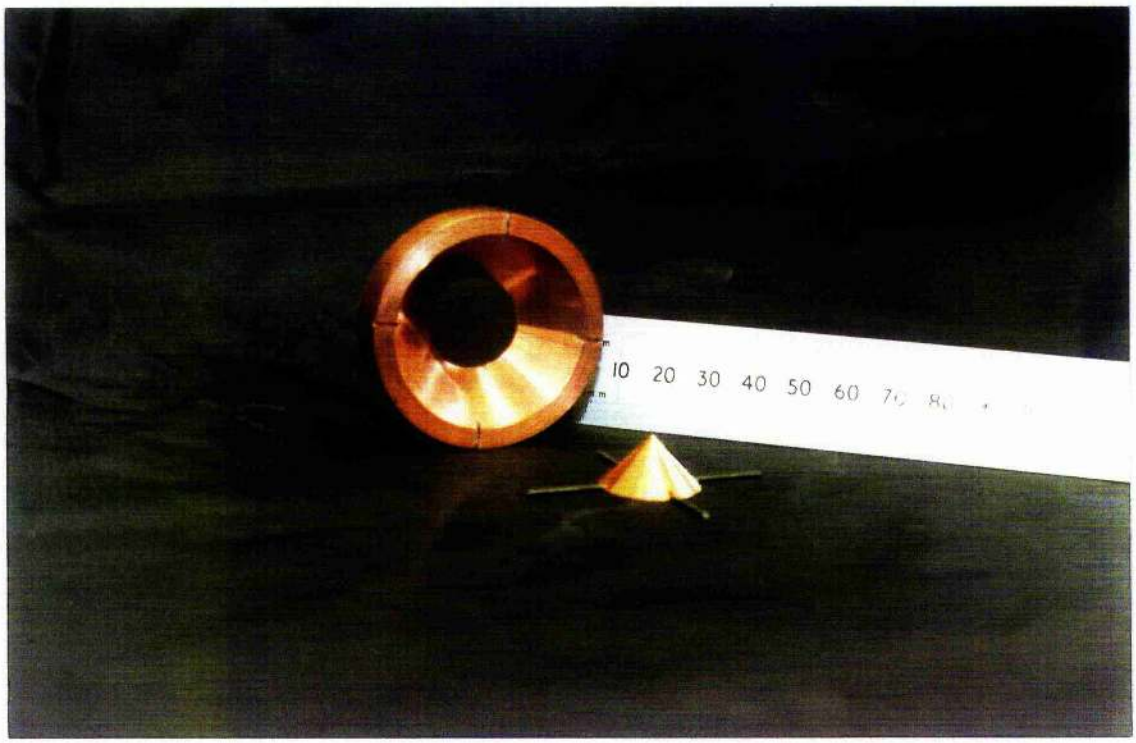

Plate 11

Annular Beam Director ("ABD") prototype components

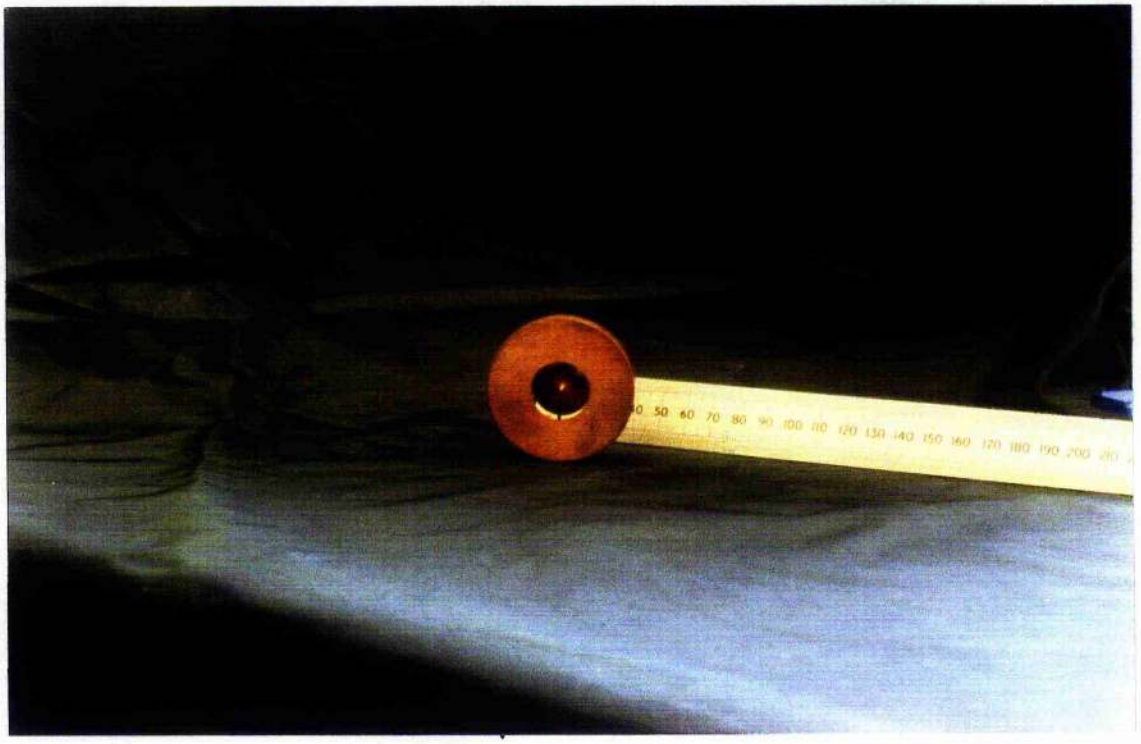

Plate 12
ABD prototype input side

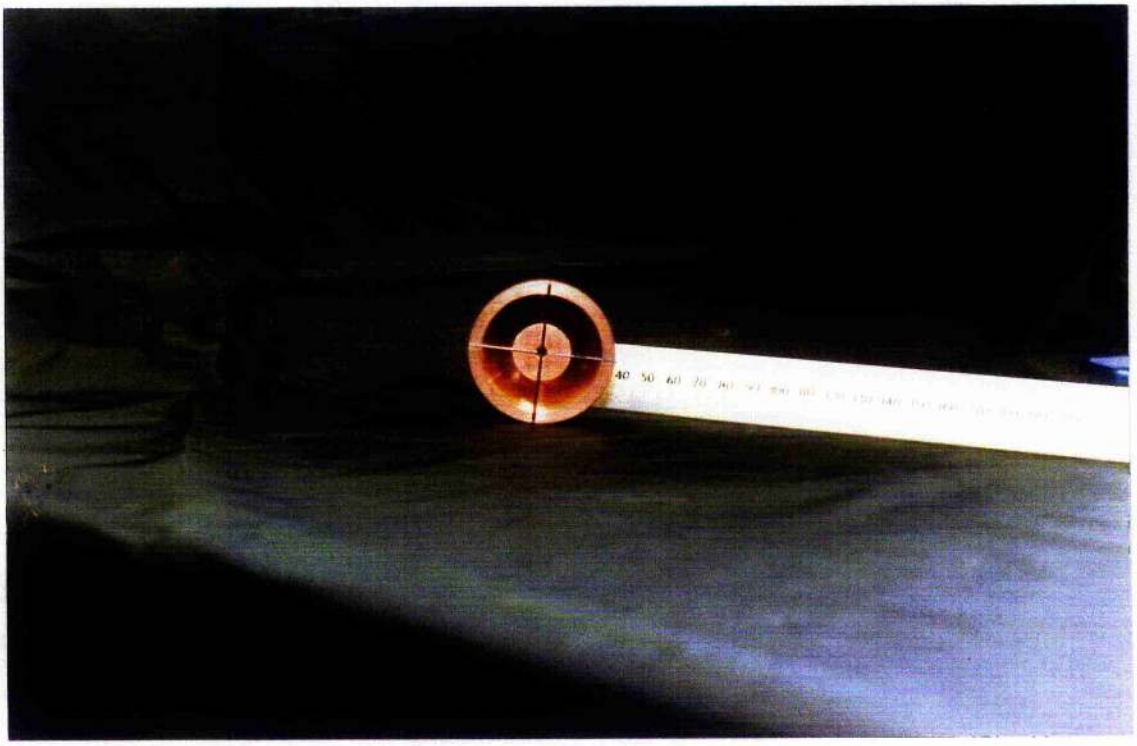

Plate 13
ABD prototype output side

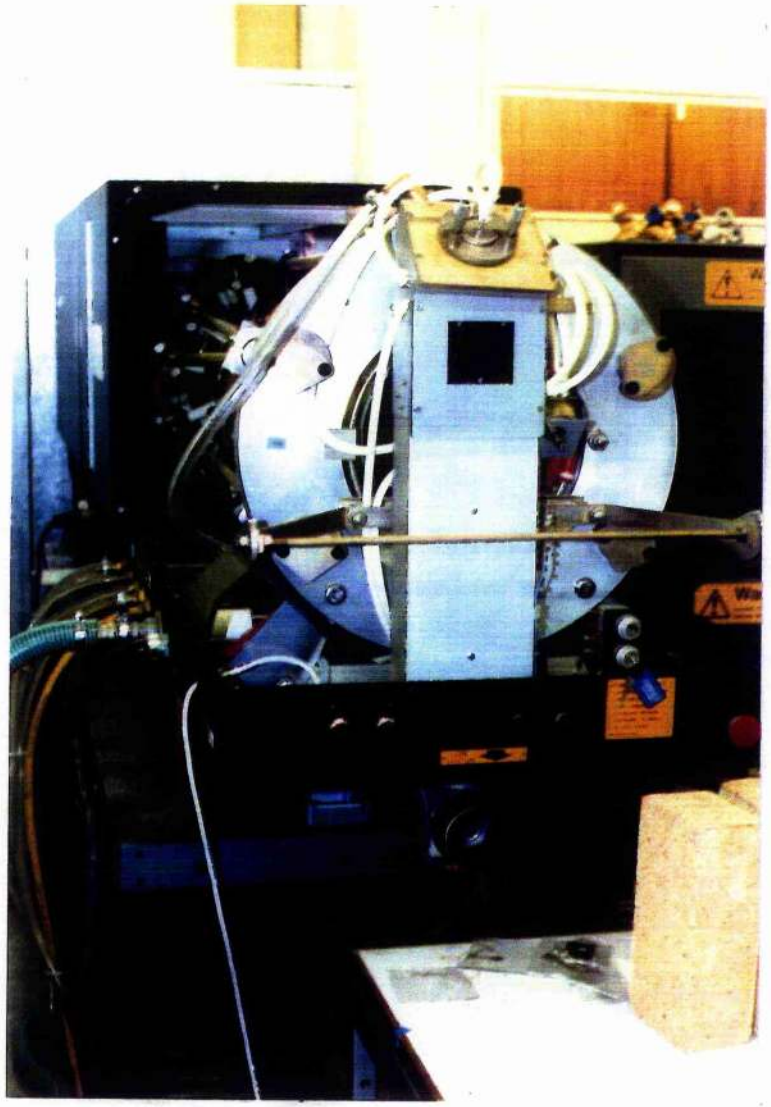

Plate 14

MFK laser-head (cover removed)

Plate 15

Laser beam track showing ABD and microwave reflector
(beam expander not shown)

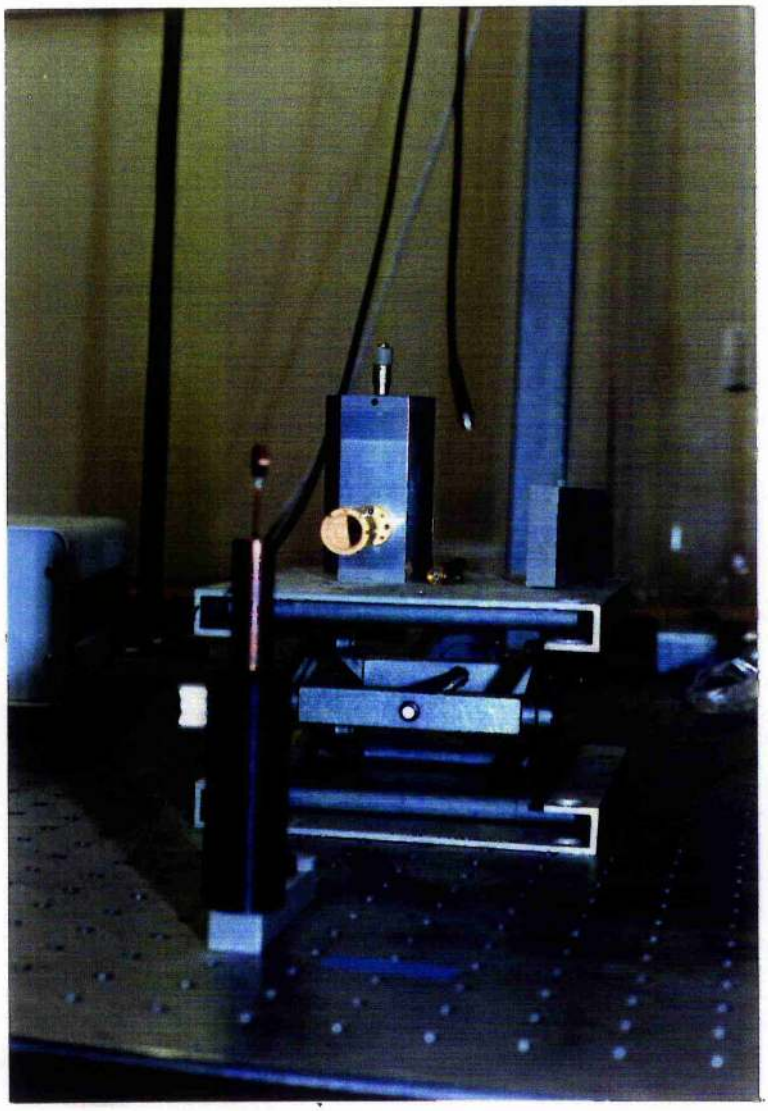

Plate 16

Microwave source with reflector

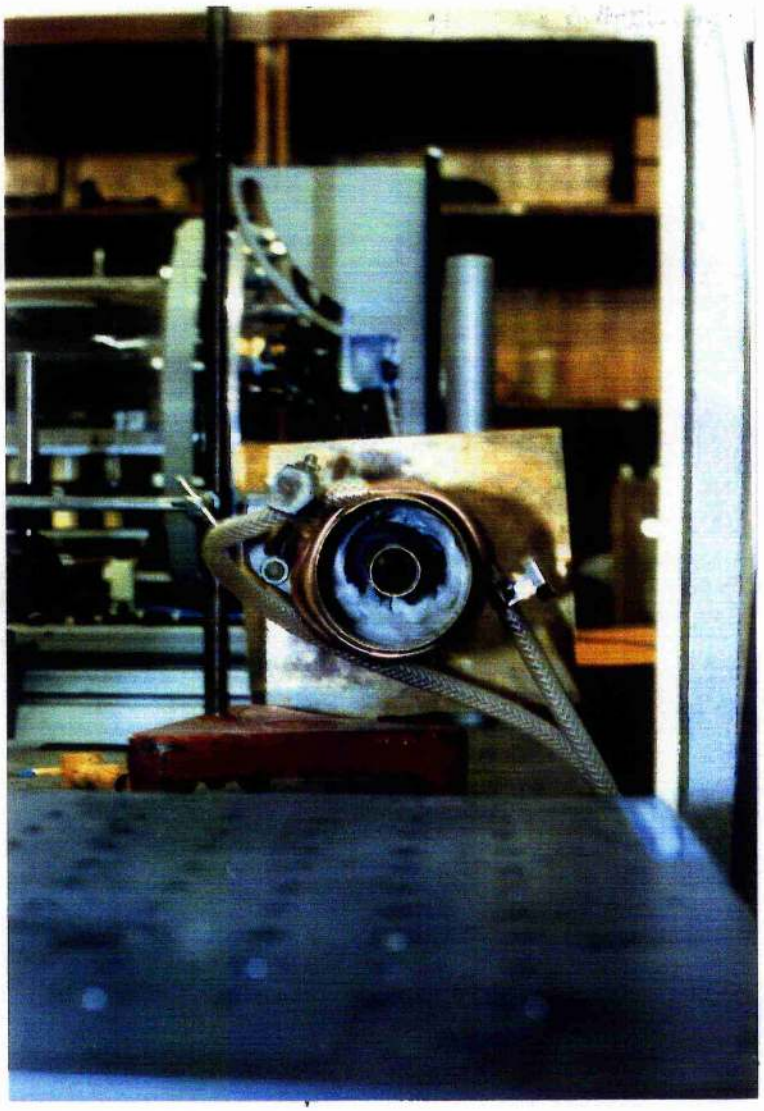

Plate 17

Annular beam dump

FIGURES FOR CHAPTER 4

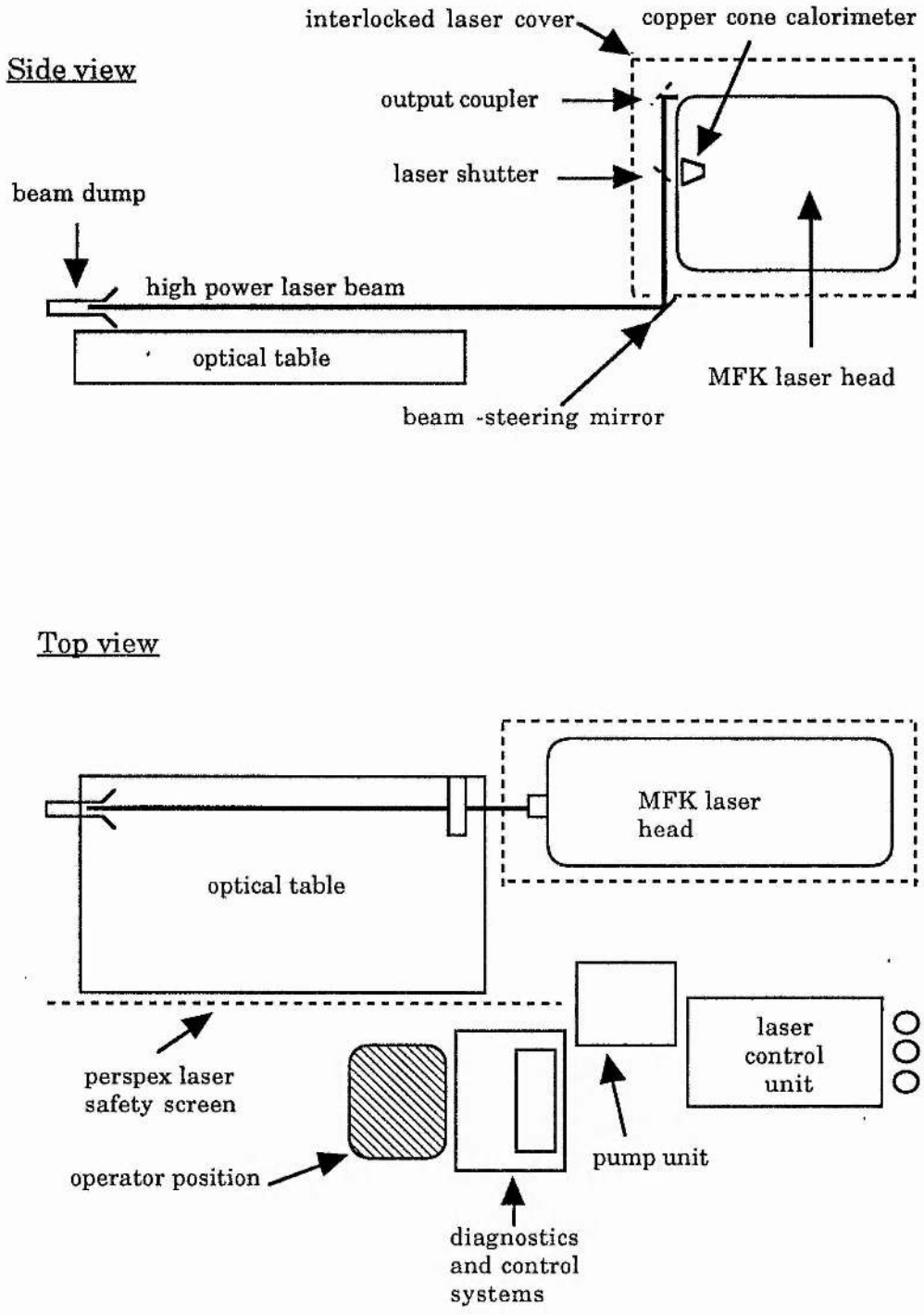

Figure 4.1 Block diagram of the experimental set-up

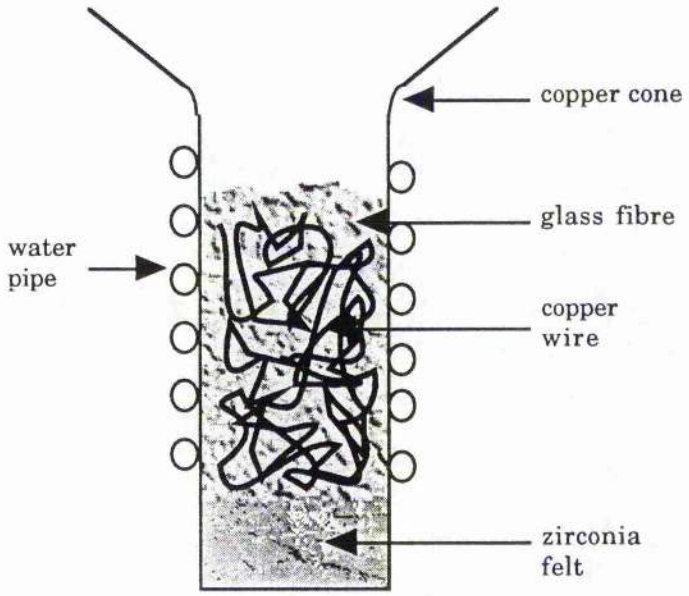

Figure 4.2 Water cooled beam dump

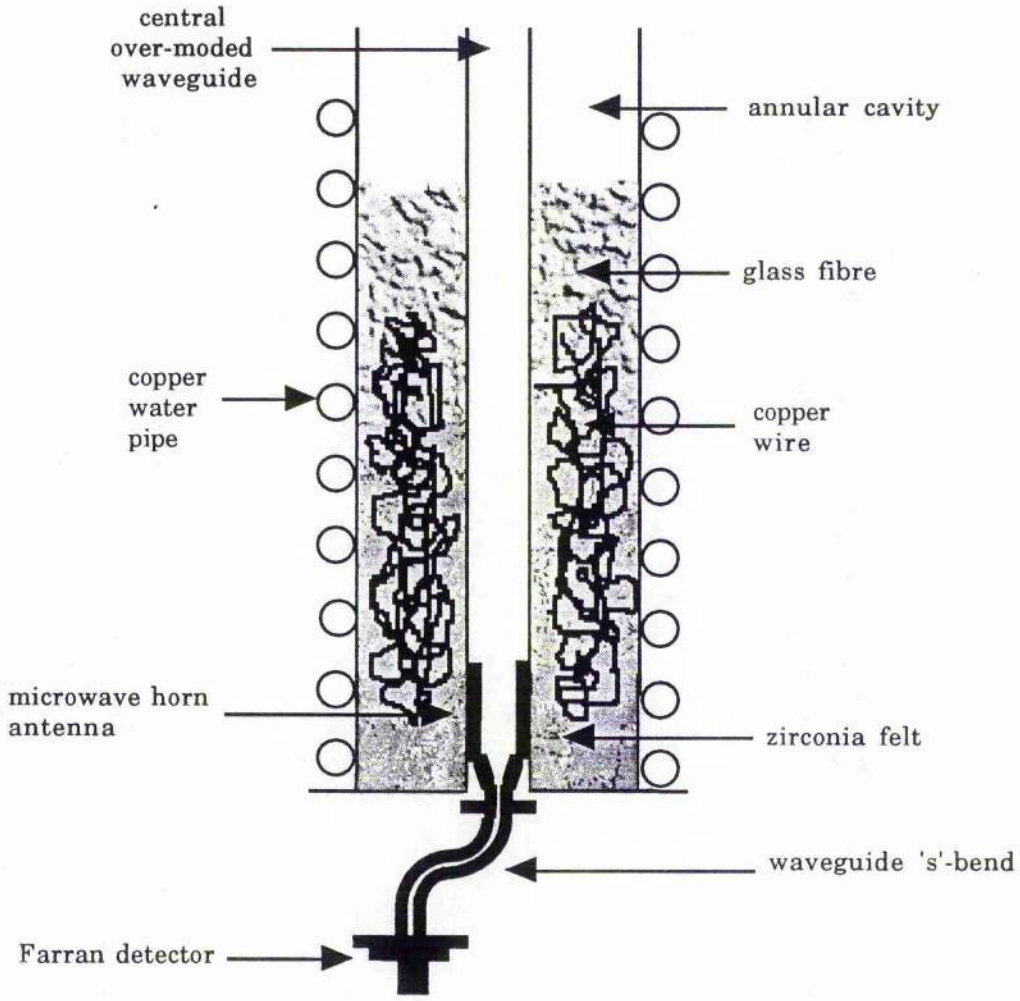

Figure 4.3 "Annular" beam dump

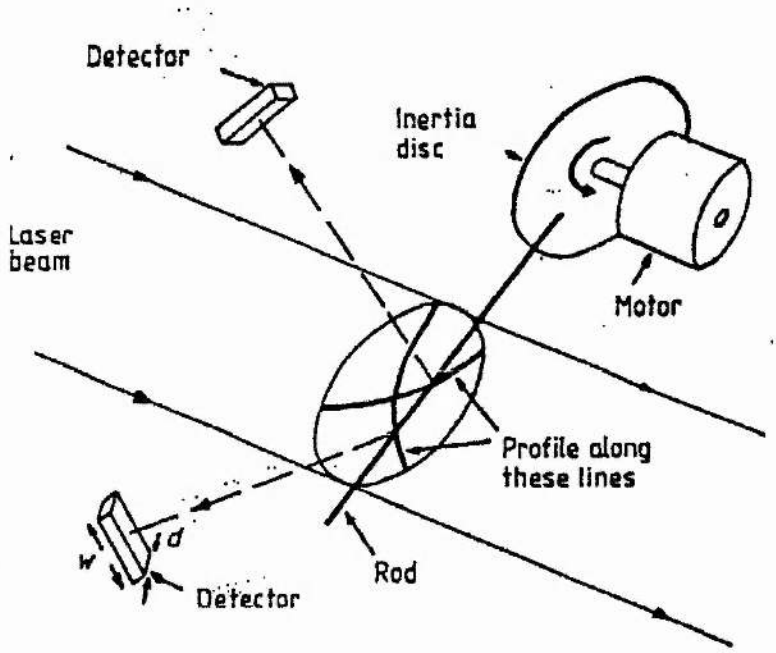

Figure 4.4 LBA schematic

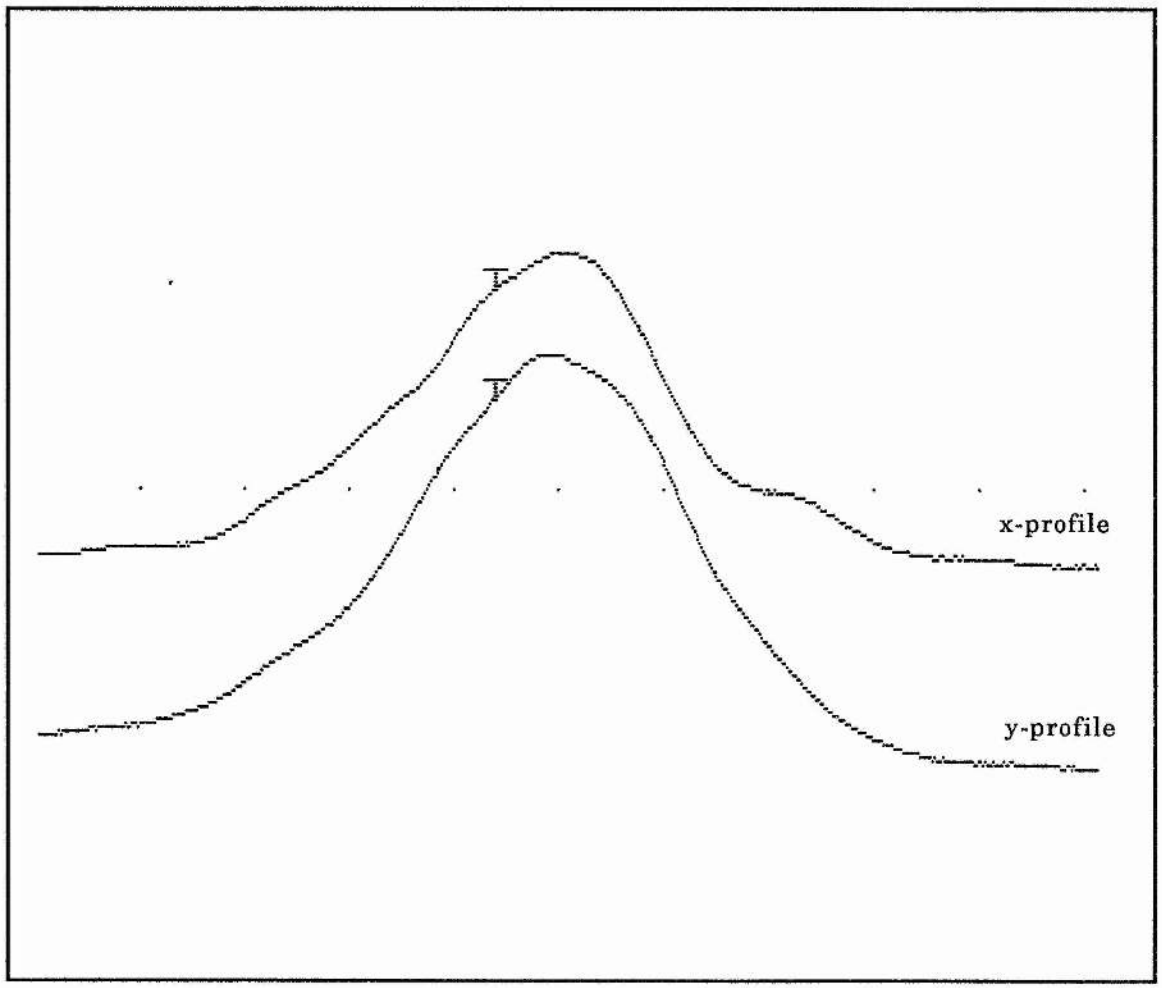

Figure 4.5 LBA traces

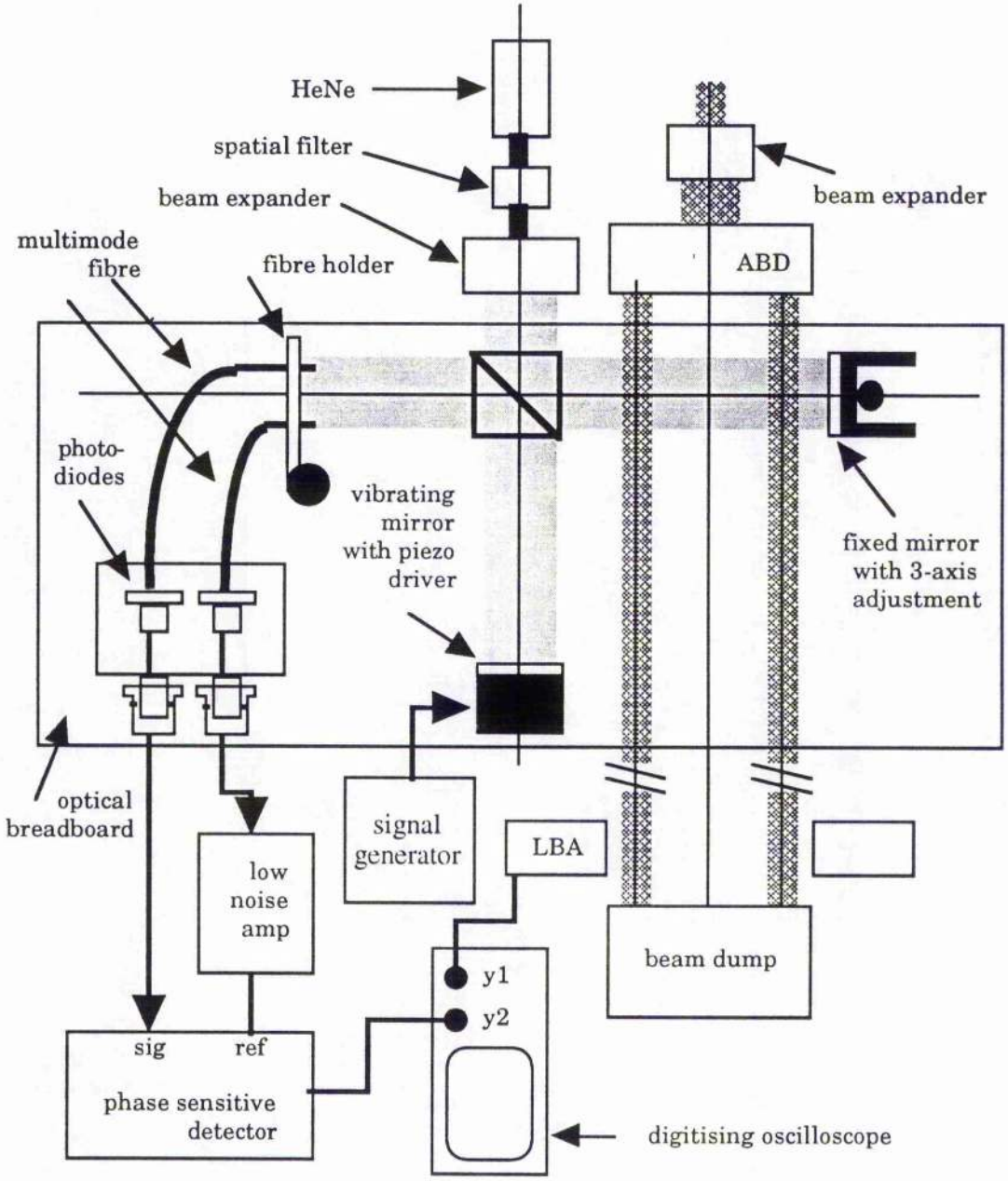

Figure 4.6 Schematic of the optical experiment

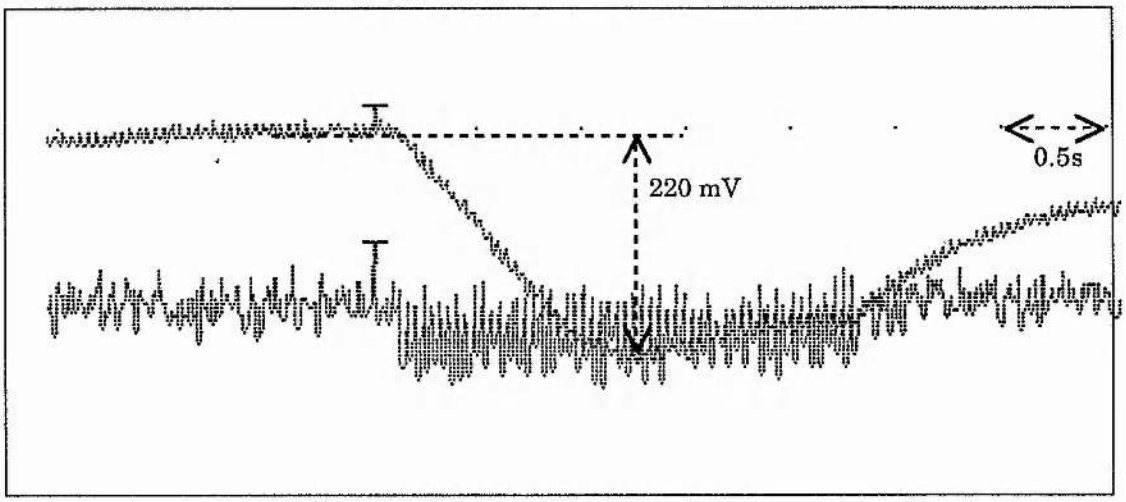

Top trace: interferometer response (output of PSD)
Bottom trace: Sync signal from the LBA, "T" indicates laser switch on, sync output is a series of pulses during the laser on time.

Figure 4.7 Output of optical interferometer

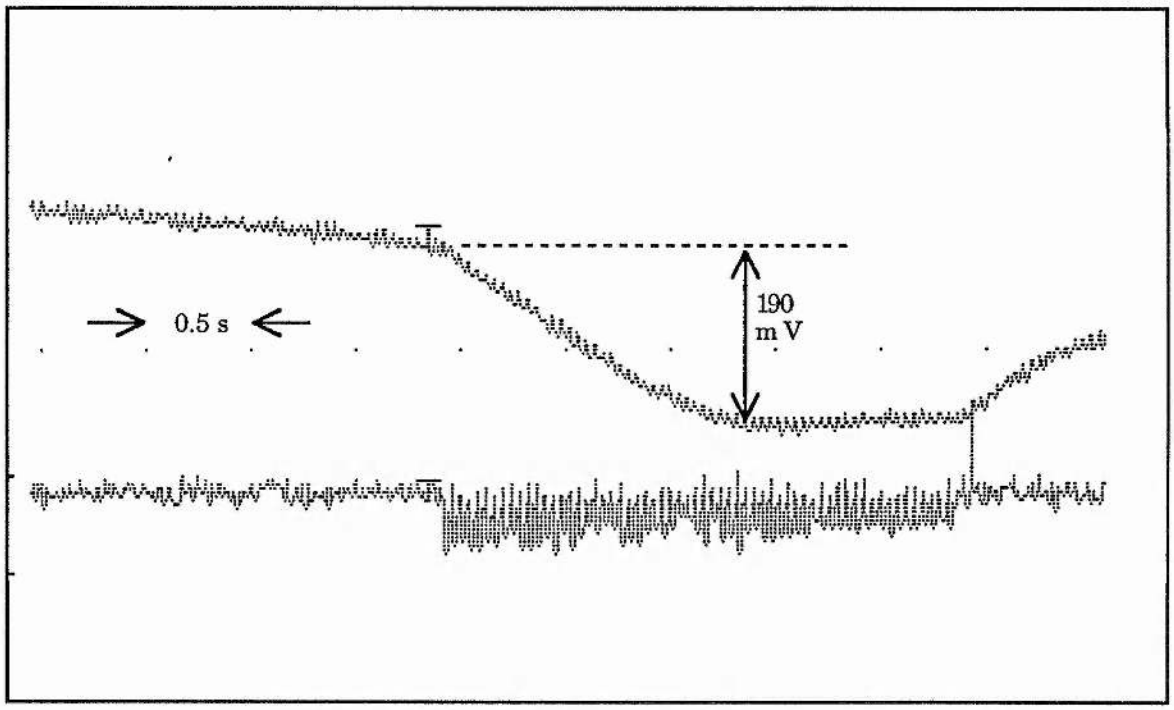

Top trace: interferometer response (output of PSD)
Bottom trace: Sync signal from the LBA, "T" indicates laser switch on, sync output is a series of pulses during the laser on time.

Figure 4.8 Output of optical interferometer

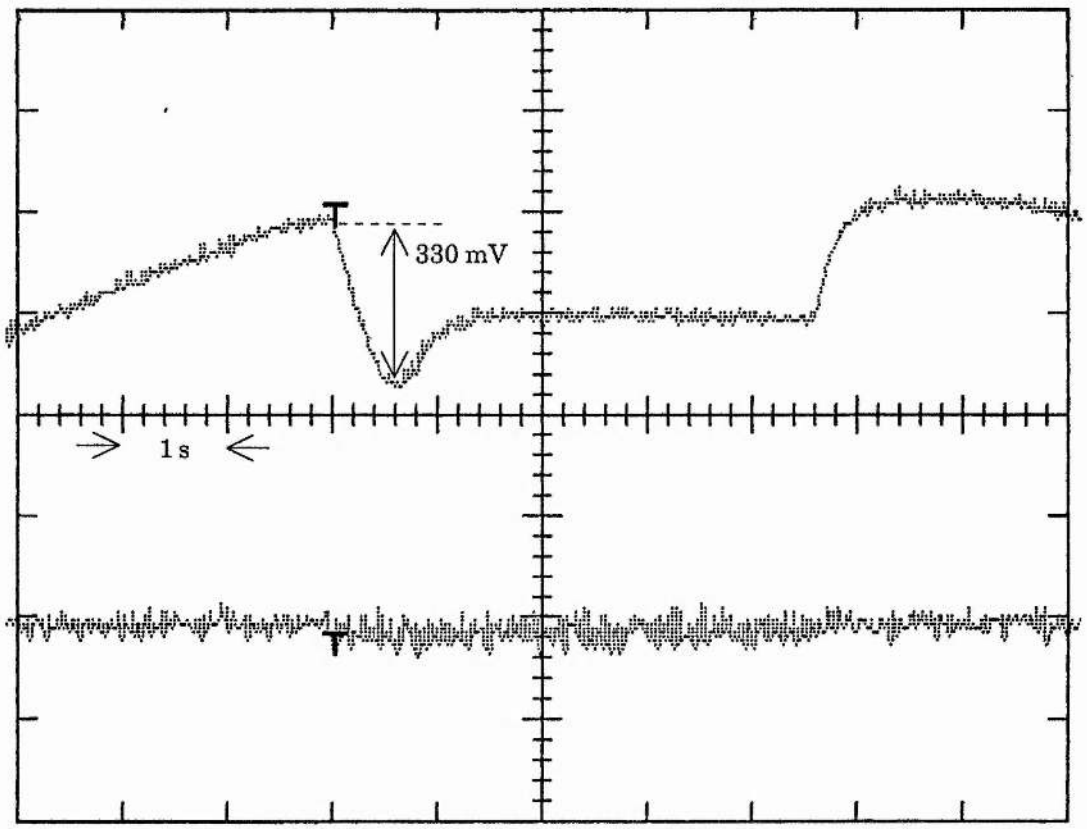

Top trace: interferometer response (output of PSD)
Bottom trace: Sync signal from the LBA, "T" indicates laser switch on, sync output is a series of pulses during the laser on time.

Figure 4.9 Output of optical interferometer

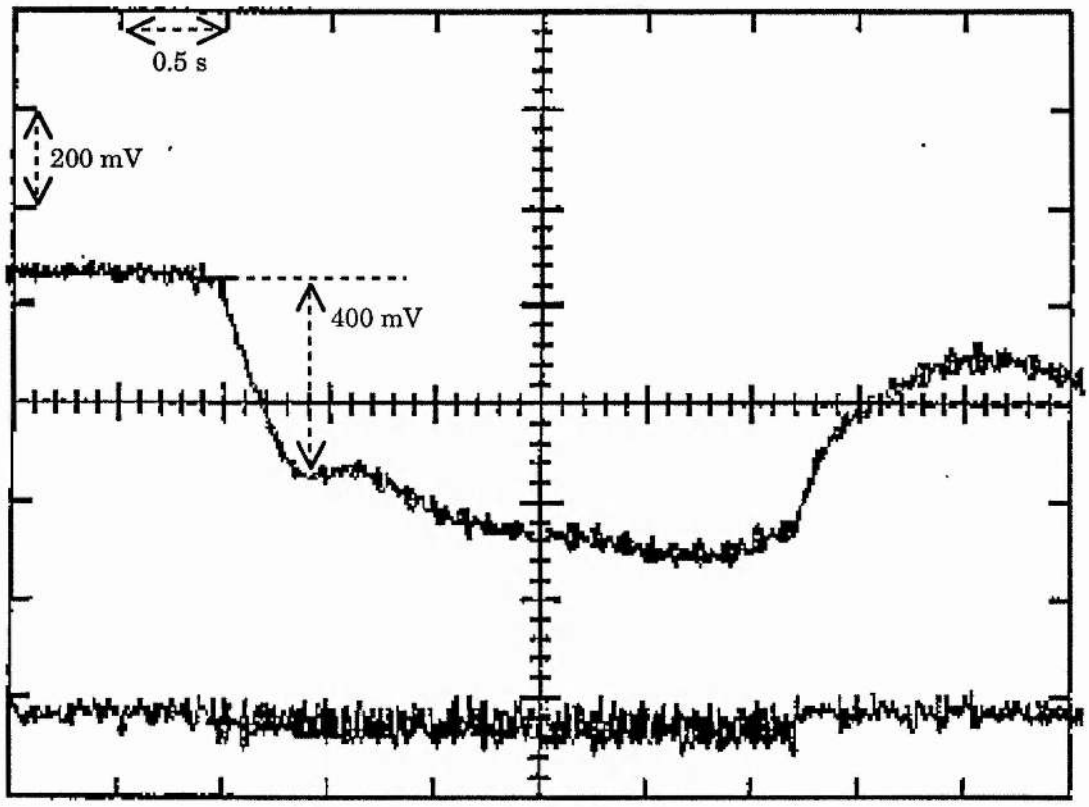

Top trace: interferometer response (output of PSD)
Bottom trace: Sync signal from the LBA, "T" indicates laser switch on, sync output is a series of pulses during the laser on time.

Figure 4.10 Output of optical interferometer

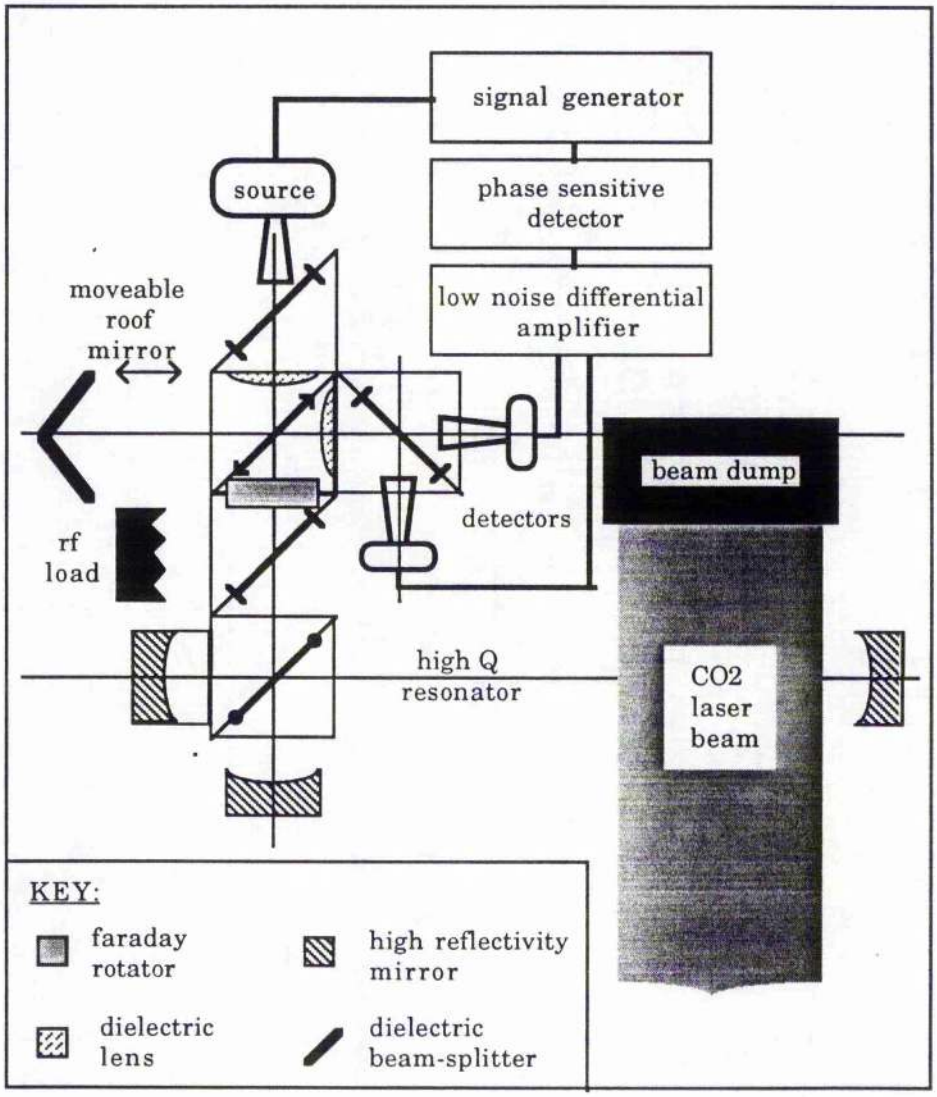

Figure 4.11 Schematic of microwave interferometer

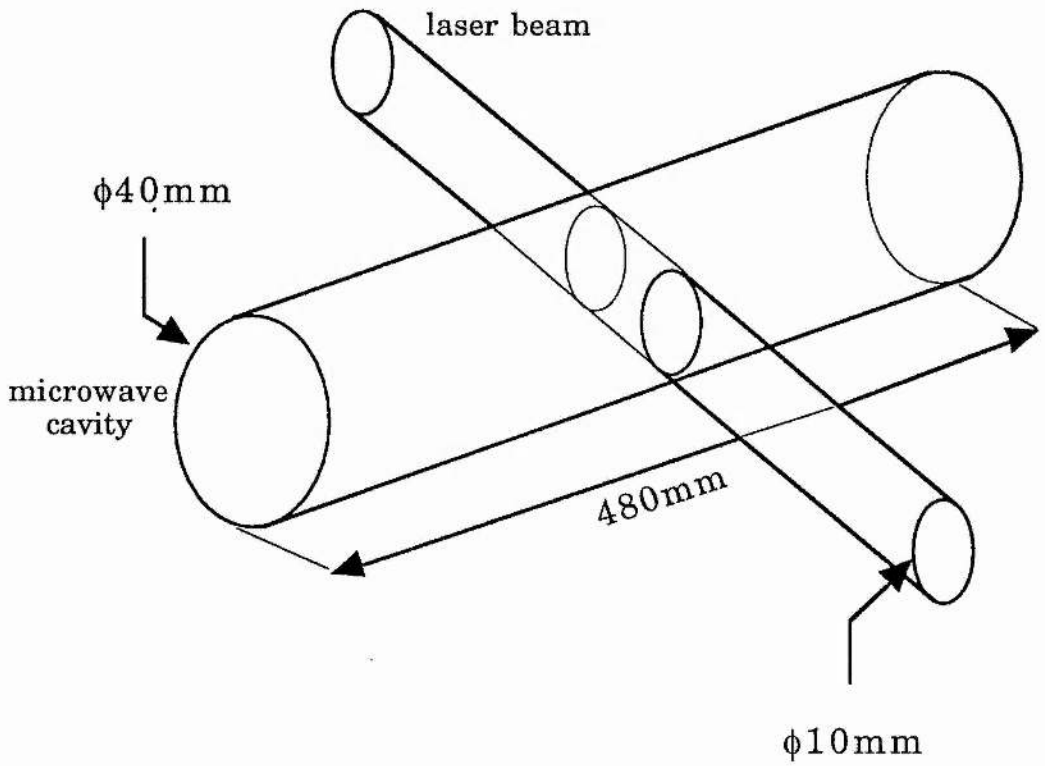

Figure 4.12 Schematic of the microwave and laser beam interaction zone

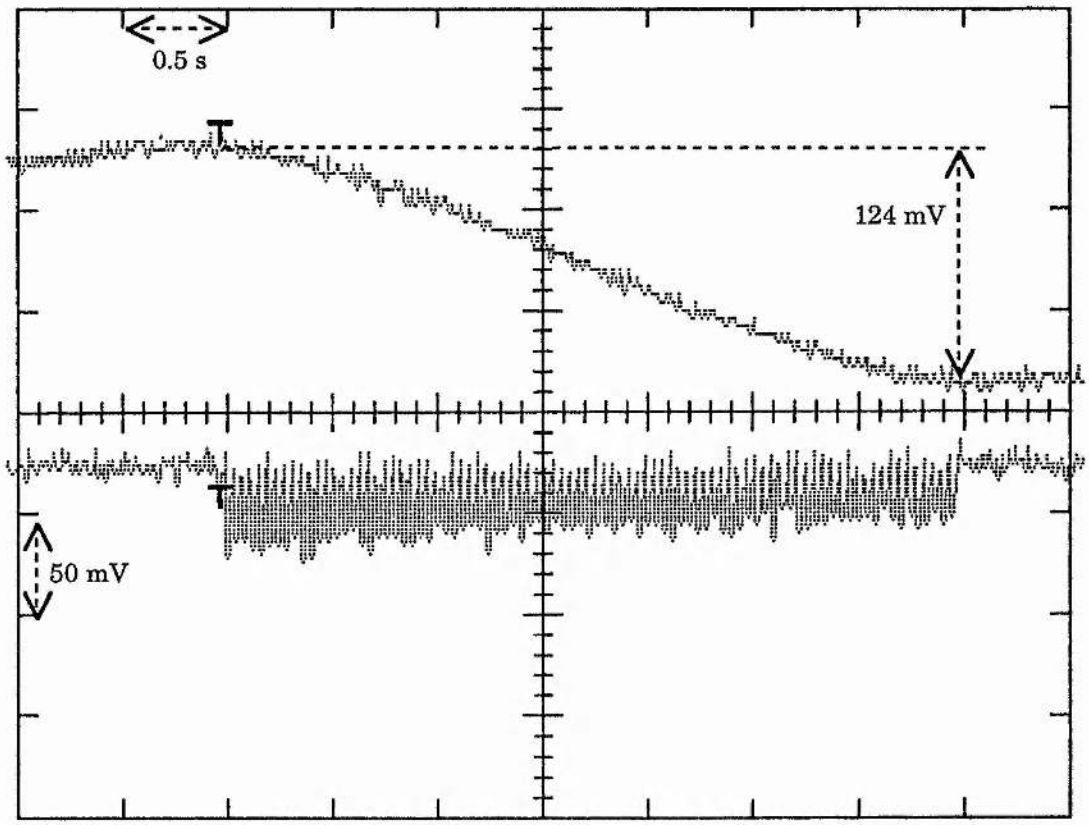

Top trace: interferometer response (output of PSD)
Bottom trace: Sync signal from the LBA, "T" indicates laser switch on, sync output is a series of pulses during the laser on time.

Figure 4.13 Output of microwave interferometer

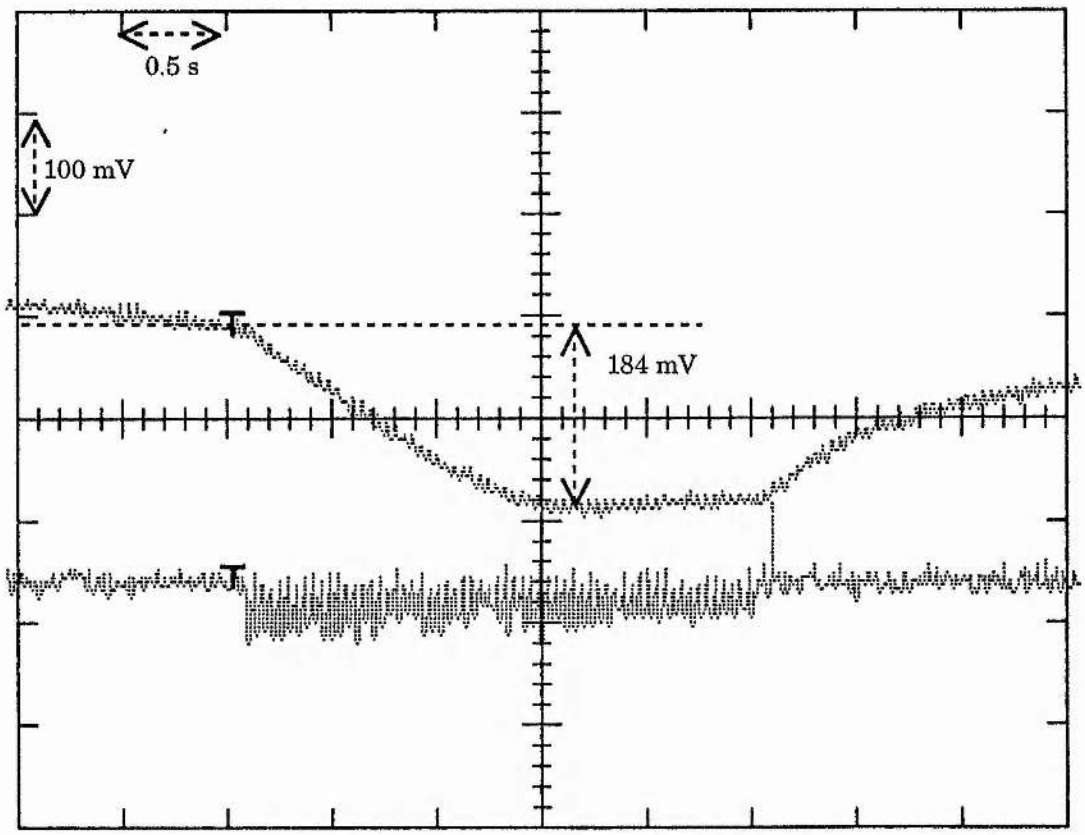

Top trace: interferometer response (output of PSD)
Bottom trace: Sync signal from the LBA, "T" indicates laser switch on, sync output is a series of pulses during the laser on time.

Figure 4.14 Output of microwave interferometer

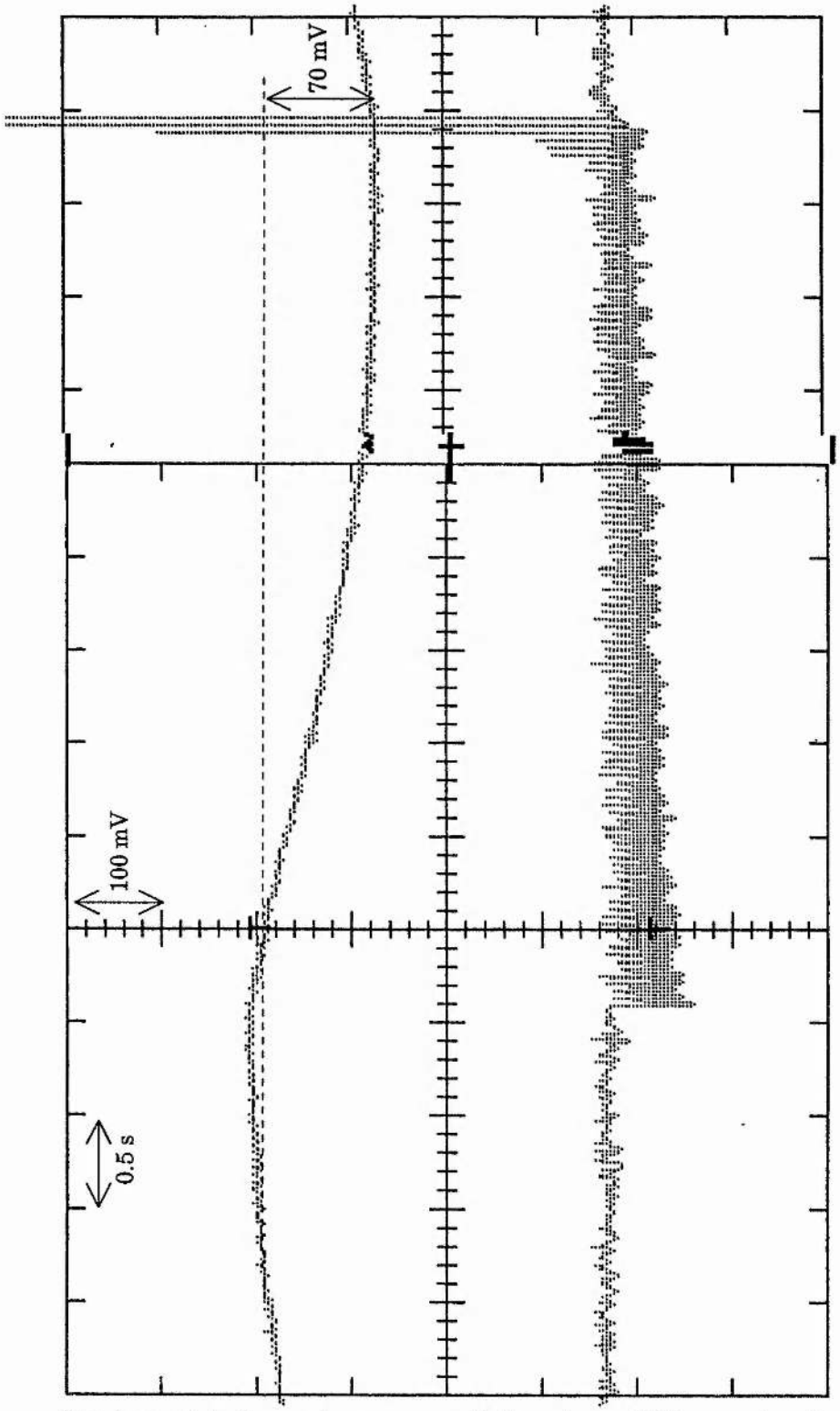

Top trace: interferometer response, Bottom trace: LBA sync signal

Figure 4.15 Output of microwave interferometer

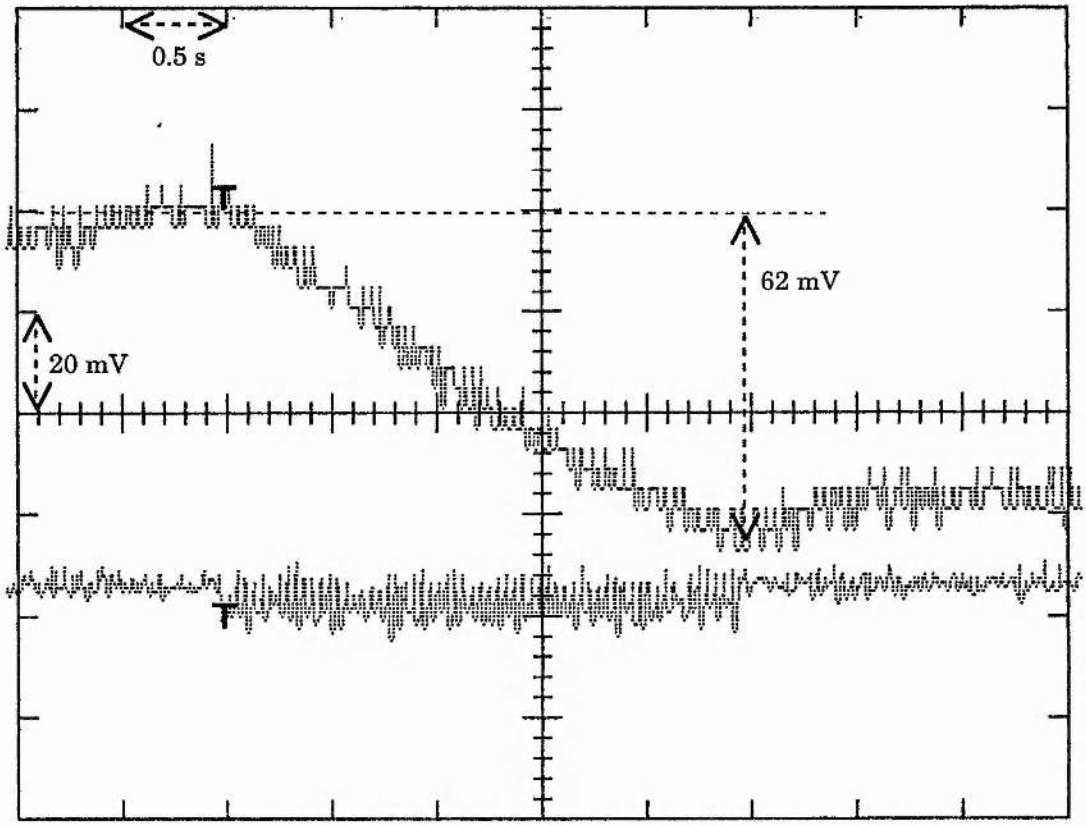

Top trace: interferometer response (output of PSD)
Bottom trace: Sync signal from the LBA, "T" indicates laser switch on, sync output is a series of pulses during the laser on time.

Figure 4.16 Output of microwave interferometer

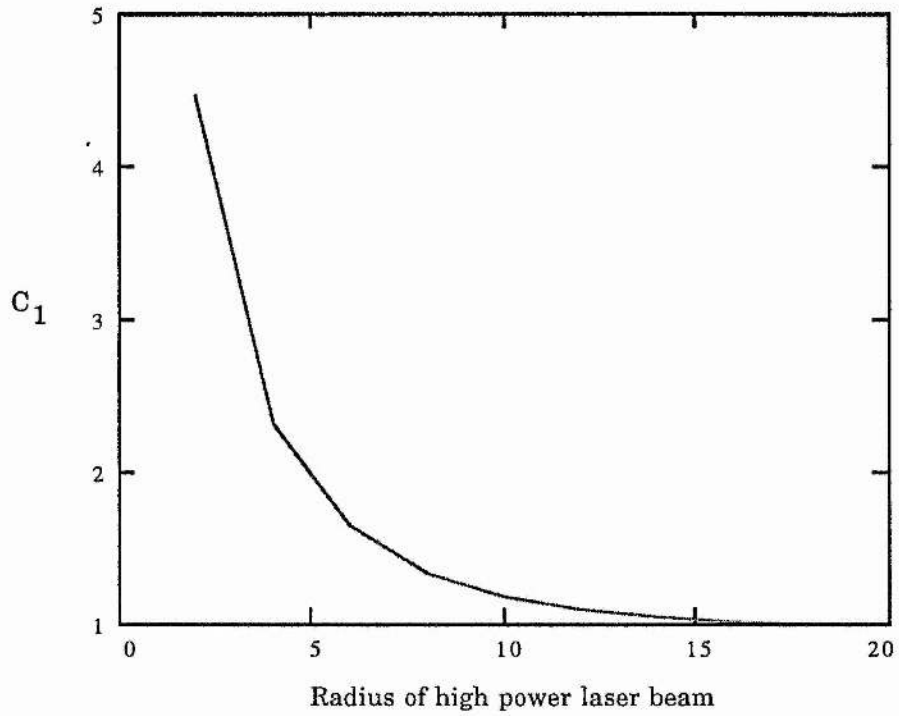

Figure 4.17 Correction factor plot of Equation (4.3.3.3)

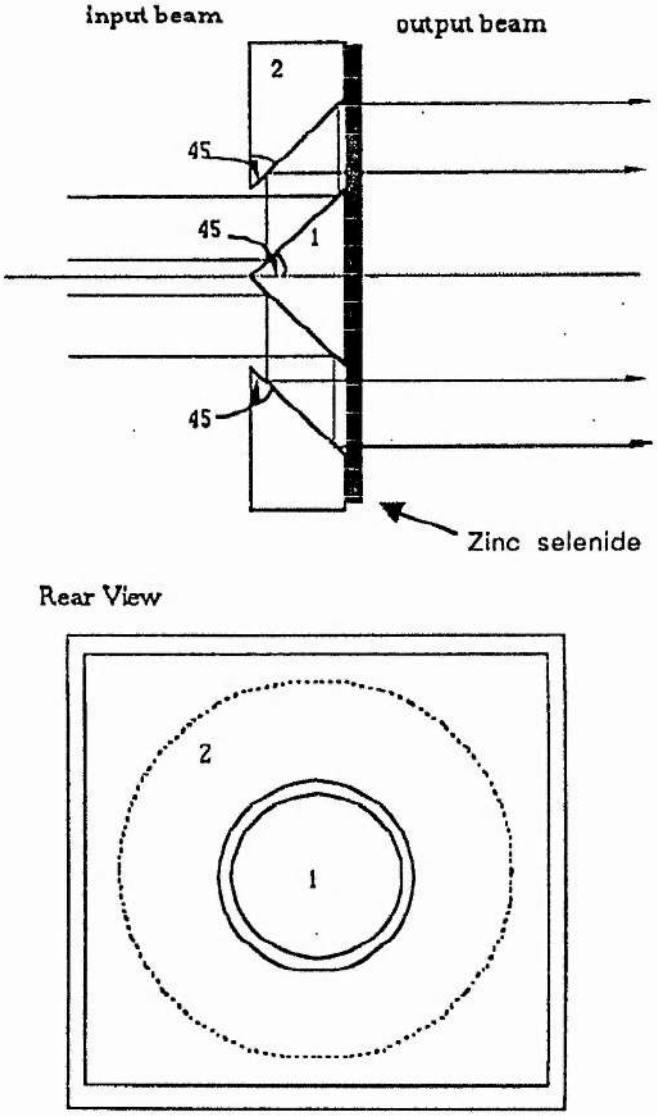

Figure 4.18a ABD design

Specification

Input Beam

1200 W Carbon Dioxide laser with 11 mm beam diameter and far-field divergence of 2 milliradian.

ABD

Collimation	Less than 1.2 milliradians
Obstruction diameter	20.5 mm
Clear aperture diameter	40.0 mm
Reflecting surfaces	Single point diamond machined copper with a 0.01 mm RMS surface finish
Reflectivity	98.8% at 10.6 μm
Window material	Zinc selenide
Form error	λ/5 at 10.6 μm over used annulus

Beam Expander

X2 Beam expander with focus facility (2.3m to infinity) to minimise laser divergence.

All optics water cooled.

Figure 4.18b ABD specification

ABD Performance

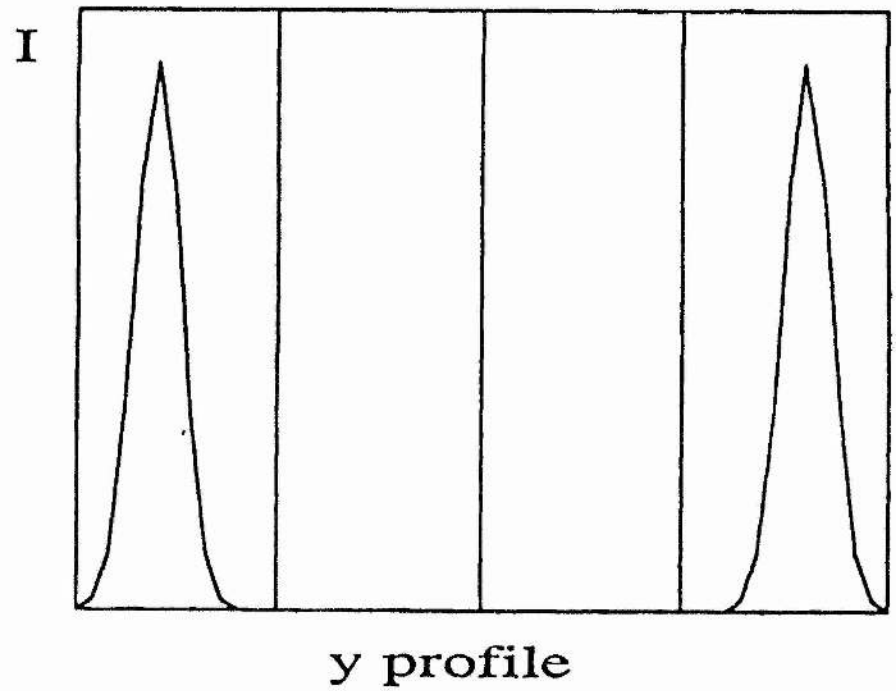

Figure 4.19a Comparison of calculated (above) and measured (below) annular beam profiles, indicating ABD performance.

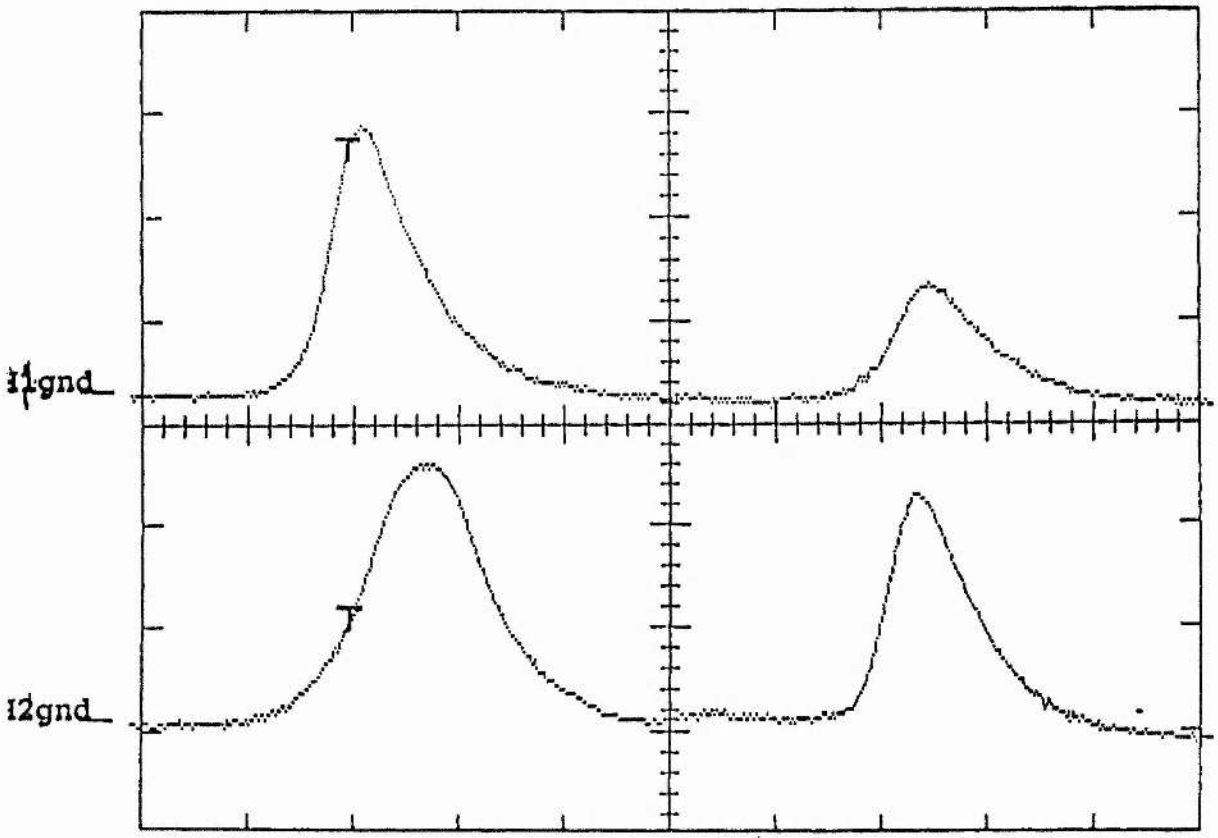

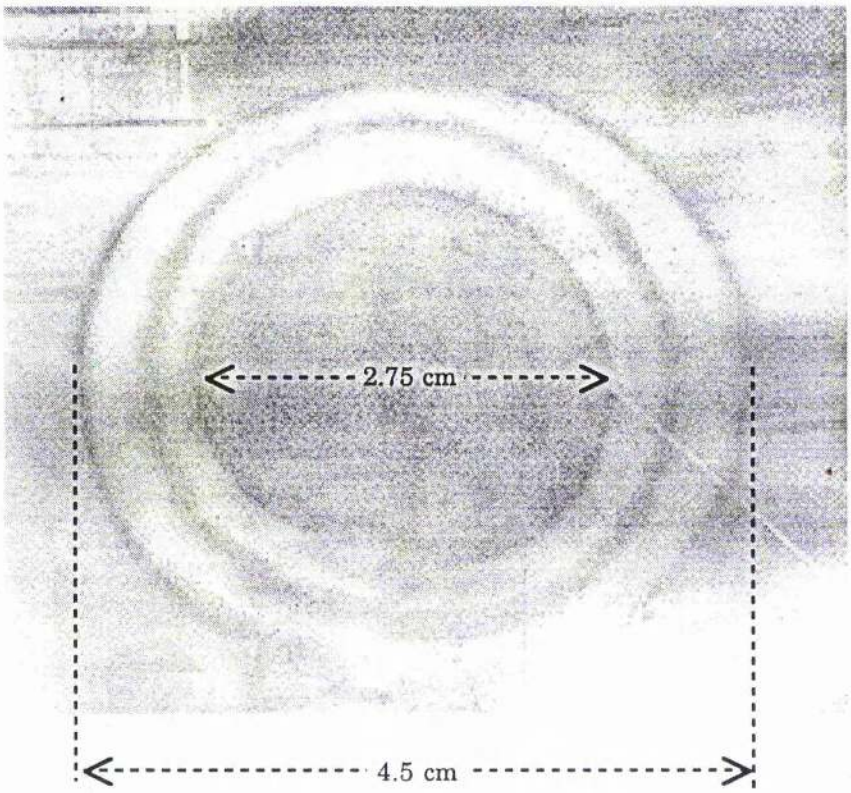

Figure 4.19b Annular burn pattern

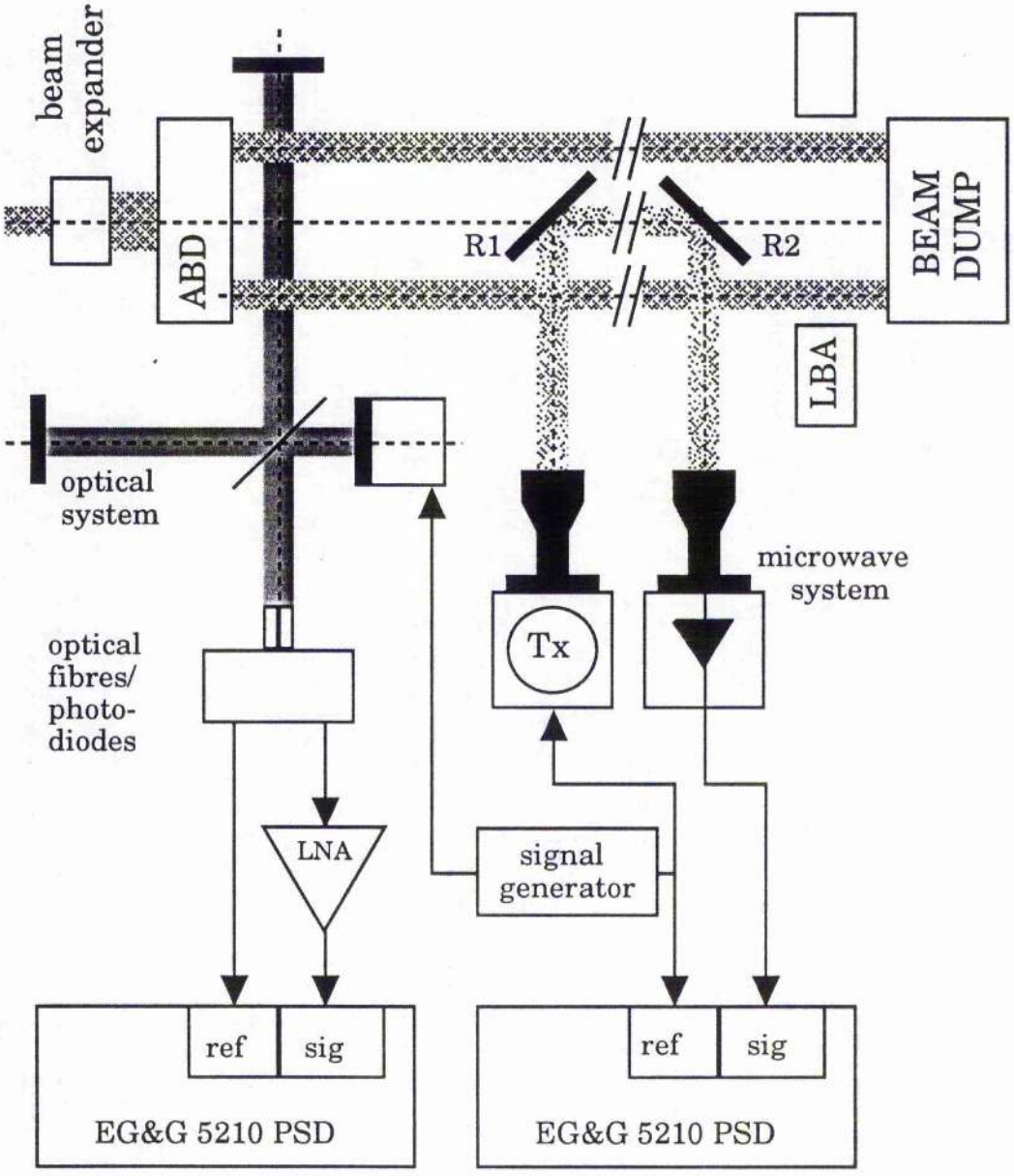

Figure 4.20 Experimental arrangement for guiding experiment

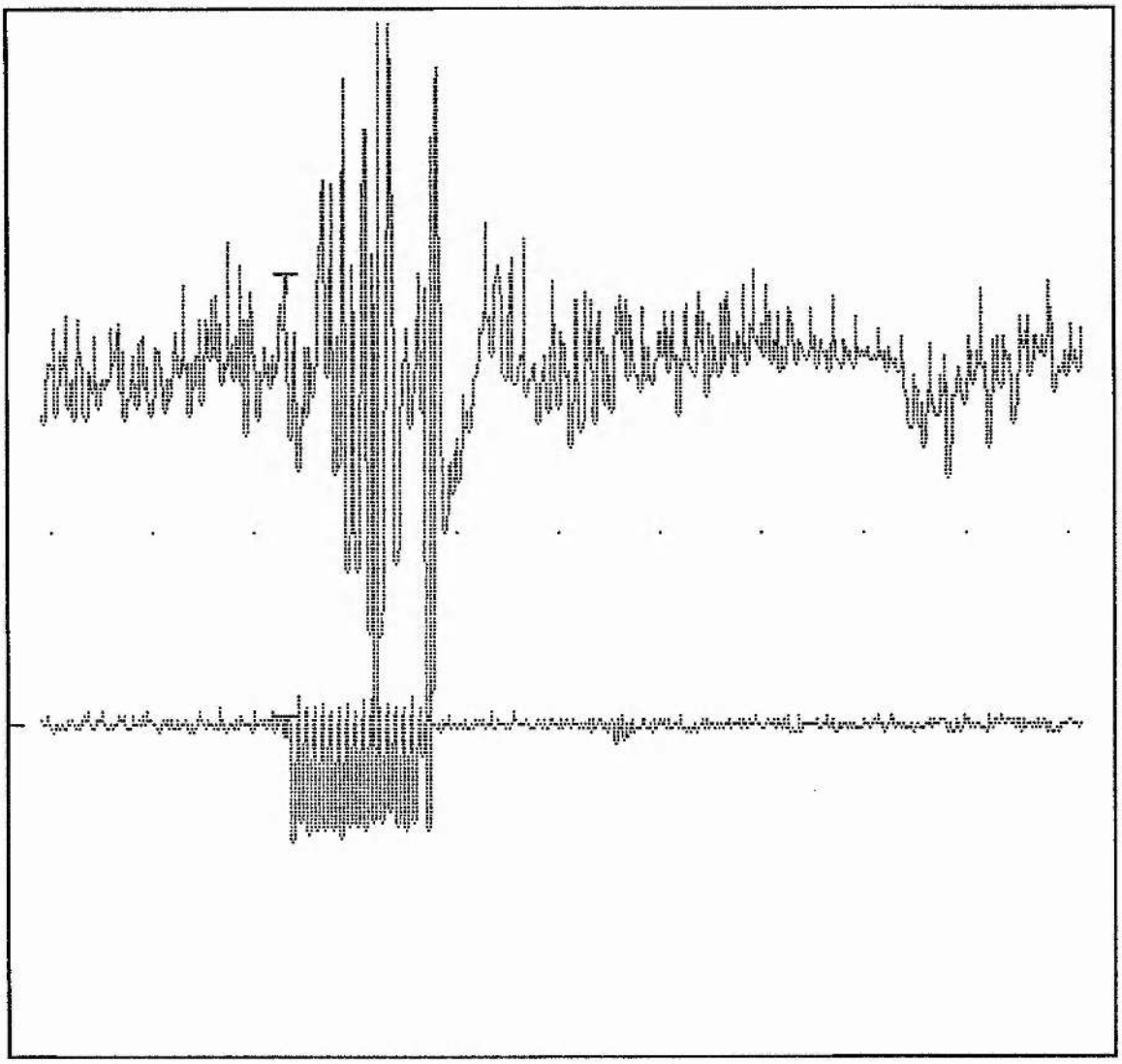

Top trace: Microwave receiver response (PSD output)
Bottom trace: Sync signal from the LBA indicating laser switch on and switch off. Timebase 0.5 s per division.
Note that the microwave signal increases significantly during the laser on time, although noise problems prohibit quantification of the effect

Figure 4.21 Guiding measurement

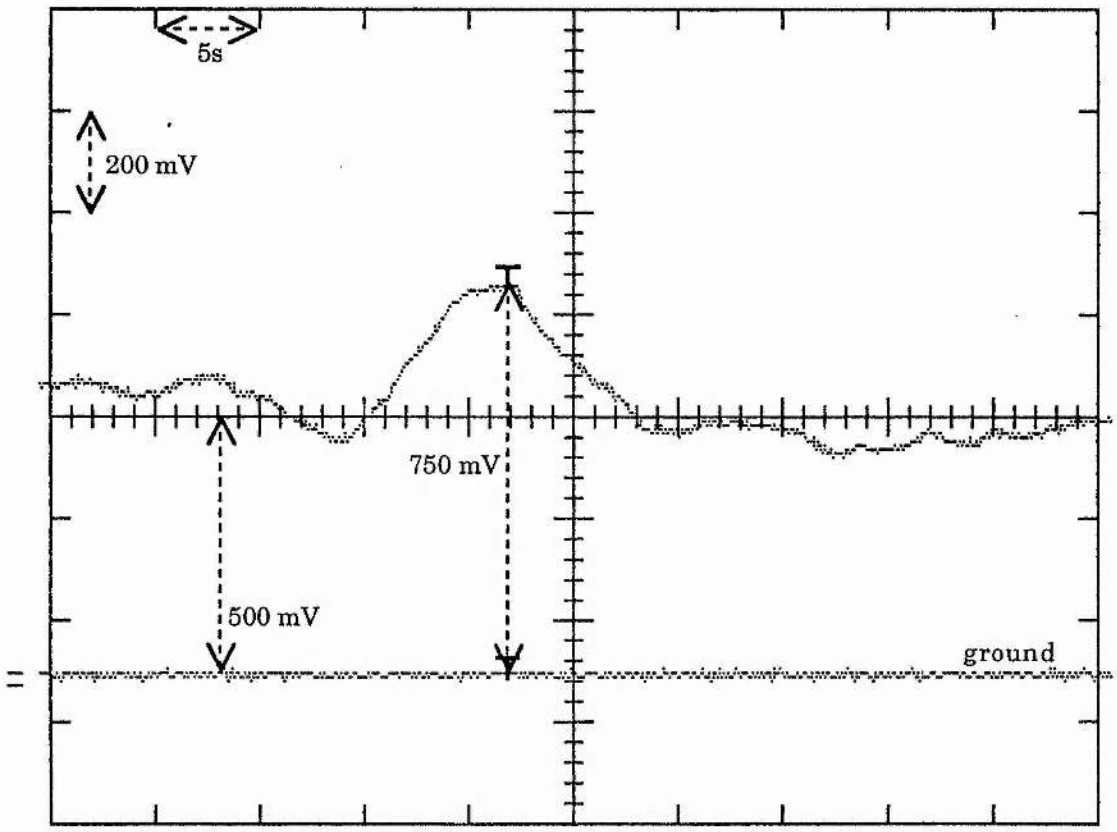

Top trace: Microwave receiver response (PSD output)

Bottom trace: ground

Figure 4.22 Guiding measurement

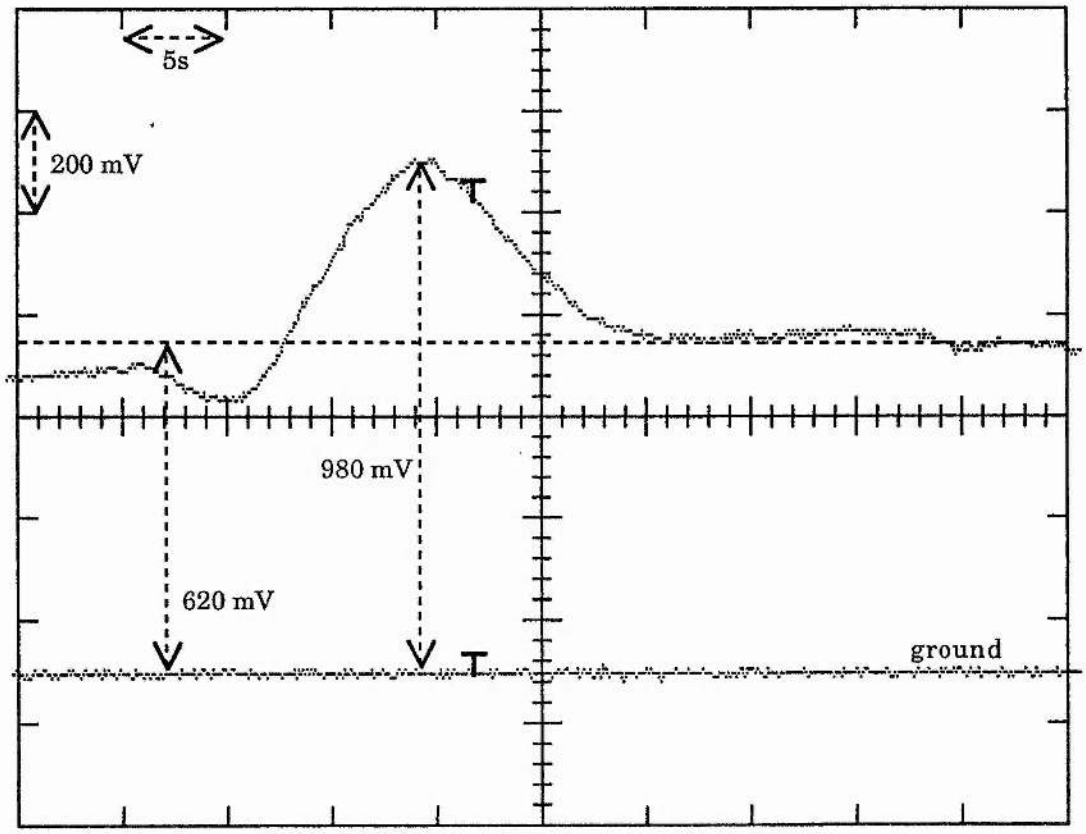

Top trace: Microwave receiver response (PSD output)

Bottom trace: ground

Figure 4.23 Guiding measurement

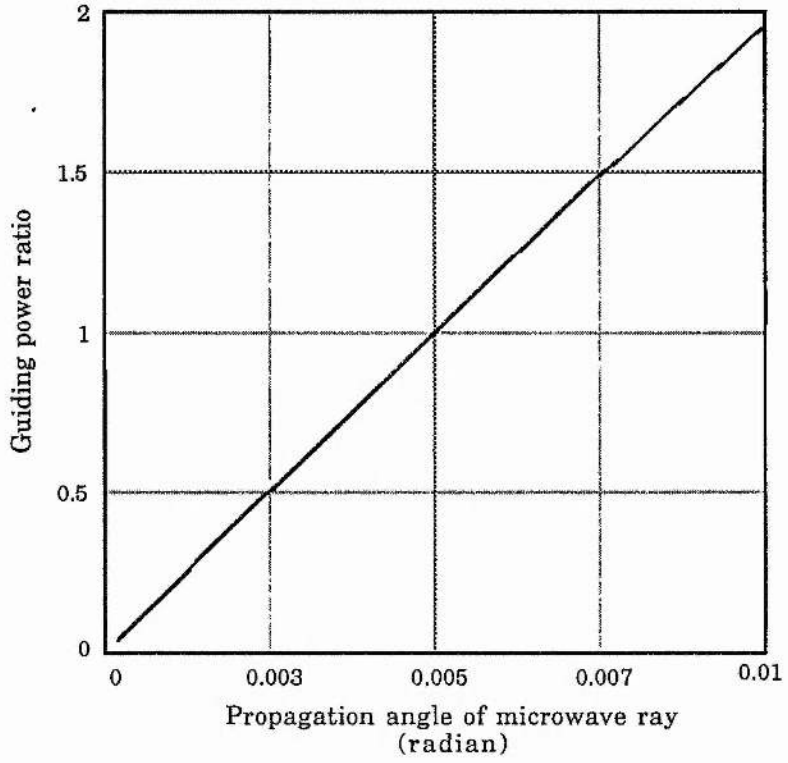

Figure 4.24 Guiding power ratio

REFERENCES FOR CHAPTER 4

1 Hirst P F, private communication, 1991

2 "Safety in Universities: Notes of Guidance Part 2:1 Lasers", published by The Committee of Vice-Chancellors and Principals of the Universities of the United Kingdom, Second Revised Edition ISBN 0 948890 05 3 (1987)

3 Lim G C and Steen W M, Journal of Physics E: Review of Scientific Instruments, **17**, p 999 (1984)

4 Dawber Bill, private communication, 1991

5 Smith G M and Lesurf J C G, IEEE Transactions on Microwave Theory and Techniques, **39**, No 12 p 2229 (1991).

5. SUMMARY AND CONCLUDING REMARKS

5.1 Summary

The essence of the idea underlying this thesis was stated simply in Chapter 1: "If the natural phenomenon of ducting could be replicated in a controlled manner, we would have a powerful technique for improving the performance of microwave systems". We have established the feasibility of using an annular laser beam to generate an atmospheric waveguide.

The waveguide is formed by tailored refractive index changes caused by absorption in the atmosphere of a small fraction of the energy of a high power laser beam. We have reviewed the status of existing work on the interaction of high power laser beams with the atmosphere (Sections 1.4 and 2.7) and related phenomena. The type and magnitude of the effects reported by researchers in the field give strong support to the concept of a laser-generated atmospheric waveguide.

We have derived and studied the equations governing the propagation of high power laser beams in the paraxial limit and their interactions (both linear and non-linear) with an absorbing atmosphere. The utility of the paraxial approximation has, in particular, been justified in relation to this class of problems (Section 2.2.1). Thermodynamic analysis (Section 2.5) has shown that total absorption coefficients of the order of 10% per km for CO_2 laser radiation at 10.6 μm are typical for

realistic atmospheres close to sea-level. The effects of turbulence have been shown to be negligible compared to those caused by absorption (Section 2.6). We have shown that, for realistic conditions, a CO_2 laser of 1 kW output power is at the threshold for thermal blooming in air. Extension of this analysis to annular geometries (Section 2.7) yielded the result that we expect strong guiding to occur for a 4.88 kW CO_2 laser for a microwave beam in the ray-optic limit. To produce guiding, refractive index changes of 4 parts in 10^6 are necessary (Section 2.7.4).

We have proposed and discussed a number of implementations of the waveguiding concept (Sections 3.2 and 3.3). It was concluded that for the purposes of an experimental verification, an Annular Beam Director ("ABD") of an on-axis design was the most practical solution. Two designs were eventually tested, one manufactured at the University of St Andrews and one manufactured by SPECAC Limited to our design (Sections 3.2.3 and 4.6). Annular laser beams were propagated over a few metres in the laboratory and measurements with a rotating wire Laser Beam Analyser (Section 4.6) indicated satisfactory performance and confirmed our design expectations.

The mechanisms which lead to the formation of the guide were considered in detail and the full paraxial form of the non-linear thermal blooming wave equation has been derived from first principles (Section 3.4). The refractive index changes produced by the laser beam were studied and both linear and non-linear cases examined (Section 3.4.1). In the linear case, a refractive index change of greater than 1 part in 10^5 is predicted for air exposed to a 1 kW CO_2 laser beam for 1 second. In the non-linear case, the iterative scheme developed predicts self-interaction and beam break-up after less than

0.5 s. The refractive index changes produced as a function of time by a laser beam of the doughnut mode have been examined and changes of 3 parts in 10^4 predicted (Section 3.4.2).

The influence of refractive index fluctuations on microwave radiation has also been considered and a ray-tracing algorithm used to investigate the behaviour of microwave radiation in an atmospheric waveguide (Section 3.5). For a step-index guide of 5 cm radius, there is strong guiding so that even with a small perturbation in refractivity, rays with á wide range of launch angles are trapped. In the case of a guide with a quadratic refractive index profile, small changes in refractive index (1 part in 10^6) produce weak guiding where only rays with trajectories very close to the optic axis are trapped. As the refractive index change increases, more divergent rays are trapped until a transition to strong guiding occurs at a critical value (changes in refractive index of the order of 1 part in 10^4).

The experimental approach employed in this thesis, reduced the overall objective of the verification of guiding to a set of simpler, modular experiments which form the individual elements of a guiding system. Once these results were obtained the individual elements were combined and atmospheric waveguiding attempted.

An overview of the experiments reported is as follows;

- Measurement of the refractive index changes produced by a high power laser beam at optical and microwave frequencies;
- The production and propagation of annular high power laser beams in the laboratory using the ABD; and

- The combination of an annular laser beam and microwave radiation in a verification of guiding.

The laser used for the experiments was a 1 kW CW CO_2 laser operating at a wavelength of 10.6 μm (Section 4.3). At optical frequencies, a specially configured Michelson interferometer was used to measure the refractive index changes produced by the laser (Section 4.4). Typical results indicate a refractive index change of 1 part in 10^6. At microwave frequencies, a millimetre wave quasi-optical FM noise measurement system developed by the Millimetre Wave Group at the University of St Andrews was used to measure the refractive index changes (Section 4.5). Refractive index changes of the order of 1 part in 10^6 have been measured for microwave radiation with a frequency of 90 GHz.

The guiding effect has been verified using an annular laser beam produced by the ABD into which microwave energy is injected using a small copper reflector located in the centre of the annulus (Section 4.7). In one implementation, the microwave energy is coupled out of the guide with a second copper reflector. In another implementation, the microwave detector unit is located on the optic axis and the laser beam is terminated in an annular beam dump. The results show clear evidence that the high power laser beam formed a waveguide, increasing the amount of microwave radiation which reached the detector by a factor of 1.5.

5.2 Concluding Remarks

Previous research work on laser beam propagation in the atmosphere has concentrated on minimising the influence of atmospheric components on the beam. In general, this is reflected in the choice of wavelengths which are located in so-called "atmospheric windows" or in the use of adaptive optics or other techniques to correct beam distortion. We have taken the "problem" of energy loss in laser propagation and applied it as a resource for the creation of a structure intended to assist the delivery of a different type of radiation. This work necessitates a different way of thinking about the physics and engineering of the processes involved. The concentration of previous research effort on eliminating propagation loss means that there is a rich field of endeavour available to those of us who would like to increase propagation loss (albeit in a controlled and useful way). In particular, further work could be done in looking at laser wavelengths which are strongly absorbed by the atmosphere (HF chemical lasers, for example), the formation of waveguides using repetitively pulsed lasers (the timing of launch of the radiation to be guided is a crucial parameter to investigate) and in outdoor tests in real conditions. The results of the research reported in this thesis suggest that the possible benefits accruing from the exploitation of atmospheric absorption of high power laser beams to generate a radiofrequency waveguide are sufficient to merit further research.